Determinants of brain region-specific age-related declines in microvascular density in the mouse brain

by

Benjamin Schager
B.A.& Sc., Quest University, 2015

A Thesis Submitted in Partial Fulfillment
of the Requirements for the Degree of

MASTER OF SCIENCE

in the Division of Medical Sciences (Neuroscience)

Supervisory Committee

Determinants of brain region-specific age-related declines in microvascular density in the mouse brain

by

Benjamin Schager
B.A.& Sc., Quest University, 2015

Supervisory Committee

Dr. Craig E. Brown, Division of Medical Sciences
Supervisor

Dr. Hector Caruncho, Division of Medical Sciences
Departmental Member

Dr. Raad Nashmi, Department of Biology
Outside Member

Abstract

It is emerging that the brain's vasculature consists of a highly spatially heterogeneous network; however, information on how various vascular characteristics differ between brain regions is still lacking. Furthermore, aging studies rarely acknowledge regional differences in the changes of vascular features. The density of the capillary bed is one vascular feature that is important for the adequate delivery of nutrients to brain tissue. Additionally, capillary density may influence regional cerebral blood flow, a parameter that has been repeatedly correlated to cognitive-behavioural performance. Age-related decline in capillary density has been widely reported in various animal models, yet important questions remain concerning whether there are regional vulnerabilities and what mechanisms could account for these regional differences, if they exist. Here we used confocal microscopy combined with a fluorescent dye-filling approach to label the vasculature, and subsequently quantified vessel length, tortuosity and diameter in 15 brain regions in young adult and aged mice. Our data indicate that vessel loss was most pronounced in white matter followed by cortical, then subcortical gray matter regions, while some regions (visual cortex, amygdala, insular cortex) showed little decline with aging. Changes in capillary density are determined by a balance of pruning and sprouting events. Previous research showed that capillaries are naturally prone to plugging and prolonged obstructions often lead to vessel pruning without subsequent compensatory vessel sprouting. We therefore hypothesized that regional susceptibilities to plugging could help predict vessel loss. By mapping the distribution of microsphere-induced capillary obstructions, we discovered that regions with a higher density of persistent obstructions were more

likely to show vessel loss with aging and vice versa. Although the relationship between obstruction density and vessel loss was strong, it was clear obstruction rates were insufficient to explain vessel loss on their own. For that reason, we subsequently used *in vivo* two-photon microscopy to track microsphere-induced capillary obstructions and vascular network changes over 24 days in two areas of cortex that showed different magnitudes of vessel loss and obstruction densities: visual and retrosplenial cortex. Surprisingly, we did not find evidence for differences in vessel pruning rates between areas, as we would have expected. Instead, we observed brain region-specific differences in recanalization times and rates of angiogenesis. These findings indicate that age-related vessel loss is region specific and that regional susceptibilities to capillary plugging and angiogenesis must be considered to explain these differences. Altogether, this work supports the overarching hypothesis that regional differences in vascular structure and function contribute to a regionally heterogeneous phenotype in the aging brain.

Table of Contents

List of Tables and Figures

List of Abbreviations

ACA: Anterior Cerebral Artery

ANOVA: Analysis of Variance

ATP: Adenosine Triphosphate

BBB: Blood Brain Barrier

C. Callosum: Corpus Callosum

CBF: Cerebral Blood Flow

CCD: Charge-coupled Device

CGM: Cortical Gray Matter

CI: Confidence Interval

FIJI: Is Just ImageJ

FITC: Fluorescein Isothiocyanate

FWHM: Full Width at Half Maximum

FrA: Frontal Association Cortex

GFP: Green Fluorescent Protein

GI/DI: Granular/Dysgranular Insular Cortex

HIF: Hypoxia-inducible Factor

HPC: Hippocampus

IOS: Intrinsic Optical Signal

LA: Lateral Amygdala

LED: Light Emitting Diode

M1/M2: Primary/Secondary Motor Cortex

MCA: Middle Cerebral Artery

NA: Numerical Aperture

PBS: Phosphate Buffered Saline

PCA: Posterior Cerebral Artery

PFA: Paraformaldehyde

pO_2: Partial Pressure of Oxygen

PRh/Ect: Peri-rhinal/Ecto-rhinal Cortex

RBC: Red Blood Cell

ROI: Region of Interest

RS: Retrosplenial Cortex

S1B: Primary Somatosensory Barrel Cortex

S1FL: Primary Somatosensory Forelimb Cortex

SGM: Subcortical Gray Matter

SNR: Substantia Nigra Reticulata

STR: Striatum

V1: Visual Cortex

VEGF: Vascular Endothelial Growth Factor

VEGFR2: Vascular Endothelial Growth Factor Receptor-2

WM: White Matter

Acknowledgments

I would first like to acknowledge with respect the Lekwungen peoples on whose traditional territory the university stands and the Songhees, Esquimalt and WSÁNEĆ peoples whose historical relationships with the land continue to this day. It was on their lands that this research was carried out.

I would also like to acknowledge the sources of funding for this research. I am very grateful to have been supported by a CIHR Frederick Banting and Charles Best Canada Graduate Scholarship. I am also grateful for the Brown Lab's funding sources that include CIHR, NSERC, CFI, and Heart & Stroke Foundation. Without these agencies, none of this work would have been possible.

To my supervisor Dr. Craig Brown, I would like to deeply thank you for inviting me into your lab and treating me with great respect. Armed with your clever ideas and your guidance, you gave me the opportunity to succeed. I'm most grateful that you gave me the freedom and confidence to make my own decisions. To my committee members Dr. Hector Caruncho and Dr. Raad Nashmi, I thank you for your time, input, and guidance. You both have terrific minds. To Dr. Neal Melvin, who first gave me an opportunity to experience science. I am eternally grateful for your support and mentorship. Rare are those who are willing to work as hard as you do to foster a love of science in others. Your work ethic, passion, and clever wit give me something to aspire to.

I would like to acknowledge and thank Alexis Kellinghusen for helping me with data collection. You strike me as someone who will live up to your own great aspirations. Good luck. I would also like to thank Emily White for performing many cranial window surgeries for my second chapter. You made my job a lot easier. Thanks also to Taimei Yang and all of the animal care staff for managing and taking great care of our animals.

To the members of the Brown Lab, Alejandra, Emily, Essie, Kim, Mo, Patrick, Reza, Rubina, Sorabh, and Sunny, as well as all the other amazing students and support staff in the Neuroscience program. You are all wonderful people and very good friends. Thank you for making me feel like I belonged here. To Essie, in particular, thank you for being a great listener and for always giving such thoughtful (and good) advice about science and beyond.

To my family, especially my mom, dad, brother, and dear friend Kade. I'm grateful for the unending support you have given me. Any success I achieve is largely attributable to you. You have simply been the best outlets, advisers, and friends.

Finally, to Brianna, the person whom I love the most. To you I owe much of my happiness. Thank you for being patient with and supportive of my decision to come to Victoria. You are an exceptional person and the perfect partner. I'm so thrilled to be coming home.

Dedication

For my mom and dad, who taught me to push myself beyond my imagined limits.

1. General Introduction

1.0 Brain energy demand and blood supply

1.0.0 Brain energy demand and blood supply

The brain performs a multitude of impressive functions simultaneously, including the mammoth task of processing great quantities of sensory information to construct our perception of, and craft our reactions to, the complex world around us. Perhaps it comes as no surprise then that the brain requires a large amount of energy to carry out these functions. In fact the cost of neurotransmission, dominated by the energetic demands of restoring ion gradients following the opening of post-synaptic ionotropic receptors and the firing of action potentials (Attwell and Laughlin, 2001), is so great that it accounts for approximately 20% of the body's resting metabolism (Kuzawa et al., 2014). These demands are noteworthy given that the brain accounts for only 2% of the body's mass (Hartmann et al., 1994). Aside from glycogen stores in astrocytes, the brain's ability to store energy is limited (Choi et al., 2003; Gruetter, 2003; Peters et al., 2004). Therefore, a constant supply of oxygen and glucose from the vascular system is necessary to produce sufficient quantities of ATP to meet this high energy demand. On top of bringing nutrients to the brain, the vasculature is equally important for removing metabolic waste from brain tissue. The human brain contains hundreds of kilometers of microvessels precisely to carry out these actions. The consequences of disrupting this vascular supply network can be predictably catastrophic. For example, in an ischemic stroke, a blockage in a major artery reduces blood flow to the tissue, causing hypoxia and widespread cell death. Strokes can leave their victims with profound long-lasting

cognitive and sensorimotor deficits, even after blood flow may be restored to the tissue. However, not all disruptions of the cerebrovascular system are so obvious. Even minor changes to vascular properties, such as hematocrit (proportion of blood that consists of red blood cells) or red blood cell (RBC) velocity, can affect oxygen extraction. Unfortunately, the human body experiences many of these small vascular changes with natural aging. While some changes in the vascular system may be compensatory in nature, others likely contribute to a decrease in the general oxygenation of brain tissue in old age, potentially contributing to the onset or exacerbation of neurological disease and cognitive decline (Moeini et al., 2018; Cruz-Hernández et al., 2019). Due to the crucial role capillaries play in nourishing the brain and maintaining its function (Cipolla, 2009), this thesis focuses on how the brain's microvasculature changes with age and what factors may influence this process. Furthermore, I herein take the stance that understanding regional differences in these microvascular elements in young, healthy subjects is an important consideration for determining how and why microvascular features, and thereby cognitive/behavioural ability, change during aging.

1.0.1 Comparing vasculature in human and rodent brains

The brains of mice and rats are a very good model to study cerebral vasculature because they share many vascular properties with the human brain. To start, vascularization of the human and rodent brains share a similar pattern, with sprouting angiogenesis populating the cortex from a pial network of vessels (Walls et al., 2008; Marín-Padilla, 2012). Given the similarities in vascular development between the species, it isn't surprising that the gross vascular anatomy is similar between species. The brains of both rodents and humans are supplied by the same major arteries that

have similar perfusion areas in each species (Kandel et al., 2012; Xiong et al., 2017). The architecture of the cortical vasculature is also similar between humans and rodents. It consists of penetrating vessels feeding and draining a meshwork of capillaries. One of the largest differences between rodents and humans is the ratio between arterioles and venules in these penetrating vessels. Humans have more penetrating arterioles than penetrating venules, while the opposite is true in rodents (Hartmann et al., 2018). The capillary beds are remarkably similar, too, though the size of the human vasculature is slightly scaled up. Capillaries are slightly longer, wider, and more spaced out in humans than in rodents, which is accompanied by slight differences in red blood cell (RBC) size (Lauwers et al., 2008; Namdee et al., 2015; Smith et al., 2019). However, capillary beds have similar branching properties in each species (Blinder et al., 2013; Smith et al., 2019), and similar density distributions across cortical layers (Schmid et al., 2017a). And even though the length and spacing of the vasculature in the human brain is slightly scaled up from that of a rodent brain, resulting is slightly reduced vascular densities, the scaling up of the vasculature is not proportional to the difference in tissue volume (Lauwers et al., 2008; Hartmann et al., 2018). In fact, one study states that the rodent vasculature is closer to a “cropped” than a “scaled” version of the human vasculature (Hartmann et al., 2018). Finally, the neurovascular unit and the blood brain barrier are made up of the same cell types and microstructural components (tight junctions, similar transporters, etc.) in rodents and in humans, though humans tend to have more astrocyte endfeet on vessels (O’Brown et al., 2018).

Given all the similarities between the vasculature in rodents and humans, it isn’t surprising to see similar trends between species in vascular aging and in the vascular

components involved in disease. For example, pericytes are equally involved in Alzheimer's pathology in rodents and humans, constricting in response to amyloid beta (Nortley et al., 2019). Most important to this thesis, age-related declines in microvascular density and cerebral blood flow (CBF) have been reported in both humans and rodents (Ohata et al., 1981; Riddle et al., 2003; Brown and Thore, 2011), though the rates of capillary loss appear to be much lower in humans than rodents, leading to similar magnitudes of capillary loss over the lifespan, but over many more years. These similarities in the vasculature promise that rodent brains are good models of studying vascular aging and disease, though careful attention must be paid when considering parameters with known differences between rodents and humans.

1.1 Vascular organization and function in the healthy nervous system

1.1.0 Gross vascular perfusion of the brain

To make sense of how age and disease-related changes in the vasculature may affect the function of the brain, we must first establish the vascular features that contribute to the optimal performance of a healthy adult brain. The blood supply to the brain arises from two primary sources: the internal branches of the carotid arteries that become the anterior and middle cerebral arteries (ACA and MCA), and the vertebral arteries that fuse together to create the basilar artery that subsequently spawns the posterior cerebral artery (PCA) (Cipolla, 2009). Each of the cerebral arteries supplies its own territory in the brain (Kandel et al., 2012). Branches of the ACA supply frontal areas of the cortex and structures close to the brain's midline, branches of the MCA supply lateral, primarily somatosensory areas of the cortex and anterior subcortical structures, and branches of the basilar artery and PCA supply some posterior areas of the cortex, posterior subcortical structures, the brain stem, and the cerebellum (Kandel et al., 2012). **Figure 1.0** shows the blood supply and perfusion territories of the mouse brain. In every case, major arteries give rise to various sizes of smaller arterioles that in turn feed a meshwork of capillaries, where the majority of bidirectional nutrient, waste, and gas exchange with the surrounding tissue takes place (Cipolla, 2009). In the healthy brain there are little to no arteriole-venule shunts, so all blood must pass through this capillary network (Shih et al., 2015). After passing through capillaries, blood in the brain travels through venules and veins before finally draining into venous sinuses, leaving the brain with metabolic waste from the cerebrospinal fluid and its own tissue-capillary

exchange (Cipolla, 2009). At nearly all levels, from major arteries to capillaries, a degree of redundancy is demonstrated by the vasculature. This redundancy protects the brain tissue from disruptive vascular events.

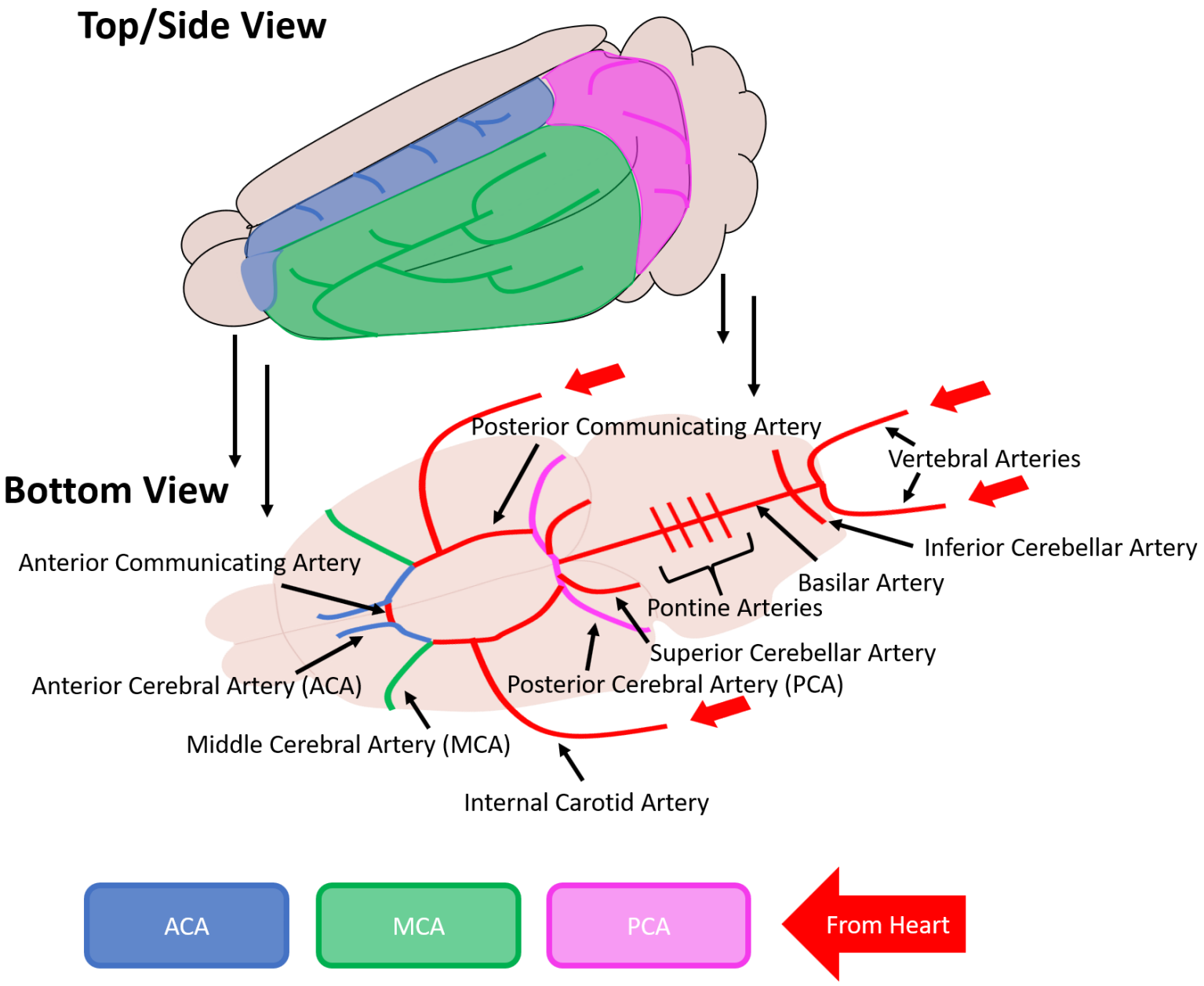

Figure 1.0. Blood supply and perfusion territories of the mouse brain. Top/side view of the cortical perfusion territories for the Anterior Cerebral Artery (ACA, blue), Middle Cerebral Artery (MCA, green), and Posterior Cerebral Artery (PCA, pink) in the mouse brain, guided by data published by (Xiong et al., 2017). Bottom view shows major arterial blood supply to the mouse brain, including collateral circulation provided by the Circle of Willis, made up of the PCA, MCA, ACA, and Posterior and Anterior Communicating Arteries.

1.1.1 Redundancy in the cerebral vasculature

Given the nervous system's high demand for energy and lack of local energy stores, redundancy in the cerebrovascular architecture is critical for preserving function in the event of a vascular insult. In large vessels, the Circle of Willis, where anterior and posterior communicating arteries connect the major cerebral arteries on both sides of the brain (see **Figure 1.0**), ensures that cerebral perfusion can be partially maintained if there is a disruption to flow in a major artery, like the internal carotid (Jung et al., 2017). The communicating arteries are an example of redundant vessels known as collaterals or anastomoses. Collaterals also exist between the internal and external carotid arteries, as well as between intracranial arteries (Jung et al., 2017). These connections, called leptomeningeal collaterals, consist of pial arterioles connecting territories of the MCA to territories of the PCA or ACA (Jung et al., 2017). Leptomeningeal collaterals are important for preserving cerebral perfusion in the event of an ischemic stroke of the MCA, PCA, or ACA, but are variable between brains in their prevalence and anatomy (Jung et al., 2017); they even differ within brains in their functional capacity for providing collateral flow (i.e. MCA-PCA collaterals are more functional than MCA-ACA collaterals) (Menon et al., 2013). Collateral circulation is a prominent feature of the vasculature on the pial surface of the cortex, too. In the pial arteriolar networks, a single occlusion leads to a rebalancing of flow (accompanied by changes in RBC velocity) that restores perfusion in vessels downstream of the occlusion. This is accomplished by a network of downstream, yet inter-connected vessels that reverse their flow to direct blood towards the location of the clot after the insult (Schaffer et al., 2006; Shih et al., 2015; Reeson et al., 2018). This redundancy makes pial circulation highly resistant to ischemic damage

resulting from a single occlusion (Schaffer et al., 2006; Shih et al., 2013, 2015; Bollu et al., 2018).

On the other hand, penetrating arterioles that dive radially into the cortex and supply the microcirculation do not have the same collateral circulation. Insults to penetrating arterioles result in large changes in RBC velocity in downstream capillaries, and areas dependent on this vascular supply are highly susceptible to ischemic damage from a single occlusion (Nishimura et al., 2010; Shih et al., 2013, 2015). Currently there is little information available on the organization of the subcortical circulation, so it remains unclear whether similar bottlenecks to perfusion exist in the subcortical vascular supply. Though the capillary beds are at the mercy of insults to penetrating arterioles, there is such great redundancy within their networks (and such widespread capillary coverage) that insults to single capillaries themselves have very little effect on nearby cells (Shih et al., 2013). In fact in healthy adult mice, capillaries stall constantly, often for minutes at a time, without immediate consequences to tissue oxygenation (Kleinfeld et al., 1998; Erdener et al., 2017; Moeini et al., 2018; Reeson et al., 2018). In the cortex, and presumably subcortically, capillaries form a highly interconnected lattice structure where connected loops of vasculature consist of an average of 8 internodal segments; therefore, 7 separate nodes may serve as a source for perfusion of the loop (Blinder et al., 2013). Capillary networks like the ones described above likely rebalance flow after an insult in the same manner as the networks on the pial surface (Shih et al., 2015). However, it is important to note that with age, the redundancy and adaptability of this network is likely to change, thereby rendering the brain more vulnerable to future insults.

1.1.2 Capillary structure and function

Densely interconnected capillary networks make up nearly all the brain's vascular length in both humans and rodents. They are structured to optimize tissue-capillary exchange while limiting damage to the brain from harmful circulating substances. Capillaries represent >90% of the total vascular length in the brain by my own estimates (~96%) and the estimates of others (Xiong et al., 2017). The importance of these small vessels is implied not only by their abundance, but also by the estimation that almost every neuron in the brain is associated with a corresponding capillary (Cipolla, 2009). In fact, the average distance from neuronal or glial somata to the nearest capillary is approximately 15-18 microns (Tsai et al., 2009; Gould et al., 2017), while, on average, spines on dendrites are only 13 microns from the nearest capillary surface (Zhang et al., 2005). The proximity between capillaries and the other cells of the central nervous system ensures that nutrients, oxygen, and waste diffuse quickly between the capillaries and the cells or synapses in the parenchyma (Zlokovic, 2005). Capillaries represent the largest increase in resistance to flow in the brain (Gould et al., 2017). Their low pressure, reduced RBC velocity, and small (~4-8μm) diameter maximize surface area and contact time for both plasma and RBCs with the endothelium, facilitating oxygen and nutrient extraction through diffusion, facilitated diffusion, and active transport.

Structurally, capillaries in the brain are different from both larger brain vessels and capillaries elsewhere in the body because of the presence of the Blood Brain Barrier (BBB). In short, the BBB tightly regulates the delivery of substances from the blood. The purpose of this regulation is twofold: to maintain proper quantities of the nutrients that the brain needs to function, and also to prevent unwanted substances

from entering the parenchyma (Daneman and Prat, 2015). Endothelial cells that comprise the vascular lumen are connected by tight junctional proteins that bring the cells very close together, preventing larger molecules from diffusing into the brain (Daneman and Prat, 2015). Owing to the absence of larger fenestrations that facilitate diffusion, which are found in the capillaries of many other tissues in the body, larger molecules, especially those that are not lipid-soluble, must enter the brain through specific channels or transporters (Daneman and Prat, 2015). For example, the endothelial cells in the brain contain specific influx transporters for important nutrients. These transporters move molecules such as glucose, lactate, and amino acids along their concentration gradients into endothelial cells and subsequently out the abluminal membrane into the parenchyma (Daneman and Prat, 2015). Endothelial cells also have many efflux transporters on their luminal membrane to return small lipophilic molecules to the blood that would otherwise have passed through the endothelium and into the brain (Daneman and Prat, 2015). Finally, the BBB regulates transport by reducing the transcytosis of blood components through cells and into the brain (Daneman and Prat, 2015). Blood vessels are found in close proximity to several different cell types that together make up the neurovascular unit. These cells include endothelial cells, mural cells (such as pericytes and smooth muscle cells), neuronal processes, microglia (that respond to vascular insults), and astrocytes (whose endfeet envelop parenchymal arterioles and capillaries almost completely) (Cipolla, 2009). These cells help maintain the proper function of the BBB and they also support other important vascular processes, such as neurovascular coupling – the process by which brain activity in a region can increase local blood flow. Astrocytes, for example, provide trophic and

metabolic products to the BBB and contribute to bidirectional signaling with endothelial and smooth muscle cells that regulates vascular tone (Filosa et al., 2016; Lécuyer et al., 2016).

Figure 1.1. The Blood Brain Barrier

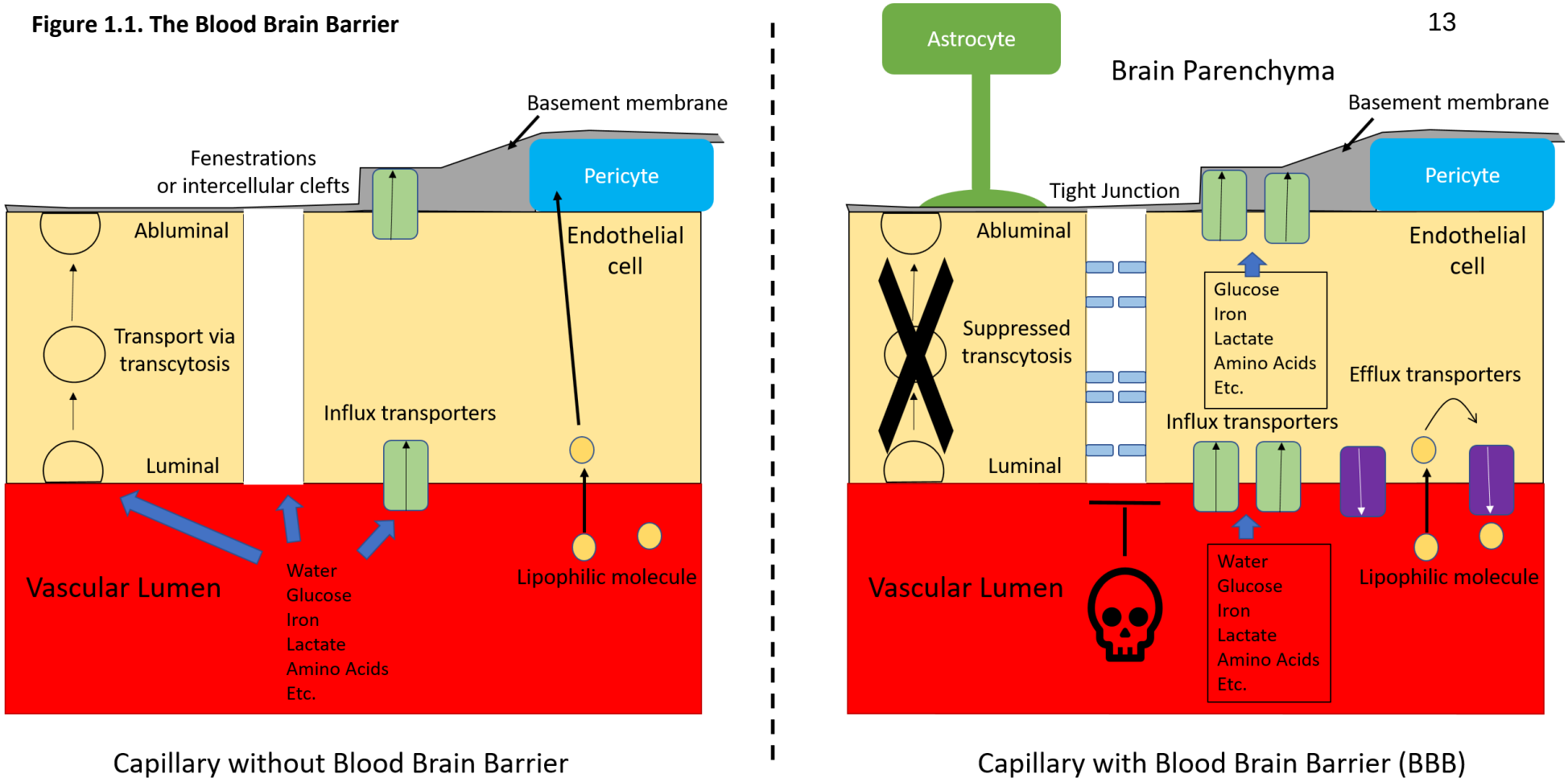

Figure 1.1. The Blood Brain Barrier. The left panel shows a cellular transport in a peripheral capillary. Whether the capillary has fenestrations or not determines the size of molecules that can simply diffuse into the parenchyma. The right panel shows a capillary in the brain. The Blood Brain Barrier (BBB) consists of tight junctions, influx and efflux transporters, and the suppression of transcytosis. Astrocytes and pericytes provide support to maintain the BBB.

In addition to their small size, the structure and microenvironment of capillaries also differentiates them from other larger vessels in the brain. Arteries or large arterioles on the pial surface of the brain are surrounded by layers of smooth muscle cells that are innervated by the peripheral nervous system (Cipolla, 2009). Smooth muscle allows these vessels to contract and dilate. Penetrating arterioles dive into the brain and are initially surrounded by Virchow-Robin spaces, an extension of the subarachnoid space that exists between the *glia limitans* and the vascular basement membrane (Iadecola, 2017). As penetrating vessels get deeper into the parenchyma, the perivascular space disappears (as the *glia limitans* and the basement membrane fuse) and the smooth muscle cell layer drops to single cell thickness (Cipolla, 2009; Iadecola, 2017). In contrast to larger vessels, brain capillaries are not associated with smooth muscle (Iadecola, 2017). Instead, other mural cells, called pericytes, are found inside the basement membrane and enwrap capillary endothelial cells with sparse projections (Attwell et al., 2016). There are several classes of pericytes that differ slightly in morphology and function depending on where they are found in the capillary network (Attwell et al., 2016). Interestingly, those close to precapillary arterioles and higher order capillaries express smooth muscle actin. These can contract to alter capillary diameter (Peppiatt et al., 2006; Mishra et al., 2016; Berthiaume et al., 2018; Nortley et al., 2019). There is still some debate on whether the contractile properties of pericytes contribute to another feature of the healthy brain: regulation of blood flow in response to neural activity and metabolic demand.

Figure 1.2. Angioarchitecture of the cerebral cortex.

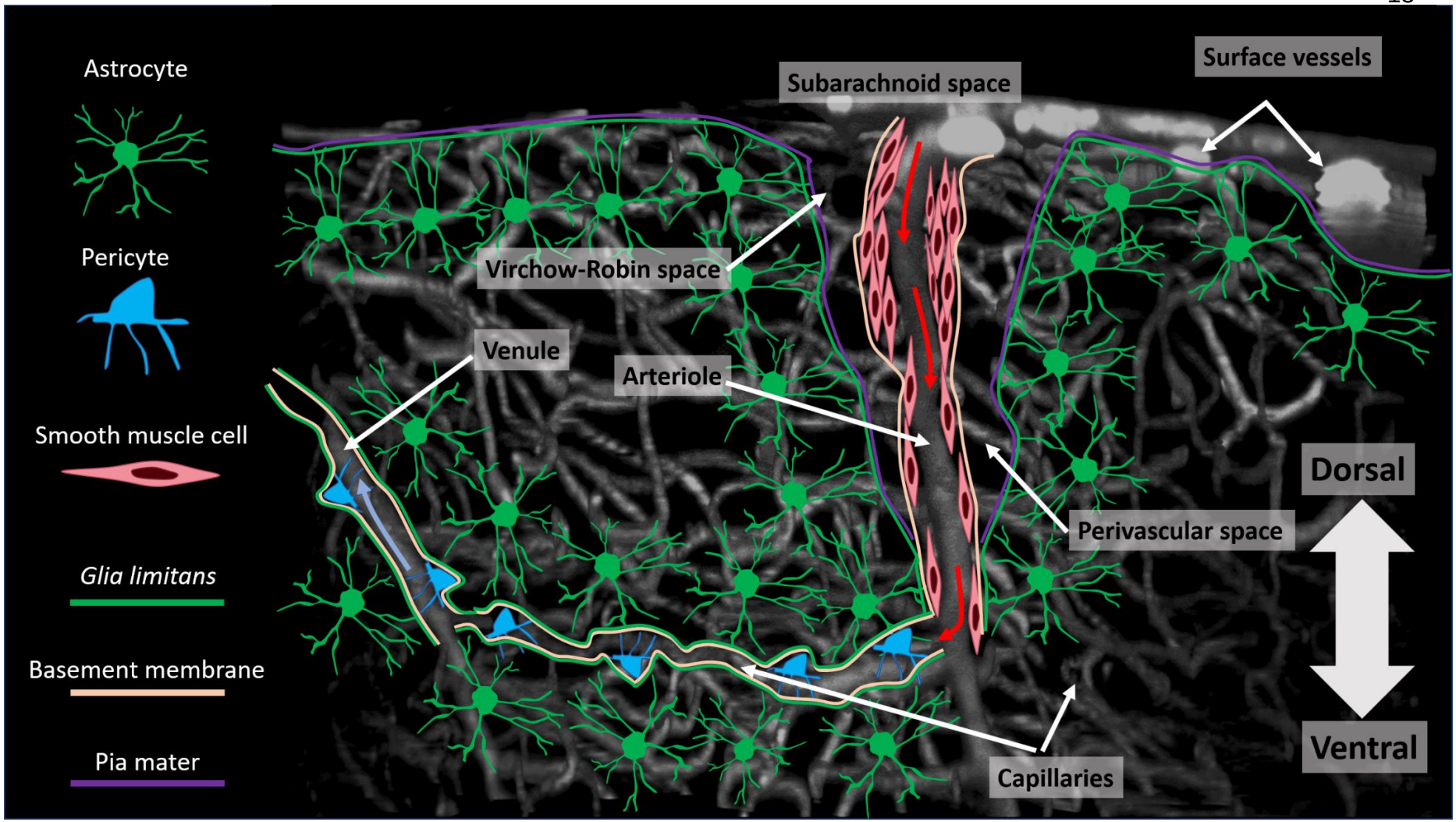

Figure 1.2. Angioarchitecture of the cerebral cortex. Figure displays the path of blood from the pial surface down a penetrating arteriole, through a capillary bed, and up a penetrating venule. Note that as the arteriole gets deeper, the basement membrane fuses with the *glia limitans* and smooth muscle cells become fewer. Pericytes line capillaries and venules.

1.1.3 Regulation of cerebral blood flow and neurovascular coupling

Another important feature of the cerebral vasculature is its ability to locally alter blood flow to meet changing energy requirements based not only on feedback from changing metabolic rates (anaerobic by-products like lactate and adenosine can affect blood flow), but also on feedforward signaling from changes in electrical activity in the brain (Roy and Sherrington, 1890; Fox and Raichle, 1986; Attwell et al., 2010; Iadecola, 2017). The change in blood flow in response to neural activity is known as neurovascular coupling or functional hyperemia. Blood flow through a capillary network is thought to be largely determined by the pressure gradient existing between the precapillary arteriole that supplies the vessels and the precapillary venule that drains them (Cipolla, 2009). As such, blood flow through the capillary network is dependent on the flow and pressure in arterioles, which can be altered by changing arteriolar diameter through smooth muscle contraction or dilation (Cipolla, 2009; Fernández-Klett et al., 2010). Neuronal activity can affect vascular tone and bring about transient changes in vascular (arteriolar and capillary) diameter through a multitude of mechanisms, some of which include signaling through astrocytes and/or pericytes (Attwell et al., 2010; Gordon et al., 2016; Mishra et al., 2016; Iadecola, 2017; Mehina et al., 2017). Some researchers even argue that capillary flow is regulated by contractile pericytes on first and second order capillaries (Peppiatt et al., 2006; Hall et al., 2014; Mishra et al., 2016; Khennouf et al., 2018). Mechanisms involved in neurovascular coupling tend to vary by the signaling cell type and location within the brain (Devonshire et al., 2012; Uhlirova et al., 2016; Mapelli et al., 2017). Furthermore, the relative importance of each pathway in producing functional hyperemia is still in question (Attwell et al., 2010; Iadecola, 2017; Longden et

al., 2017; Mapelli et al., 2017; Hogan-Cann et al., 2019). Beyond the relative importance of various signaling pathways, there are still two primary points of contention: the contribution of astrocytes to fast transient changes in either arteriolar or capillary diameter, and the importance of capillary pericyte-mediated local diameter changes to the instigation of functional hyperemia (Hall et al., 2014; Hill et al., 2015; Bazargani and Attwell, 2016; Mishra et al., 2016; Tran et al., 2018; Institoris et al., 2019). Clearly, pericytes can be contractile and responsive to neuronal activity (Khennouf et al., 2018; Rungta et al., 2018), and while it is unknown whether they *instigate* functional hyperemia, they are undoubtedly important for its progression (Khennouf et al., 2018; Rungta et al., 2018). Pericyte degeneration leads to a breakdown of neurovascular coupling (Kisler et al., 2017b), characterized by decreased capacity to increase CBF in response to neuronal activity, reduced tissue oxygenation, and increased buildup of anaerobic metabolites (Kisler et al., 2017b). While there is debate concerning the mechanisms that underlie functional hyperemia, there is no question that it drives a large heterogeneity in RBC velocity and flux (# of RBCs per second) in the brain that is critical to meeting dynamic metabolic demands (Cipolla, 2009).

It is well known that capillaries display a large heterogeneity in RBC flux (Lee et al., 2013; Li et al., 2016). Factors that contribute to this heterogeneity in flow include functional hyperemia and differences in the resistance of individual capillaries, which helps to determine preferred paths for RBCs (Schmid et al., 2017b). According to a simple parallel capillary model, an increase in blood flow (as accompanies functional hyperemia) should affect each capillary passively, increasing the flux slightly in each (Lee et al., 2016). This model predicts that an increase in flow should slightly elevate

the standard deviation in flux, or in other words cause an increase in flux heterogeneity (Lee et al., 2016). However, experimental evidence shows that there is instead a local reduction in standard deviation of flux following sensory stimulation despite there being an increase in the mean flux (Gutiérrez-Jiménez et al., 2016; Lee et al., 2016). This homogenization of flow theoretically and experimentally appears to increase the efficiency of oxygen extraction (Jespersen and Østergaard, 2012; Lee et al., 2016; Li et al., 2019a). While it is unclear exactly how this homogenization happens, it has been proposed that changes in capillary diameter through pericyte contractility may be involved (Lee et al., 2016). Homogenization of flow in response to neural activity is an interesting finding because it suggests that energy needs may not be met only with changes in arterial diameter and CBF. Theoretically, a change in CBF is not needed to improve oxygenation when homogenization of flow can itself improve the efficiency of oxygen extraction (Jespersen and Østergaard, 2012). Nonetheless, functional hyperemia produces a dynamic regional heterogeneity in CBF to meet energy demands while also increasing the efficiency of oxygen extraction.

1.1.4 Regional heterogeneity in the cerebral vasculature

CBF heterogeneity is not only a product of functional hyperemia, it is heterogeneous even in resting states (Craigie, 1945; Iadecola, 2017). As it turns out, CBF is not the sole vascular parameter that varies systematically by brain region. In fact, we've now asserted that vessel caliber, vessel structure, CBF, the extent of vascular redundancy, and the mechanisms that underlie neurovascular coupling all vary depending on the brain region in question. It is obvious that regional heterogeneity is a hallmark of the cerebral vasculature. Moreover, regional heterogeneity in the

vasculature may relate to local energy demands of the tissue (Craigie, 1945; Iadecola, 2017). Some vascular parameters change with depth below the pial surface. For example, vascular density and perhaps tissue oxygenation (there are conflicting reports (Sakadžić et al., 2010; Schmid et al., 2017b)) are quite low in layer 1 of the neocortex, which contains few cell bodies, but both parameters appear to increase significantly in deeper layers (Tsai et al., 2009; Blinder et al., 2013; Lyons et al., 2016; Schmid et al., 2017a). Simulations of blood flow in the brain also indicate that the number of possible unique paths through a capillary bed, RBC velocities, and locations of the largest pressure drops for RBCs (happening in capillaries in superficial layers and in arterioles in deeper layers) also vary by cortical depth (Schmid et al., 2017b). The location of the largest pressure drop is especially important for functional hyperemia, since changes in vascular diameter at these locations have the greatest effect on blood flow (Schmid et al., 2017b). In sensory areas of the cortex, layer IV has the highest density of neurons and, presumably, the greatest oxygen consumption (Attwell and Laughlin, 2001; Tsai et al., 2009; Blinder et al., 2013). Predictably, it also boasts the greatest capillary density, the most homogeneous distribution of capillary oxygenation and RBC flux, and the highest efficiency of oxygen extraction (Tsai et al., 2009; Blinder et al., 2013; Li et al., 2019a). Vascular parameters not only vary by cortical depth, they also vary by gross anatomical area — especially between the gray matter and the white matter of the brain.

Following with the trend of baseline metabolic demand predicting elements of vascular supply, the vascular supply of white matter appears to vary from gray matter in a few key respects (Noumbissi et al., 2018). First of all, the white matter contains fewer

neuronal cell bodies and dendrites, the greatest sites for energy consumption in the brain, than gray matter (Attwell and Laughlin, 2001). However, white matter contains many more myelinated axonal fibres than gray matter (Noumbissi et al., 2018). The vascular structure in the white matter reflects these differences. In comparison to capillaries in the gray matter, those in the white matter are longer and run largely parallel to the axonal fibres. Further, the number of vessels is also notably reduced (Cavaglia et al., 2001), presumably because fewer sites for tissue-capillary exchange are needed to meet the reduced local energy demand. Though CBF is lower in white matter relative to gray matter (Leenders et al., 1990), RBC velocity and flux are actually higher in the white matter, likely because there is a reduced number of vessels that must pass a great volume of blood (Li et al., 2019b). As would be predicted with greater flux and shorter transit times, there evidence that the efficiency of oxygen extraction may also be reduced in white matter (Leenders et al., 1990; Hyder et al., 2016; Oghabian and Jafari, 2018). Aside from features that affect blood flow and nutrient abundance, there are differences in the BBB composition between gray and white matter, too. Specifically, the white matter is enriched in several BBB-related proteins (such as adherens junction α-catenin, claudin-5, and occludin in endothelial cells, and astrocyte GFAP in endfeet) and capillaries taken from white matter have stronger barrier properties (i.e. less leakage) than those taken from gray matter (El-Khoury et al., 2006; Nyúl-Tóth et al., 2016; Noumbissi et al., 2018).

Aside from strictly gray or white matter distinctions, vascular properties, including vessel density, vary between individual brain regions and even within gross anatomical structures. In the rodent brain, the thalamus and dorsal areas of the cortex (including

somatosensory areas) tend to have higher vascular densities, while the hypothalamus, lateral cortical areas, and the white matter tend to have lower vascular densities (Cavaglia et al., 2001; Xiong et al., 2017). Vascular densities and BBB properties even vary within structures. For example, there are reported differences in vascular density between striate and extra-striate visual cortex (Schmid et al., 2017a), and between CA1 and CA3 of the hippocampus (Cavaglia et al., 2001). Moreover, CA1 vessels were also more likely to leak following reperfusion after an ischemic event than vessels in the CA3, demonstrating differences in BBB integrity (Cavaglia et al., 2001). In general, the subcortical vasculature has been profoundly understudied, especially outside the hippocampus. However, other differences in vasculature between cortical and subcortical areas likely exist. For example, Devonshire and colleagues assert that the pattern of vascular innervation and the diameter of arteries relative to their peripheral branches are different for subcortical structures than for cortical structures (Rieke, 1987; Devonshire et al., 2012; Xiong et al., 2017). In all, numerous traits of the cerebral vasculature are regionally heterogeneous in nature. This heterogeneity may affect how vascular networks change over time, which finally evokes a discussion of microvascular plasticity: the mechanisms by which the microvasculature adapts to its environment.

1.1.5 Microvascular plasticity

Microvascular networks in the brain are plastic, maintaining the ability to sprout new vessels, prune old ones, alter diameter, and clear obstructing emboli, all in the goal of maintaining a network that is suited to meeting local energy demands. In development, the vasculature has a large capacity for sprouting new vessels. Vascularization of the brain happens via angiogenesis, the process by which new

vessels sprout from existing ones. Blood vessels infiltrate from the peri-neural vessel plexus in a process driven by gradients of growth factors (primarily VEGF) secreted by subventricular neural progenitor cells (Milner, 2014). Endothelial cells release matrix metalloproteinases that degrade the extracellular matrix and allow endothelial cells to proliferate (Milner, 2014). The leading cell (called the tip cell) extends filopodia that contain receptors for VEGF and Angiopoietin that help direct cell migration toward the source of the growth factors (Milner, 2014). Signalling of many other proteins are required for vessel stabilization, lumen formation, attraction of other neurovascular unit cells, and construction of the blood brain barrier (Milner, 2014). Hypoxia is a major driver of angiogenesis in development. Hypoxic conditions increase the expression of hypoxia-inducible factor (HIF) proteins, which are transcription factors that increase VEGF expression (Milner, 2014). In mice, a large number of angiogenic events continue to occur after birth before exhibiting a rapid decline in prevalence after approximately 1.5 months (Harb et al., 2013). While angiogenic events occur at a high frequency in early development, studies in mice and zebrafish show that there is a concomitant simplification of the vasculature, caused by a large number of pruning events (Chen et al., 2012; Harb et al., 2013). In developing zebrafish, signals such as endothelial sheer stress help to determine the fate of sprouted vessels. Specifically, those vessels with lower blood flow velocity are more likely to be pruned from the vascular network than vessels with higher velocity. These pruning events appear to happen via endothelial cell migration and not cell death (Chen et al., 2012). Chen and colleagues postulate that animals develop an angioarchitecture suited to meet the brain’s energy supply by sprouting vessels where energy demand is not being met, and pruning vessels where

their presence is redundant (Chen et al., 2012). A simplified visual representation of hypoxia-mediated angiogenesis and subsequent network simplification can be found in **Figure 1.2**. Time-lapse 2-photon imaging shows that, in somatosensory cortex, angiogenesis and pruning drop to very low levels by 3 months of age in a mouse and disappear almost completely in old (~25 month-old) animals (Harb et al., 2013). However, that does not indicate that the brain's vasculature loses its *capacity* for plasticity in adulthood.

Figure 1.3. Hypoxia-mediated angiogenesis and sheer stress-related pruning.

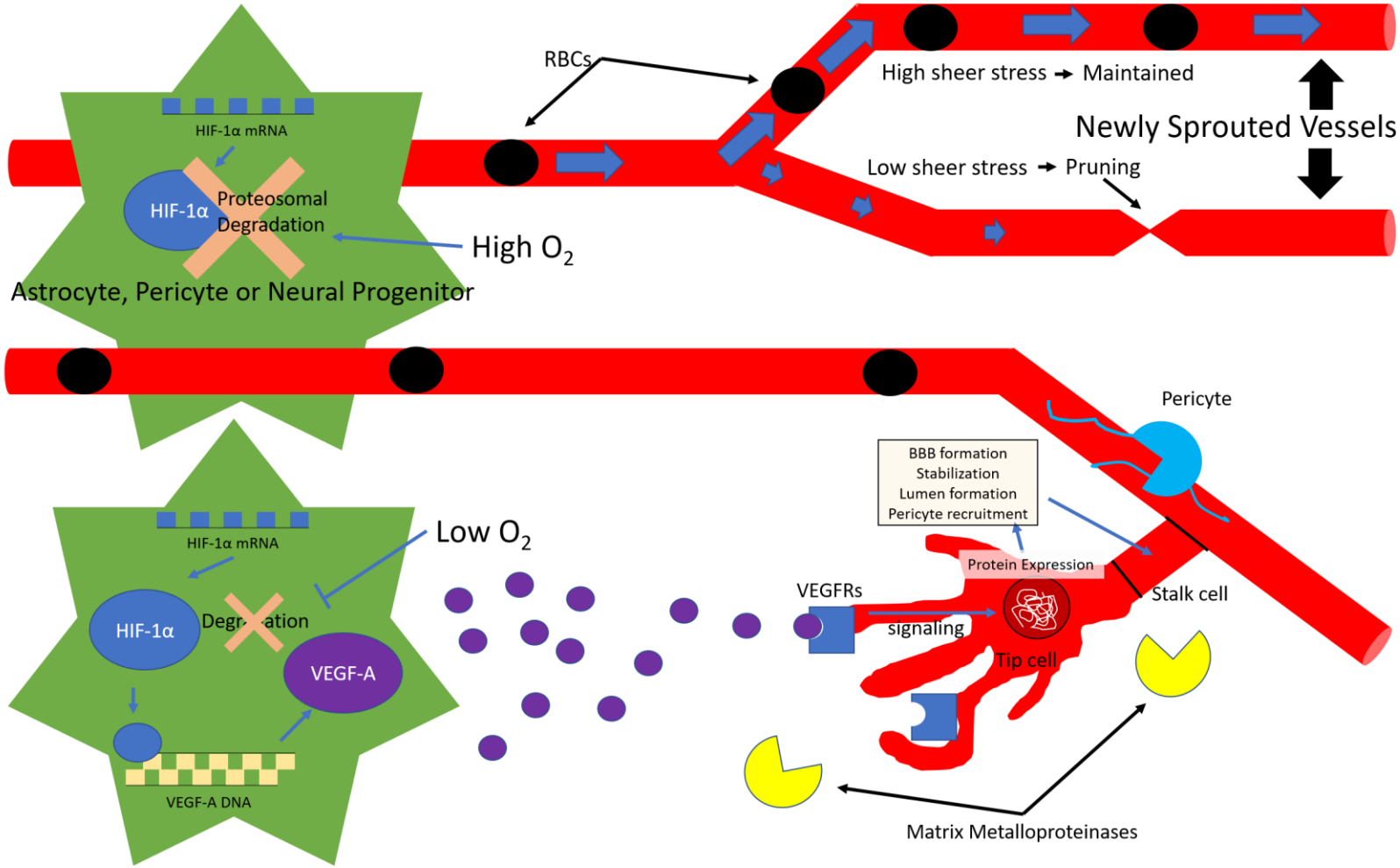

Figure 1.3. Hypoxia-mediated angiogenesis and sheer stress-related pruning. Figure shows that in areas of low hypoxia, HIF-1α protein is no longer degraded, leading to VEGF-A gradient. VEGF-A signaling promotes tip cell formation, guides tip cell migration, and stimulates the production of other signaling molecules involved in vessel maturation. Endothelial sheer stress promotes cell survival. Newly sprouted vessels may be pruned when there is little flow through them, leading to low endothelial sheer stress.

Plasticity in the adult brain appears to be largely driven in response to vascular challenges. One common challenge to the vasculature is obstruction. Obstruction can occur in vessels of any size, including in large vessels, where emboli can cause ischemic strokes. However, obstructions are particularly common in the microvasculature, where small diameter and low pressure tubes must pass large and sometimes adherent materials, including red blood cells, white blood cells, fibrin clots, atheromatous plaques, and other types of cellular debris (Lam et al., 2010; Santisakultarm et al., 2014; Erdener et al., 2017; Reeson et al., 2018; Cruz-Hernández et al., 2019). Small vessels usually quickly clear the embolus and re-establish flow after obstruction (also known as “recanalization” by washout, a process where emboli are pushed back into the circulation) (Erdener et al., 2017; Reeson et al., 2018). Though the mechanisms for embolus washout are currently unknown, there are hypotheses that they may involve neural activity and/or vascular endothelial growth factor receptor-2 (VEGFR2) signaling (Erdener et al., 2017; Reeson et al., 2018). However, microvessels and arterioles sometimes recanalize after obstruction via a process called angiophagy, wherein endothelial processes envelop the embolus and transport it outside of the vessel (Lam et al., 2010; Grutzendler et al., 2014; Reeson et al., 2018; van der Wijk et al., 2019). Research indicates that this process becomes delayed with age (Lam et al., 2010). In larger vessels, such as penetrating arterioles that lack abundant collateral circulation, failed embolus washout combined with delayed or failed extravasation can lead to prolonged hypoxia and cell death in the local tissue (Lam et al., 2010). These events may produce microinfarcts, which researchers have associated with dementia and correlated with cognitive dysfunction (Vermeer et al., 2007; Shih et al., 2013, 2015;

van der Wijk et al., 2019). In smaller vessels (i.e. capillaries), angiophagy is less prevalent and failure to recanalize does not have the immediate large-scale hypoxic consequences that are associated with obstruction in larger vessels (Shih et al., 2013; Reeson et al., 2018). Instead of flow being re-established by embolus extravasation, capillary obstruction results in vessel pruning in approximately 30% of capillaries that are occluded for greater than 20 minutes (Cudmore et al., 2017; Reeson et al., 2018). In Reeson and colleagues' 2018 study, the loss of vessels due to capillary obstruction in the somatosensory cortex was not compensated for by angiogenic sprouting and was thus hypothesized to drive an age-related reduction in capillary density that has been widely reported in mice, rats, monkeys, and humans (Reeson et al., 2018).

Although angiogenesis does not occur in the forelimb somatosensory cortex in response to small perturbations, such as capillary obstructions (Reeson et al., 2018), there are several reports that claim angiogenesis can be deployed in the adult brain. For example, a number of studies have shown that mice and rats exposed to chronic hypoxia retain the ability to grow new vessels (Shweiki et al., 1992; Swain et al., 2003; Ndubuizu et al., 2010; Harb et al., 2013; Masamoto et al., 2014), though by some accounts that capacity decreases with advanced age (Harb et al., 2013). When angiogenesis occurs in response to hypoxia, vessels preferentially sprout from superficial areas of cortex into regions with low capillary density surrounding penetrating arterioles (Masamoto et al., 2014). These new vessels are subsequently enveloped by astrocyte endfeet, a process which may aid in the stabilization of the BBB (Masamoto et al., 2014). Hypoxia associated with stroke is also thought to result in a degree of angiogenesis and remodeling (Brown et al., 2007a). Furthermore, there is a large body

of literature suggesting that exercise can induce angiogenesis (Isaacs et al., 1992; Kleim et al., 2002; Swain et al., 2003; Ding et al., 2006; Gao et al., 2014; Morland et al., 2017), and that vessel density may increase into middle age in humans, rats, and mice (Hunziker et al., 1979; Meier-Ruge et al., 1980; Wilkinson et al., 1981; Hinds and McNelly, 1982; Villena et al., 2003; Moeini et al., 2018). However, it is important to consider that many of these angiogenesis studies use indirect approaches based on protein expression or metrics that rely on vessel diameter to show increases in vascular density and infer angiogenesis. The positive results of these studies were tempered by the fact that several *in vivo* imaging studies that directly assess changes in the same vascular structures over time found scant or no evidence for angiogenesis (Mostany et al., 2010; Tennant and Brown, 2013; Cudmore et al., 2017; Dorr et al., 2017). However, it is important to note that all these *in vivo* two-photon imaging studies were focused on somatosensory and motor cortex, usually in the context of a vascular challenge like stroke or chronic hypoxia. It is conceivable that rates of angiogenesis may vary in a region-dependent manner, as there has yet to be any systematic study on angiogenesis across different brain regions.

Finally, vascular plasticity may also consist of remodeling without sprouting, as can happen with long-lasting changes in diameter. When this happens in arteries and arterioles, it is called arteriogenesis. This phenomenon is caused by an increase in sheer stress that drives upregulation of cell adhesion molecules, which subsequently attracts leukocytes. These leukocytes release growth factors and cytokines that ultimately elicit diameter changes (Yanev and Dijkhuizen, 2012). In mice, similar long-lasting changes in the diameter of capillaries can also be induced by extended exposure

to hypoxia (Masamoto et al., 2014) and by advanced aging (Hicks et al., 1983; Moeini et al., 2018). The brain's capacity for plasticity is greatly affected with age. Pro-angiogenic molecules become scarce (Murugesan et al., 2012), natural angiogenesis stops, the capacity for challenge-induced angiogenesis diminishes, vessels widen, and recanalization mechanisms fail. These and other vascular changes are now being considered as important factors contributing to dementia and cognitive decline in aging.

1.2 Cognitive and vascular changes in the aging brain

1.2.0 Vascular changes related to aging and dementia

A multitude of vascular properties must work together to meet the complex energy demands of the brain. Specifically, the gross angioarchitecture and microstructure of vessels optimizes the specialized delivery of specific nutrients in a regionally heterogeneous manner based on baseline need, while maintaining the ability to alter the pattern of perfusion with changing neural activity levels and metabolic demand. Moreover, vascular networks exhibit a capacity for plasticity to mitigate the consequences of those systems failing. Many of the core features of the vasculature that maintain optimal nervous system function change with age, however. There is now substantial evidence indicating that these changes compound to offset the balance of energy supply and demand, evoking some of the cognitive and behavioural deficits that characterize normal aging and dementia.

In humans, natural aging results in an increased risk for vascular disease and is accompanied by many macro and microvascular changes. These changes in humans include atherosclerosis (build up of plaque/debris around vessel walls), an increase in circulating adhesion molecules, loss of vascular tone and reactivity, microinfarcts and microbleeds, vascular amyloid deposition, thickening of the vascular basement membrane, increased collagen deposition in venous vessels, reduced metabolism, degeneration of pericytes in both function and number, reduced CBF, and a decline in vascular density (Hunziker et al., 1979; Merat et al., 2000; Richter et al., 2003; Zaletel et al., 2005; Stephan et al., 2009; Brown and Thore, 2011; Fabiani et al., 2014; Scioli et al., 2014; Bagi et al., 2018; Berthiaume et al., 2018). Rodent studies have replicated

many of these age-related changes and have further demonstrated: a) decreases in the partial pressure of oxygen in both vessels and brain tissue, b) more heterogeneous tissue oxygenation (including the presence of micro-pockets of hypoxic tissue), c) increases in capillary flow and RBC flux, d) greater heterogeneity in RBC speeds, e) a reduction in hematocrit and f) reduced angiogenic capacity in response to hypoxic challenge (Black et al., 1989; Park et al., 2007; Ungvari et al., 2013; Berthiaume et al., 2018; Moeini et al., 2018). Many of these changes (which are summarized in **Figure 1.4**) can lead to a reduction in the amount of oxygen and glucose delivered to the tissue, an inability to alter blood flow to meet transient increases in energy demand, BBB breakdown, and both an increased prevalence of and decreased capacity to respond to vascular insults (such as hypoxia).

Given the decline in vascular functionality, it comes as no surprise that vascular changes, such as those listed above, correlate with poor cognition and many are considered either risk factors or symptoms that contribute to various dementias (such as Alzheimer's disease, vascular dementia, and Parkinson's disease) (Buée et al., 1994; de la Torre, 2002; Zlokovic, 2005; Vermeer et al., 2007; Bell and Zlokovic, 2009; Stephan et al., 2009; Guan et al., 2013; Iadecola, 2013; Snyder et al., 2015; Nielsen et al., 2017; Tarantini et al., 2017). In fact, research in humans shows that vascular predictors are both the earliest and strongest predictors of Alzheimer's dementia (Iturria-Medina et al., 2016). This 2016 study showed that vascular abnormalities began to show up in most brain regions at earlier stages of disease progression than any other predictor of Alzheimer's, including amyloid deposition. Moreover, vascular decline also correlated more strongly with disease progression than any of the other markers (Iturria-

Medina et al., 2016). The vascular changes that happen in patients with Alzheimer's disease include declines in vascular density and CBF, the latter of which, in particular, has been strongly correlated with cognitive performance (Buée et al., 1994; Kisler et al., 2017a; Nielsen et al., 2017). One recent animal study, that we will return to in the next section, even showed an increase in memory performance when CBF was improved in a mouse model of Alzheimer's disease (Cruz-Hernández et al., 2019).

Figure 1.4. Summary of age-related cerebrovascular changes.

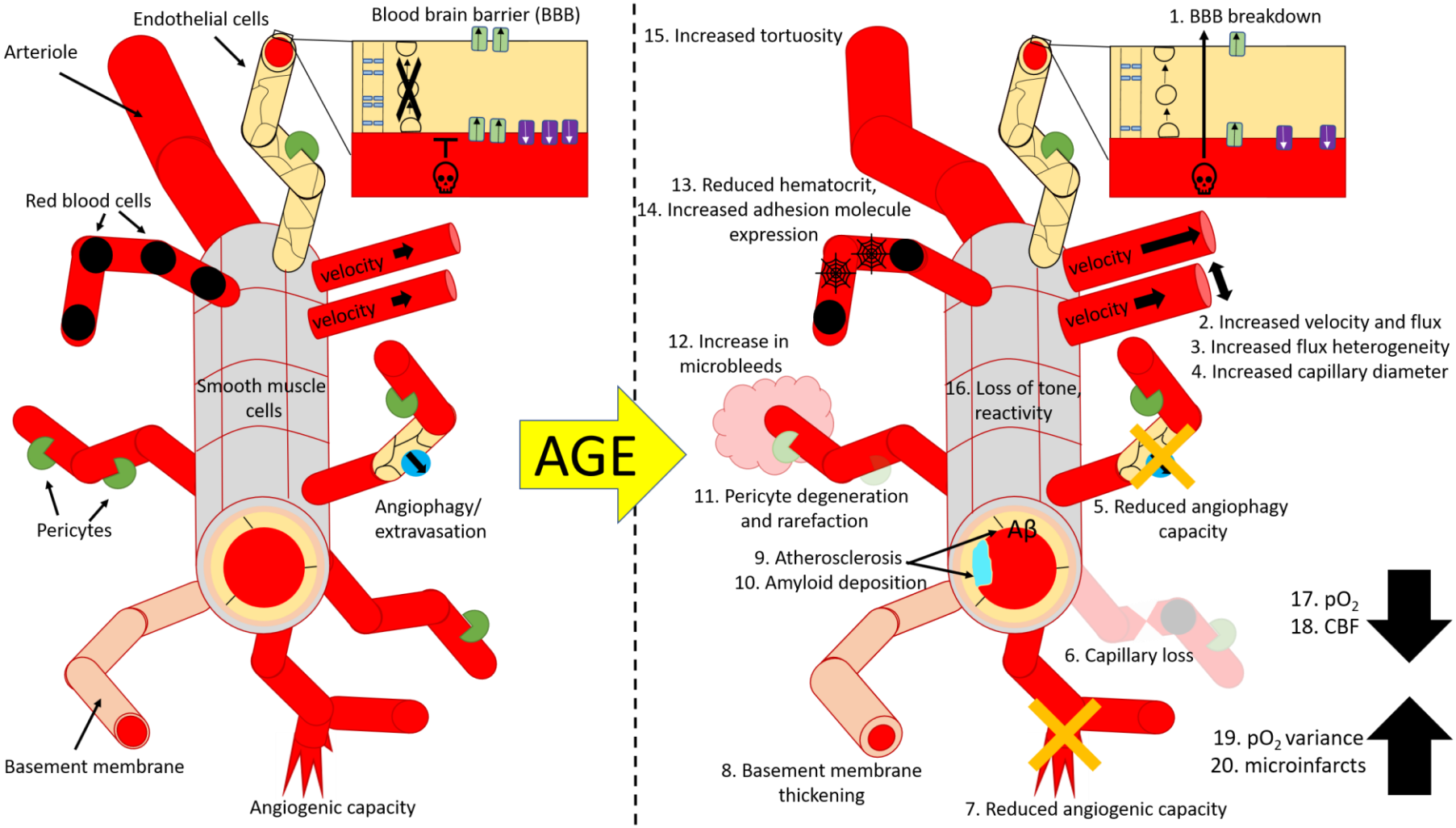

Figure 1.4. Summary of age-related cerebrovascular changes. Left panel shows vascular features in young subjects for reference comparing with age-related changes in the right panel. pO_2: partial pressure of oxygen. CBF: cerebral blood flow. Aβ: Amyloid beta.

1.2.1 On the merit of explaining regional differences in vascular decline

Understanding regional heterogeneity in vascular properties, as well as the spatial heterogeneity in the age-related changes of those elements, has not consistently been considered an important part of understanding age and disease-related processes. However, one region where this heterogeneity has started to be appreciated is in the white matter, and this consideration has proven fruitful in finding a contributing factor to the cognitive symptoms associated with aging and dementia. Cerebral white matter experiences many vascular changes with age, including vasodilator dysfunction, increased arteriolar tortuosity, microinfarction, and decline in CBF (Brown and Thore, 2011; Bagi et al., 2018). Moreover, imaging studies in humans show that white matter integrity is very important for maintaining cognitive function (Gunning-Dixon and Raz, 2000; Kennedy and Raz, 2009; Gold et al., 2010; Bennett and Madden, 2014). One study shows that white matter integrity in aged subjects correlates with better performance on tests to measure task-switching, episodic memory, working memory, processing speed, and inhibition (Kennedy and Raz, 2009). That study further demonstrates the importance of exploring regional differences in age-related decline as the researchers show that deficits in each cognitive faculty were inversely related to integrity in different parts of the white matter (Kennedy and Raz, 2009). We know that white matter may be particularly susceptible to hypoperfusion and ischemia due to being supplied by the distal branches of long penetrating arterioles from ACA-MCA watershed zones, with some white matter areas (like those above the ventricles) having limited collateral circulation from other sources (Brown and Thore, 2011). Perhaps further consideration of how the vasculature differs between brain regions will explain

how and why age-related changes in behaviour manifest. Further, this variety of study could identify other regions that may be particularly vulnerable to aging.

Age-related declines in CBF have been correlated with cognitive dysfunction and dementia, are accompanied by changes in metabolism (Leenders et al., 1990; Moeller et al., 1996), and have been widely reported in humans (Krejza et al., 1999; Shin et al., 2007), rats (Ohata et al., 1981), and monkeys (Noda et al., 2002). CBF also appears to decline in a region-specific manner (Hagstadius and Risberg, 1989; Leenders et al., 1990; Martin et al., 1991; Chen et al., 2011). Chen and colleagues (2011) used arterial spin labeling magnetic resonance imaging (ASL MRI) to demonstrate that, not only is CBF regionally heterogeneous in young people, but its decline also displays brain-region specificity. Specifically, they show that white matter and cortical areas show substantial declines in CBF, but indicate that many subcortical structures do not show a relationship between age and CBF (Chen et al., 2011). There could be functional implications of this regional heterogeneity in CBF decline given that many imaging studies in humans have shown that higher CBF correlates with increased performance on tasks measuring executive functioning, attention, and memory in healthy subjects (Leeuwis et al., 2018), patients with vascular disease (such as type 2 diabetes) (Bangen et al., 2018), and patients with dementia (Nielsen et al., 2017).

Since CBF has frequently been associated with cognitive performance, a topic of interest is to understand what factors contribute to its regionally heterogeneous decline. A recent study investigating a mouse model of Alzheimer's disease found that neutrophils occluded a portion (~1-2%) of cerebral capillaries, but that when the number of those obstructions was reduced (with a high concentration of an antibody initially

used to mark the neutrophils), they found an increase in CBF of approximately 15% that was accompanied by improvements in memory tasks, such as Novel Object Recognition (Cruz-Hernández et al., 2019). This study implies that the number of viable, flowing capillaries correlate with effective CBF. This makes reasonable sense in a hypothetical condition. Reducing the number of vessels in parallel increases the resistance in a branch of a fluid system, which reduces flow through that branch. Though adherent neutrophils may not contribute to the decline in CBF in healthy subjects (they reported fewer stalls in wild-type animals and the antibody did not change CBF) (Cruz-Hernández et al., 2019), the loss of capillary density might. In fact, regional capillary density has been previously shown to strongly correlate to regional CBF (Gjedde and Diemer, 1985). And further, hypoxia, which is thought to stimulate angiogenesis, has been shown to prevent cognitive dysfunction and capillary density reductions that usually occur in mice who have experienced whole brain radiation (Warrington et al., 2011, 2012, 2013). Thus, capillary density may be particularly important for CBF and for cognitive performance.

1.3 Determinants of capillary density: questions, hypotheses, and rationales

1.3.0 Literature review of reports on age-related microvascular density

Age-related changes in the density of capillaries in the brain, typified by the loss of vessels, has been widely reported in humans and multiple animal systems. I've constructed a comprehensive review of these studies in **Table 1** that immediately highlights several problems with the existing literature on age-related changes in vessel density. These concerns include a wide variety of reported changes in magnitude that is coincident with a general lack of consensus, reporting of relative changes in density based on protein expression, and sampling of many single areas in isolation. First, although the majority of studies report a decline in vascular density, there are a wide range of results reported. There are reports of ~50% declines in vascular density (Amenta et al., 1995a; Viboolvorakul and Patumraj, 2014), no change at all (Black et al., 1989), or even ~50% increases in vascular density (Villena et al., 2003). This variability appears to be compounded by the different metrics used to calculate vascular density. In the same study, it is possible for a group to report a ~5% decline and a ~35% decline in vascular density in the same area, depending on whether they report density based on vessel length or vessel number (Amenta et al., 1995a). Studies that report little change in vascular density may do so because they report metrics that are sensitive to concomitant changes in vascular diameter, such as fractional area or volume of vessels (Moeini et al., 2018).

Next, many measurements of vascular density are based on immunohistochemistry and therefore rely on protein expression that may change with age. For example, many of the older studies relied on alkaline phosphatase enzymatic reactions to visualize vessels, even though it is known that alkaline phosphatase chronically underestimates capillary density (Göbel et al., 1990). Therefore, groups generally report only relative changes over time rather than realistic vessel densities. It is also currently unknown whether vessel loss exhibits a homogeneous distribution in the brain, since there has yet to be a broad survey of vessel densities throughout the regions of the brain. Though many different brain regions have been sampled, each study uses different methodologies and metrics to measure vessel density, so the magnitudes of loss cannot be realistically compared between brain regions. Only 3 studies report vessel loss in a minimum of three different areas, and none report data in more than three. Furthermore, all of these three studies rely on various forms of immunohistochemistry, and only one has close to enough statistical power to compare the magnitude of vessel loss between areas (Amenta et al., 1995a; Ndubuizu et al., 2010; Murugesan et al., 2012). Finally, adding to all these concerns, only one study (out of all vessel loss studies) provided evidence for a mechanism to explain these observed age-related changes in microvascular density (Reeson et al., 2018). The shortcomings of this previous research combined with the reported region-specific decline in CBF prompted us to ask two major guiding research questions, each with specific hypotheses based on the literature I have reviewed to this point.

Table 2.0. Summary of previous research estimating vessel loss with aging.

Author	Animal	Area	Method	Age	months	metric	% change	% change / 12 months
(Hunziker et al., 1979)	Human	Precentral gyrus	Alkaline phosphatase	19-94 y/o (group means approx 32-90)	696	length	-2	0
(Hunziker et al., 1979)	Human	Precentral gyrus	Alkaline phosphatase	19-94 y/o (group means approx 32-90)	696	volume	1	0
(Meier-Ruge et al., 1980)	Human	Putamen	Alkaline phosphatase	19-94 y/o (group means approx 32-90)	696	length	60	1
(Meier-Ruge et al., 1980)	Human	Putamen	Alkaline phosphatase	19-94 y/o (group means approx 32-90)	696	volume	84	1.5
(Meier-Ruge et al., 1980)	Human	Cortex	Alkaline phosphatase	19-94 y/o (group means approx 32-90)	696	length	-4	-0.1
(Meier-Ruge et al., 1980)	Human	Cortex	Alkaline phosphatase	19-94 y/o (group means approx 32-90)	696	volume	-3	-0.1
(Bell and Ball, 1981)	Human	Hippocampus	Alkaline phosphatase	38-74 y/o	432	length	-16	-0.4
(Mann et al., 1986)	Human	Frontal cortex	Alkaline phosphatase	26-96 y/o	840	length	-46	-0.7
(Mann et al., 1986)	Human	Frontal cortex	Alkaline phosphatase	26-96 y/o	840	area	-35	-0.5
(Mann et al., 1986)	Human	Temporal cortex	Alkaline phosphatase	26-96 y/o	840	length	No change	0
(Mann et al., 1986)	Human	Temporal cortex	Alkaline phosphatase	26-96 y/o	840	area	No change	0
(Bell and Ball, 1990)	Human	Visual cortex	Alkaline phosphatase	31-79 y/o	576	length	-16	-0.3
(Abernethy et al., 1993)	Human	PVN hypothalamus	Alkaline phosphatase	30-85 y/o	660	length	-49	-0.9
(Abernethy et al., 1993)	Human	Supraoptic hypothalamus	Alkaline phosphatase	30-85 y/o	660	length	No change	0
(Buée et al., 1994)	Human	Cortex	Vascular HSPG	49-79 y/o	360	area	-28	-0.9
(Farkas et al., 2006)	Human	White matter	Hematoxylin-eosin staining	40-90y/o	600	length	No change	0
(Brown et al., 2007b)	Human	White matter	Alkaline phosphatase	57-90 y/o	396	area	-64	-1.9
(Brown et al., 2007b)	Human	Cortex	Alkaline phosphatase	57-90 y/o	396	area	-69	-2.1
(Burns et al., 1981)	Macaque	Frontal cortex	Microfil	10-20y/o	120	area	-22.2	-2.2
(Burns et al., 1981)	Macaque	Frontal cortex	Microfil	4-20y/o	192	area	-27.8	-1.7
(Sturrock, 1977)	Mouse	Indusium griseum					No change	
(Murugesan et al., 2012)	Mouse	Cortex	CD31	7-23 m/o	16	length	-19.3	-14.5
(Murugesan et al., 2012)	Mouse	White matter	CD31	7-23 m/o	16	length	-34.5	-25.9
(Murugesan et al., 2012)	Mouse	Hippocampus	CD31	7-23 m/o	16	length	-26.4	-19.8
(Moeini et al., 2018)	Mouse	S1 barrel cortex	Fluorescent plasma label	7.5-26 m/o	18.5	volume	-17	-11
(Reeson et al., 2018)	Mouse	S1 cortex	Evans Blue plasma label	3.5-16.5 m/o	13	number	-8	-7.4
(Klein and Michel, 1977)	Rat	Frontal and Occipital cortex	Windel's thionin	6-25 m/o	19	number	-21	-13.3
(Bär, 1978)	Rat	Occipital cortex		6-30 m/o	24		19	9.5
(Knox and Oliveira, 1980)	Rat	Cortex	Toluidine blue	4-23 m/o	19	number	-7.9	-5
(Burns et al., 1981)	Rat	Frontal cortex	Microfil	35-800 d/o	25.5	area	39	18.4
(Wilkinson et al., 1981)	Rat	Cortex	Latex and luconyl blue perfusion	13-120 w/o	27	number	10	4.4
(Hinds and McNelly, 1982)	Rat	Olfactory bulb	Toluidine blue	3-36 m/o	33	length	-15	-5.5
(Casey and Feldman, 1985)	Rat	Brainstem	Toluidine blue	3-33 m/o	30	volume	-27.4	-11
(Buchweitz-Milton and Weiss, 1987)	Rat	Cortex	Alkaline phosphatase, FITC dextran	9-30.5 m/o	21.5	length	-29.5	-16.5
(Hughes and Lantos, 1987)	Rat	Cortex	Toluidine blue	3-22.5 m/o	19.5	number	10	6.2
(Meier-Ruge and Schulz-Dazzi, 1987)	Rat	Parietal cortex	Alkaline phosphatase	12-36 m/o	24	volume	1	0.5
(Meier-Ruge and Schulz-Dazzi, 1987)	Rat	Parietal cortex	Alkaline phosphatase	12-36 m/o	24	length	-7.5	-3.8
(Black et al., 1989)	Rat	Visual cortex	Toluidine blue	12-22 m/o	10		No change	
(Jucker and Meier-Ruge, 1989; Jucker et al., 1990)	Rat	Hippocampus	Alkaline phosphatase	18-27.5 m/o	9.5	number	-21	-26.5
(Jucker and Meier-Ruge, 1989; Jucker et al., 1990)	Rat	Parietal cortex	Alkaline phosphatase	18-27.5 m/o	9.5	number	-26	-32.8
(Amenta et al., 1995a)	Rat	Frontal cortex	Alkaline phosphatase	12-24 m/o	12	number	-41.8	-41.8
(Amenta et al., 1995a)	Rat	Frontal cortex	Alkaline phosphatase	12-24 m/o	12	length	-30.1	-30.1
(Amenta et al., 1995a)	Rat	Occipital cortex	Alkaline phosphatase	12-24 m/o	12	number	-36.9	-36.9
(Amenta et al., 1995a)	Rat	Occipital cortex	Alkaline phosphatase	12-24 m/o	12	length	-5.6	-5.6
(Amenta et al., 1995a)	Rat	Hippocampus	Alkaline phosphatase	12-24 m/o	12	number	-48.7	-48.7
(Amenta et al., 1995a)	Rat	Hippocampus	Alkaline phosphatase	12-24 m/o	12	length	-25	-25
(Amenta et al., 1995b)	Rat	Frontal cortex	Alkaline phosphatase	12-27 m/o	15	number	-28.2	-22.6
(Amenta et al., 1995b)	Rat	Frontal cortex	Alkaline phosphatase	12-27 m/o	15	length	-11.6	-9.3
(Amenta et al., 1995b)	Rat	Occipital cortex	Alkaline phosphatase	12-27 m/o	15	number	-17.8	-14.2
(Amenta et al., 1995b)	Rat	Occipital cortex	Alkaline phosphatase	12-27 m/o	15	length	-12.2	-9.7
(Amenta et al., 1995b)	Rat	Ammons horn	Alkaline phosphatase	12-27 m/o	15	number	-26.5	-21.2
(Amenta et al., 1995b)	Rat	Ammons horn	Alkaline phosphatase	12-27 m/o	15	length	-14.7	-11.8
(Amenta et al., 1995b)	Rat	Dentate	Alkaline phosphatase	12-27 m/o	15	number	-19.4	-15.5
(Amenta et al., 1995b)	Rat	Dentate	Alkaline phosphatase	12-27 m/o	15	length	20.4	16.3
(Villena et al., 2003)	Rat	LGN	Toluidine blue	3-28 m/o	25	length	69.3	33.3
(Villena et al., 2003)	Rat	LGN	Toluidine blue	3-28 m/o	25	number	19.4	9.3
(Villena et al., 2003)	Rat	LGN	Toluidine blue	3-28 m/o	25	volume	36.4	17.5
(Villena et al., 2003)	Rat	LGN	Toluidine blue	3-28 m/o	25	area	29	13.9
(Villena et al., 2003)	Rat	LGN	Toluidine blue	18-28 m/o	10	length	-3.1	-3.7
(Villena et al., 2003)	Rat	LGN	Toluidine blue	18-28 m/o	10	number	-3.2	-3.8
(Villena et al., 2003)	Rat	LGN	Toluidine blue	18-28 m/o	10	volume	-6.3	-7.6
(Villena et al., 2003)	Rat	LGN	Toluidine blue	18-28 m/o	10	area	-4.7	-5.6
(Villar-Cheda et al., 2009)	Rat	Substantia Nigra	RECA1	4-14 m/o	10	number	-14	-16.8
(Villar-cheda et al., 2009)	Rat	Substantia Nigra	RECA1	4-24 m/o	20	number	-21	-12.6
(Ndubuizu et al., 2010)	Rat	Cortex	GLUT-1	3-24 m/o	21	number	-10.3	-5.9
(Ndubuizu et al., 2010)	Rat	Corpus Callosum	GLUT-1	3-24 m/o	21	number	-2.6	-1.5
(Ndubuizu et al., 2010)	Rat	Striatum	GLUT-1	3-24 m/o	21	number	2.8	1.6
(Ndubuizu et al., 2010)	Rat	Hippocampus	GLUT-1	3-24 m/o	21	number	-10.3	-5.9
(Shao et al., 2010)	Rat	White matter	Collagen 4	7-27 m/o	20	length	-18.6	-11.2
(Shao et al., 2010)	Rat	White matter	Collagen 4	7-27 m/o	20	volume	-23.5	-14.1
(Zhang et al., 2012)	Rat	Hippocampus	RECA1	5-34 m/o	29	length	-40	-16.6
(Desjardins et al., 2014)	Rat	S1 cortex	Fluorescent plasma label	3-24 m/o	21	number	-18.7	-10.7
(Desjardins et al., 2014)	Rat	S1 cortex	Fluorescent plasma label	3-24 m/o	21	volume	-20.6	-11.8
(Tang et al., 2016)	Rat	Cortex & Striatum	Lectin	3-24 m/o	21	number	-3.5	-2
(Tang et al., 2016)	Rat	Cortex & Striatum	GLUT-1	3-24 m/o	21	number	-10.6	-6.1
(Schager and CE Brown, current)	Mouse	Corpus Callosum	FITC Dextran Plasma Label	3.5-19.5 m/o	16	length	-26.8	-20.1
(Schager and CE Brown, current)	Mouse	Fimbria	FITC Dextran Plasma Label	3.5-19.5 m/o	16	length	-11.6	-8.7
(Schager and CE Brown, current)	Mouse	FrA	FITC Dextran Plasma Label	3.5-19.5 m/o	16	length	-7.8	-5.9
(Schager and CE Brown, current)	Mouse	GI/DI	FITC Dextran Plasma Label	3.5-19.5 m/o	16	length	-3.3	-2.5

(Schager and CE Brown, current)	Mouse	PRh/Ect	FITC Dextran Plasma Label	3.5-19.5 m/o	16	length	-16	-12
(Schager and CE Brown, current)	Mouse	M1/M2	FITC Dextran Plasma Label	3.5-19.5 m/o	16	length	-10	-7.5
(Schager and CE Brown, current)	Mouse	S1FL	FITC Dextran Plasma Label	3.5-19.5 m/o	16	length	-7.2	-5.4
(Schager and CE Brown, current)	Mouse	RS	FITC Dextran Plasma Label	3.5-19.5 m/o	16	length	-7.9	-5.9
(Schager and CE Brown, current)	Mouse	V1	FITC Dextran Plasma Label	3.5-19.5 m/o	16	length	-2.1	-1.6
(Schager and CE Brown, current)	Mouse	HPC	FITC Dextran Plasma Label	3.5-19.5 m/o	16	length	-9.9	-7.4
(Schager and CE Brown, current)	Mouse	STR	FITC Dextran Plasma Label	3.5-19.5 m/o	16	length	-4.6	-3.4
(Schager and CE Brown, current)	Mouse	Thalamus	FITC Dextran Plasma Label	3.5-19.5 m/o	16	length	-4.3	-3.2
(Schager and CE Brown, current)	Mouse	Hypothalamus	FITC Dextran Plasma Label	3.5-19.5 m/o	16	length	-11.1	-8.3
(Schager and CE Brown, current)	Mouse	LA	FITC Dextran Plasma Label	3.5-19.5 m/o	16	length	-0.1	-0.1
(Schager and CE Brown, current)	Mouse	SNR	FITC Dextran Plasma Label	3.5-19.5 m/o	16	length	-7.3	-5.5

Table 1.0. Summary of previous research estimating vessel loss with aging

Review of existing literature on microvascular loss, excluding studies that focused on arterioles or larger vessels. Information subject species, brain region, method of vascular labeling, age, measurement metric, and time-adjusted magnitude of change in vessel density. Negative values indicate vessel loss. Some values are approximations based on interpretations of figures.

1.3.1 Research Question #1: Does microvascular loss occur in a regionally heterogeneous manner in the brain?

Hypothesis 1: Microvascular loss is greatest in the white matter and areas that experience a decline in CBF with age.

Rationale 1: As outlined above, I have identified a possible relationship between CBF and vascular density. If a drop in vascular density influences CBF, it would follow that areas that experience a decline in cerebral blood flow, specifically cortical and white matter areas from the study by Chen and colleagues (2011), would also present with a decline in vascular density. I also identified that the white matter is highly susceptible to vascular insults with natural aging and in disease. If declines in capillary density are either a risk factor for or a result of these vascular insults, then it would follow that the white matter would display a decline in vascular density. It is of note that both lines of reasoning used to develop this hypothesis would predict a decline in the capillary density of the white matter.

1.3.2 Research Question #2: What factors determine microvascular density changes with age?

Research Question 2.1: Does the rate of microvascular obstruction differ between brain regions and can it predict regional patterns of microvascular loss?

Hypothesis 2.1: There is a strong positive correlation between areas that experience many long-lasting microvascular obstructions and areas that experience a large magnitude of microvascular loss.

Rationale 2.1: Above, I referred to a study by Reeson and colleagues (2018) that demonstrated that in somatosensory cortex, ~30% of long-lasting capillary obstructions precipitate pruning events that are not compensated for by angiogenic sprouting (Reeson et al., 2018). These events occur at a frequency that, when modeled in a hypothetical population of capillaries, closely predicts the magnitude of capillary loss seen in an experimental group of animals. If pruning rates for obstructed capillaries are the same in the rest of the brain as they are in somatosensory cortex, and no areas display compensatory angiogenic sprouting, then regional differences in capillary loss should be explained by varying regional susceptibilities to microvascular obstruction (which we determined using fluorescent microspheres to model capillary obstructions, as was done by Reeson et al. (2018)).

Research Question 2.2: If microvascular obstruction rates do not predict microvascular loss, are there differences in pruning rates, recanalization rates, angiophagy, or compensatory angiogenesis that could explain why obstruction rates are not sufficient to predict microvascular loss?

Hypothesis 2.2: Greater rates of angiophagy are associated with areas that have obstruction rates that predict greater-than-observed magnitudes of vessel loss.

Rationale 2.2: In Reeson and colleagues' 2018 study, it was reported that angiophagy occurred very rarely (~2% of events where fluorescent microspheres were recanalized) in the somatosensory cortex and that approximately half of the vessels that were pruned following obstruction were recanalized first. If the relationship between obstruction rate, determined using fluorescent microspheres, and capillary loss is not strong, it may be because of a combination of any of the following possibilities outlined in **Figure 1.5**:

1. Angiophagy occurs at a greater frequency in some areas, leaving a microsphere in the tissue without pruning a capillary,

2. Pruning rates following recanalization differ between areas, leaving more pruning events in the absence of microspheres in some areas,

3. Some areas require more time to recanalize than others and still experience a substantial number of recanalization events even after 3 days without vessel pruning taking place,

4. Some areas experience angiogenesis that compensates for vascular pruning,

5. Obstruction, recanalization, pruning, or angiogenesis have rates that change over time in a region-dependent manner.

Given that angiophagy is common in arterioles (Lam et al., 2010; Grutzendler et al., 2014; van der Wijk et al., 2019), and that we discovered one outlier area that experienced many obstructions but only brain average vessel loss, I hypothesized that some areas, including that outlier, might have higher rates of angiophagy than other areas.

Figure 1.5. Alternative explanations in histological assessment of microspheres.

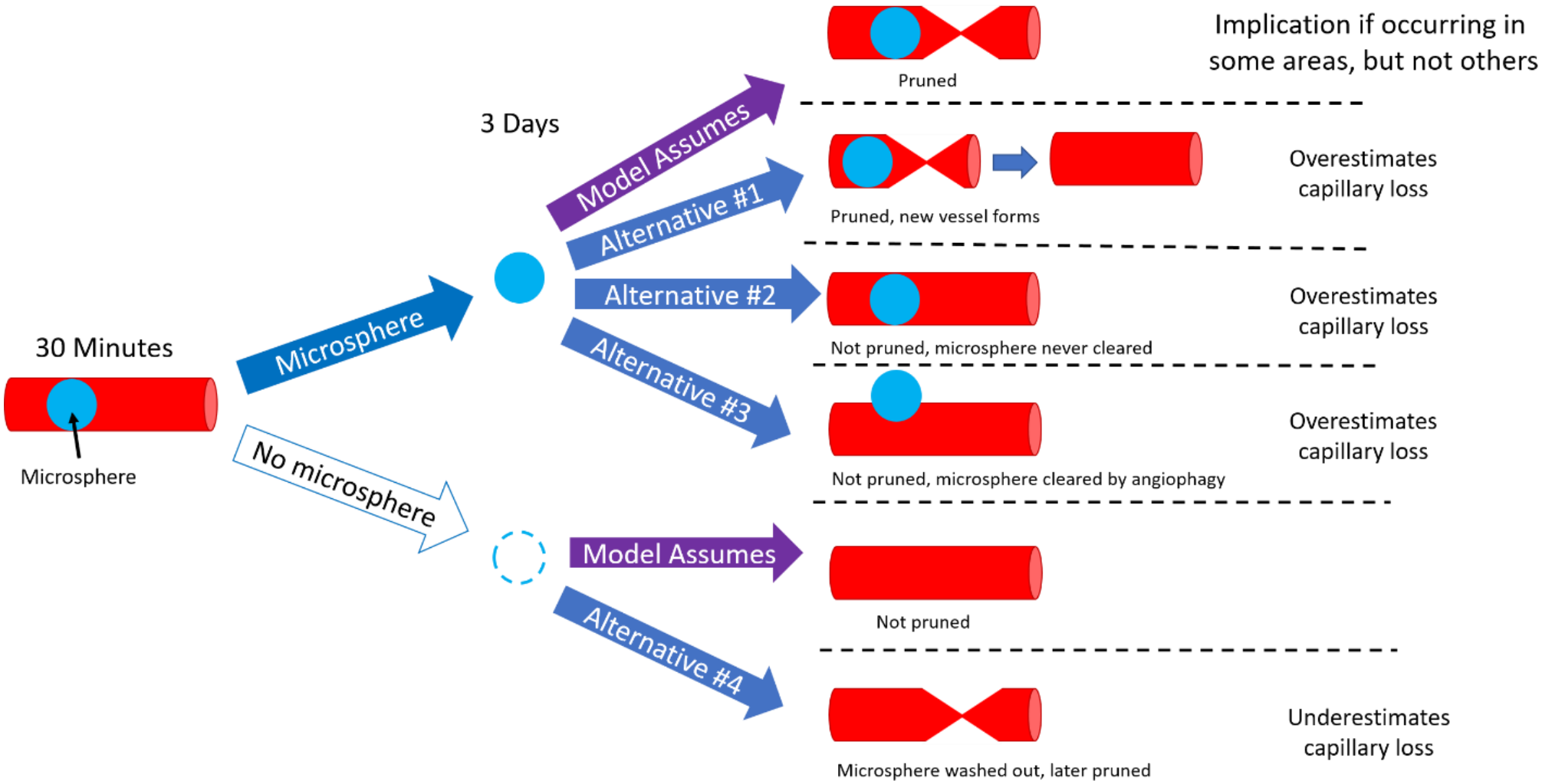

Figure 1.5. Alternative explanations in histological assessment of microspheres. We assume that a microsphere still in the brain tissue 3-days after injection indicates that a pruning event has taken place. However, it is also possible that another vessel was grown after pruning (Alternative #1). Or, it's possible that no pruning event took place because the microsphere was never cleared (or cleared after 3-days, Alternative #2), or extravasated (Alternative #3). Similarly, we assume that no microsphere indicates that no pruning event has taken place. However, a portion of capillaries are pruned following recanalization (Alternative #4). Violation of these assumptions does not invalidate the microsphere model as long as the rates of each are similar across all brain regions. However, if any of these alternatives are more prevalent in a certain area, the microsphere model will either overestimate (when microsphere remains but no vessel loss occurs) or underestimate (when vessel loss occurs despite recanalization) the magnitude of microvascular loss in that area.

2. Chapter 1: Susceptibility to capillary plugging can predict brain region specific vessel loss with aging

This chapter consists of a modified version of a manuscript published in the Journal of Cerebral Blood Flow and Metabolism in January 2020 (Schager and Brown, 2020):

> **Schager B**, Brown CE (2020) **Susceptibility to capillary plugging can predict brain region specific vessel loss with aging.** J Cereb Blood Flow Metab. DOI: 0271678X19895245.

B.S. and C.E.B conceived the study and wrote the manuscript. B.S. performed experiments and analyzed data.

2.0 Abstract

Vessel loss in the aging brain is commonly reported, yet important questions remain concerning whether there are regional vulnerabilities and what mechanisms could account for these regional differences, if they exist. Here we imaged and quantified vessel length, tortuosity and width in 15 brain regions in young adult and aged mice. Our data indicate that vessel loss was most pronounced in white matter followed by cortical, then subcortical gray matter regions, while some regions (visual cortex, amygdala, insular cortex) showed little decline with aging. Regions supplied by the anterior cerebral artery were more vulnerable to loss than those supplied by middle or posterior cerebral arteries. Vessel width and tortuosity generally increased with age but neither correlated strongly with regional vessel loss. Since capillaries are naturally prone to plugging and prolonged obstructions often lead to vessel pruning, we hypothesized that regional susceptibilities to plugging could help predict vessel loss. By mapping the distribution of microsphere-induced capillary obstructions, we discovered that regions with a higher density of persistent obstructions were more likely to show vessel loss with aging and vice versa. These findings indicate that age-related vessel loss is region specific and can be explained, at least partially, by regional susceptibilities to capillary plugging.

2.1 Introduction

Without substantial local energy stores, the brain demands a constant supply of oxygen and nutrients (Attwell and Laughlin, 2001; Peters et al., 2004). In order to meet this demand the brain is densely supplied with capillaries which are narrow, low-pressure, high surface area vessels that comprise the majority of cerebral vascular length and are always in close proximity (~13-18 μm) to neurons and glia (Zhang et al., 2005; Tsai et al., 2009; Blinder et al., 2013; Gould et al., 2017). As such, it is not surprising that age and disease-related vascular changes that result in reduced capillary number and perfusion correlate with and contribute to cognitive impairment and dementia, including Alzheimer's Disease and Vascular Dementia (Ruitenberg et al., 2005; Iadecola, 2013; Østergaard et al., 2015; Joo et al., 2017; Nielsen et al., 2017). Indeed, a recent study revealed a direct link between capillary blood flow and cognition by showing that unplugging cortical capillaries could improve blood flow and memory in a mouse model of Alzheimer's disease (Cruz-Hernández et al., 2019).

Although it is well appreciated that capillary networks are important for maintaining brain function with aging, there still exists debate over the extent to which vascular density changes over the lifetime. For example, several rodent studies indicate there is profound vessel loss within a few regions over 1-2 years of age, whereas other studies indicate no change at all (Riddle et al., 2003; Ndubuizu et al., 2010; Brown and Thore, 2011; Xu et al., 2017). Further, to our knowledge no aging study has systematically surveyed vascular changes across a multitude of brain regions. Given long standing evidence that certain brain regions are particularly vulnerable to functional decline with aging, such as white matter tracts, frontal cortex and hippocampus (Gunning-Dixon and

Raz, 2000; Raz et al., 2005; Alexander et al., 2012), comparing vessel loss across many different regions within the same animals could provide valuable comparative data. In addition, cerebral blood flow (CBF) declines in a regionally heterogeneous manner with age (Chen et al., 2011), and may be partially determined by the density of flowing capillaries (Gjedde and Diemer, 1985; Cruz-Hernández et al., 2019). As such, we hypothesize that microvascular loss is greatest in the white matter and areas that experience a decline in CBF with age. Revealing such differences will be useful for future “omic” research that seeks to understand regional diversity in aging processes at a molecular level (Badhwar et al., 2017; Mattson and Arumugam, 2018).

Another unresolved issue in the aging literature concerns the mechanisms that account for age-related vessel loss. While this is a multifactorial problem involving the relative balance between vessel rarefaction and perhaps sprouting, it is likely that the capillary’s inherent susceptibility to clogging, due to adherent white blood cells or debris circulating in the blood (cholesterol, fibrin), could be an important factor. Recently our group and others demonstrated that a small fraction of cortical capillaries experience short and long-lasting obstructions, even in healthy animals (Santisakultarm et al., 2014; Erdener et al., 2017; Reeson et al., 2018). Of note, about ~30% of these persistent obstructions led to vessel pruning with little evidence of compensatory sprouting (Reeson et al., 2018). Using this information, we were able to approximate vessel loss with aging that closely matched our experimentally derived estimate (Reeson et al., 2018). However, one major limitation of our previous study was that only one brain region was sampled (primary somatosensory cortex) and therefore it is unknown if there are brain region specific differences in the susceptibility for capillaries to become

obstructed, and perhaps experience greater vessel loss with age. Specifically, we hypothesize that there is a strong positive correlation between areas that experience many long-lasting microvascular obstructions and areas that experience a large magnitude of microvascular loss.

Here, we attempt to reconcile some of these discrepancies in the aging literature by performing a broad survey of vascular changes in length, tortuosity and width in 15 different brain regions, including differences that may arise between different classes of brain matter (white vs gray; cortical vs subcortical) or perfusion territory. In order to directly label all patent vessels, we intravenously injected a fluorescent dye *in vivo* and then developed an automated approach for detecting and analysing fluorescently labelled vessels in *post-mortem* tissue sections. Furthermore, to help explain regional differences in vessel loss, we induced capillary obstructions with fluorescent microspheres in adult mice and surveyed capillary obstruction rates in each brain region. Our experiments reveal considerable regional heterogeneity in vessel loss with aging that varies based on tissue class and perfusion territory. Further, we find a significant correlation between a specific brain region's susceptibility to capillary plugging and vessel loss with aging. Collectively, these findings suggest that vascular networks within certain brain regions may be more vulnerable to the deleterious effects of aging.

2.2 Methods

2.2.0 Animals.

In order to optimize sampling from our animal colony for the assessment of vascular density with aging, we used young adult (3-5.5-month-old, mean=3.5, male: n=20, female: n=5) and aged (16.5-22-month-old, mean=19.3, male: n=40) mice. Since we had very few aged female mice in our colony, we could not make meaningful sex-based comparisons in our study. The mice were derived from 3 different strains: a) C57BL/6J (young adult: n=36, aged: n=9), b) *Tek*-GFP (young adult: n=4, aged: n=4) (The Jackson Laboratory, 003658), and c) *Tek*-CreER^{T2} X *Kdr*$^{+/fl}$ (aged: n=12) [*Tek*-CreER^{T2} line(Forde et al., 2002) (EMMA 00715) bred with *Kdr*$^{fl/fl}$ line (Hooper et al., 2009)] strains. from C57BL/6J (young adult: n=36, aged: n=9), *Tek*-GFP (young adult: n=4, aged: n=4) (The Jackson Laboratory, 003658), and *Tek*-CreER^{T2} X *Kdr*$^{+/fl}$ (aged: n=12) [*Tek*-CreER^{T2} line (Forde et al., 2002) (EMMA 00715) bred with *Kdr*$^{fl/fl}$ line (Hooper et al., 2009)] strains. Statistical comparisons revealed no difference in capillary density between aged C57BL/6J mice and *Tek*-CreER^{T2} X *Kdr*$^{+/fl}$ mice (Unpaired with Welch's correction for unequal variances $t_{(9.781)}$=0.8246, p=0.4293), therefore data from these two strains were pooled. The *Tek*-GFP aged animals were strain-matched with an equal number of young and aged *Tek*-GFP mice. Since an age-by-strain two-way ANOVA revealed no significant age-strain interaction (2-way ANOVA interaction $F_{(1,65)}$=0.1673, p=0.6838), *Tek*-GFP mice were also pooled with the rest of the mice in both young and aged groups. All mice were housed under a 12-hour light/dark cycle with *ad libitum* access to water and standard laboratory diet. All experiments were conducted according to the guidelines set by the Canadian Council of Animal Care and

approved by the University of Victoria Animal Care Committee (protocol 2016-016). Reporting of this work complies with ARRIVE guidelines. Animal training certificate: #17-020-AC.

2.2.1 Tissue preparation, imaging and vessel analysis.

For vessel density quantification, lysine fixable FITC dextran (100µL; 2% w/v in 0.9% saline; ThermoFisher, molecular weight 40kDa, D1845) was intravenously injected and left to circulate for 8min prior to decapitation. The brain was extracted, bisected along the midline and fixed in 4% paraformaldehyde (PFA) in 0.1M phosphate buffered saline (PBS) overnight at 4°C before being transferred to 0.1M PBS. Brains were sectioned in the coronal plane at 50µm thick using a Leica vibratome (T1000). Every 6th section was mounted on a gel-coated slide, and cover-slipped with Fluoromount G (ThermoFisher, 00-4958-02). FITC labeled vessels in the brain were imaged using a 488nm laser on an Olympus confocal microscope with a 10x objective (NA 0.40). Since aging brains can exhibit autofluorescence in extra-vascular spaces which needs to be accounted for, we excited samples with a 561nm laser and collected light using a Texas Red emitter filter (575-675nm). Confocal image stacks were collected in 4µm z-steps at a pixel resolution of 1.242µm/pixel. Two to three image stacks for each of the 15 brain regions sampled were captured in each animal within the coloured boundaries outlined in **Figure 2.1A**. Care was taken to ensure sampling at rostro-caudal levels was comparable between groups.

Images were analyzed using a custom-built macro for FIJI-ImageJ (version 1.52e). First, the macro worked by creating a maximal intensity image projection of 8 images from each stack in both green (FITC-vessel signal) and red channels

(autofluorescent background signal). Autofluorescent signal was corrected for by subtracting images in the red channel from the green channel (**Fig. 2.0A**). In order to optimize the automated detection of vessel segments in the image, we used a WEKA Trainable Segmentation machine learning plugin from ImageJ and trained our macro using 20 separate images with user defined vessel segments (Arganda-Carreras et al., 2017). Once the WEKA Trainable Segmentation plugin successfully differentiated fluorescent signal in vessels from background (see yellow and pink outline in **Fig. 2.0A**), images were segmented and then skeletonized. In order to correct for small gaps in connected capillaries (caused by dips in fluorescent plasma signal within the vessel), capillary end segments were connected if they were within 12µm of each other and within a linear slope of 60° on either side of the fitted straight-line segment. A slope of 60° was determined empirically as it did not result in false positive connections given that connected capillaries do not often change direction by >60 degrees in a 12µm segment of vessel. Dependent variables that were measured included total vascular length (sum of length in all 2-3 images divided by sum of volume in all 2-3 images), mean vessel diameter (total area of dye/vascular length averaged across 2-3 images), and median tortuosity (arc-chord ratio, sum of all arc/branch lengths divided by sum of all chord lengths in all 2-3 images). Since signal segmentation tends to overestimate vessel area, which was used to generate width measurements, we needed to calculate a transforming factor. This was done by measuring the full width at half maximum (FWHM) diameter of randomly selected vessels (9-11 vessels in 5 animals) in both the raw maximum projection and the segmented image. Segmented image-derived diameters were calibrated by dividing by the transforming factor of 2.056, the average

ratio between diameter in the segmented image to diameter in the raw image. Reported values for Tissue Class and Arterial Supply are based on the average of all the mean values for each area that falls in that classification. Area classifications are stated in **Table 2.0**.

To validate our automated analysis, estimates of vessel density and tortuosity generated from our custom macro were compared to ground truth, user defined estimates generated by an independent and blinded observer. User-measured vessel length was plotted against macro-generated length and linear regression was performed (**Fig. 2.0B**). The equation of the regression line was used to transform the vascular length measurements generated by the macro (**Fig. 2.0B,C**). Similarly, tortuosity (measured as arc-chord ratio, **Fig.2.0D**) from user-drawn images was plotted against macro-generated tortuosity (**Fig. 2.0E,F**). To ensure that changes in tortuosity could not arise from changes in vessel diameter, the difference between the hand-drawn and macro-generated tortuosity was plotted against the mean capillary diameter in each image and regression was performed, showing no relationship between the variables (**Fig. 2.0G**). Additionally, to determine whether tortuosity changes could be an artifact of increasing diameter, we modeled a capillary segment with a chord length of 60 microns and recorded the measured tortuosity as both diameter and vector tortuosity increased in two conditions: 1. With relatively few resolution constraints (10 pixels/µm resolution, **Fig. 2.0H left panel**), and 2. With the resolution used in our imaging (0.805pixels/µm, **Fig. 2.0H right panel**). For each level of vector tortuosity, we plotted the % difference from the vector tortuosity (tortuosity of the a line with a width of 1 pixel in the 10 pixels/µm condition) for each tortuosity measured from the vessel segment with a vessel

diameter increasing from 3.5µm to 10µm in 0.1µm increments, determined the strength of the relationship and slope of the best-fit line of this relationship, and plotted the slope and r^2 for each level of tortuosity. No relationship was observed between diameter and tortuosity at tortuosity values observed in our images in either resolution condition.

Some confocal image stacks could not be properly analyzed by our automated program due to uneven signal across the specimen (e.g. caused by poor sectioning). Therefore, out of 3,022 image stacks collected, 39 were identified as an outlier (1.29% of total) by the Repeated Grubbs Test and excluded from the analysis.

Analysis of specific brain regions was restricted based on a user-defined region of interest (ROI) that excluded vessels >20µm diameter. We should note that larger vessels (8-20µm diameter) were included in the analysis; however, a random sample of images showed that vessels >8µm diameter accounted for approximately just 4±1.5% (mean±SD) of the total vascular length (n=5). Given this information, age-related changes in vascular structure are overwhelmingly represented (~96%) by changes at the capillary level.

Pockets of vessel sparse sub-regions were quantified using a custom-built macro for FIJI that subdivided image skeletons into ROIs created from the intersection of 211x211µm squares (44,550µm^2) and the ROI drawn for the image, and reported local vascular density (m/mm^3) for subsections larger than 1/3 the area of a full-size square. The fraction of subsections with less than 50% of the mean vascular density (for young adult mice) for that specific brain region were reported. To try to explain the large magnitude of microvascular loss in the corpus callosum, subsections were subsequently classified as either ventral (>70 µm of ROI perimeter shared with ventral

border of the striatum or lateral ventricle), or dorsal (<70 μm of ROI perimeter shared with ventral border). The difference in the proportion of low-density subsections (between the ventral areas and dorsal areas) was compared in young adult and aged animals. Further, the vessel density for each subregion (ventral vs. dorsal) was quantified as the average of the densities for all subsection ROIs in each class for each animal. Vessel densities for aged animals were normalized to the young adult mean to generate estimates of vessel loss for ventral and dorsal areas of corpus callosum in aged animals, which were subsequently compared.

To test the hypothesis that structural changes in cortical or callosal thickness (or by proxy volume) affect vessel density, we plotted cortical (and callosal) thickness against cortical (and callosal) vascular density in both age groups, with the logic that if volume changes were affecting vascular density, animals with lower area thicknesses would show some kind of trend in density. To further probe this hypothesis, we plotted the magnitude of the change in thickness against the change in vessel density for each area that we obtained a thickness measurement for, and then performed linear regression. No relationships were found.

We also tested the hypothesis that tortuosity or diameter in young-adult animals, or the age-related changes in diameter or tortuosity, would relate to vascular loss (perhaps smaller or more tortuous vessels are more likely to be lost, perhaps areas that lose more vessels do so because they are more likely to lose their tortuous vessels, or perhaps diameter or tortuosity increases to compensate for the regional loss in vessels) by plotting vessel loss for each area against the young-adult values or the age-related changes for each area, and then performing linear regression.

Figure 2.0. Validation of automated approach for analyzing vessels.

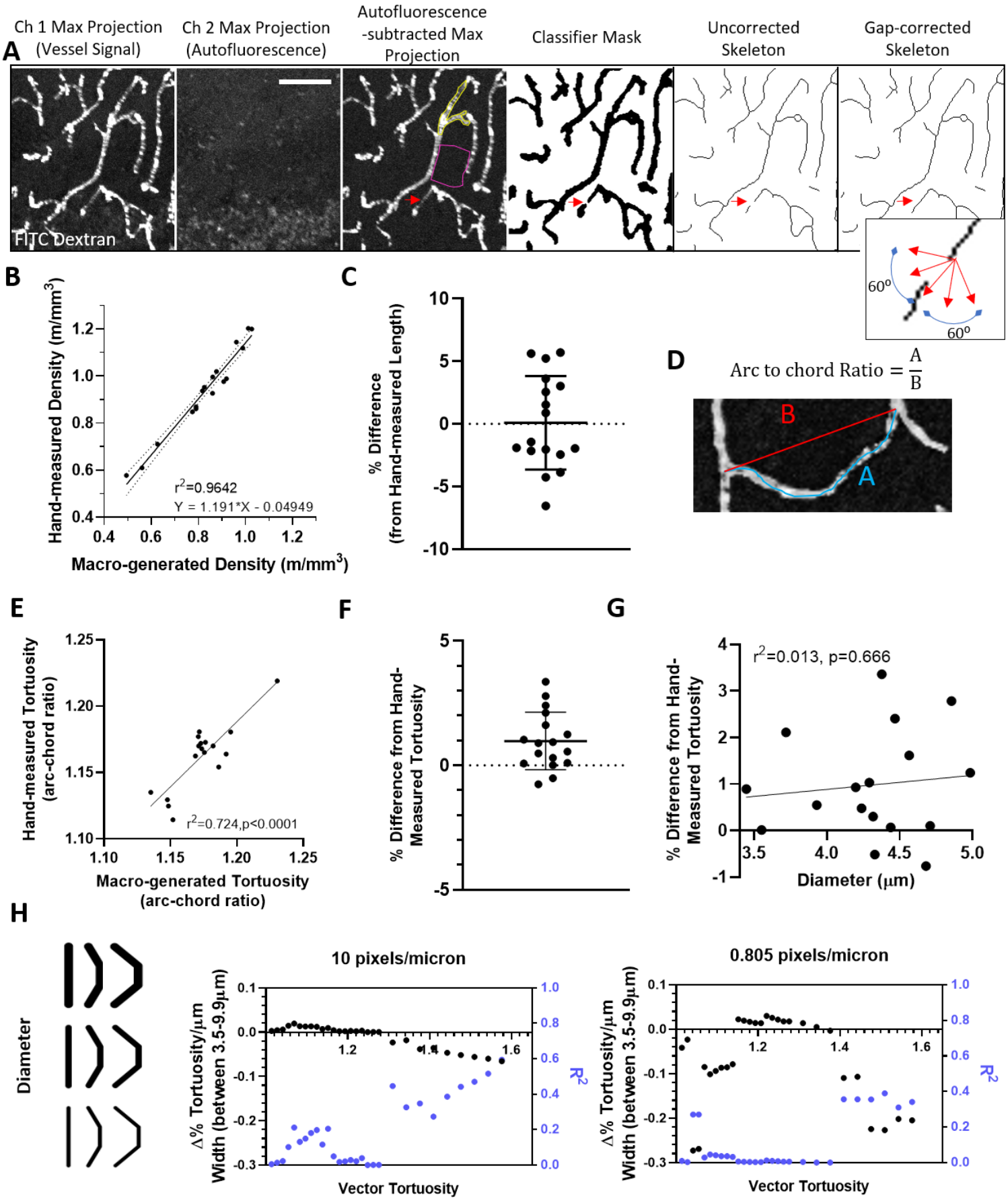

Figure 2.0. Validation of automated approach for analyzing vessels. (**A**) Confocal image stacks from channel 1 (FITC labelled vessels) and 2 (tissue autofluorescence) were first maximally projected with autofluorescent signal subtracted from the original image. Using a supervised learning plugin to segment fluorescent signal from background (signal outlines in yellow with background in pink), the image was skeletonized. Gaps in vessel signal (red arrows) were corrected if capillary segments were within 12μm of each other and within a linear slope of 60° on either side of the fitted straight-line segment (see inset). Scale bar = 50μm. (**B**) Vessel lengths for each image were estimated from the automated macro and then plotted relative to lengths generated from a blind observer. Note the extremely tight relationship (r^2=0.964) between automated and observer defined estimates. (**C**) Difference in lengths estimated by the two approaches after translation of macro-generated values (mean ± S.D.). (**D**) Image illustrating arc-chord ratio, a measurement of tortuosity. (**E**) Tortuosity measurements for each image (n=17) were estimated from the automated macro and then plotted relative to those generated from a blind observer. (**F**) Difference in tortuosity estimated by the two approaches (mean ± S.D.). (**G**) Regression analysis of mean vessel diameter generated for the 17 images plotted against the difference in tortuosity generated by the two approaches. This analysis shows that vessel diameter does not influence the macro-generated estimate of tortuosity. (**H**) Relationship between increases in vessel width and corresponding measured changes in tortuosity plotted against the vector tortuosity of the model capillary. Left panel show a cartoon of the 60μm model capillary increasing in both width and tortuosity. For each vector tortuosity (every column in the cartoon) tortuosity of the capillary was measured at diameters

increasing from 3.5µm to 10µm in 0.1µm increments. The slope (and the strength) of the linear relationship between the measured tortuosity and the vessel diameter was plotted against every vector tortuosity modelled in the middle and right panels. The middle panel shows this relationship in a very high-resolution scenario, while the right panel displays the relationship at the imaging resolution that we used.

Figure 2.1. Sampling guide and representative images of the vasculature across different brain regions in young adult and aged mice.

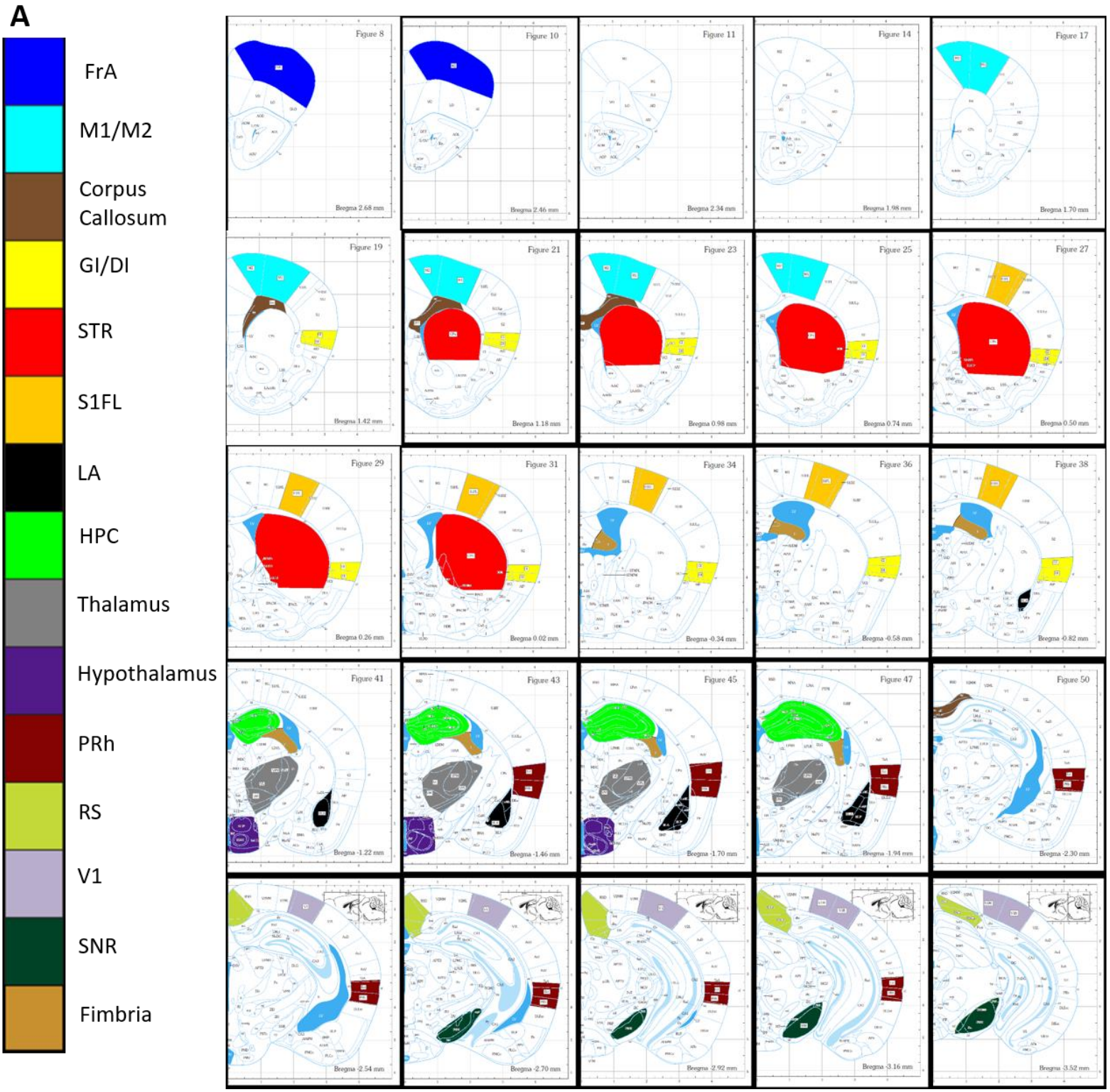

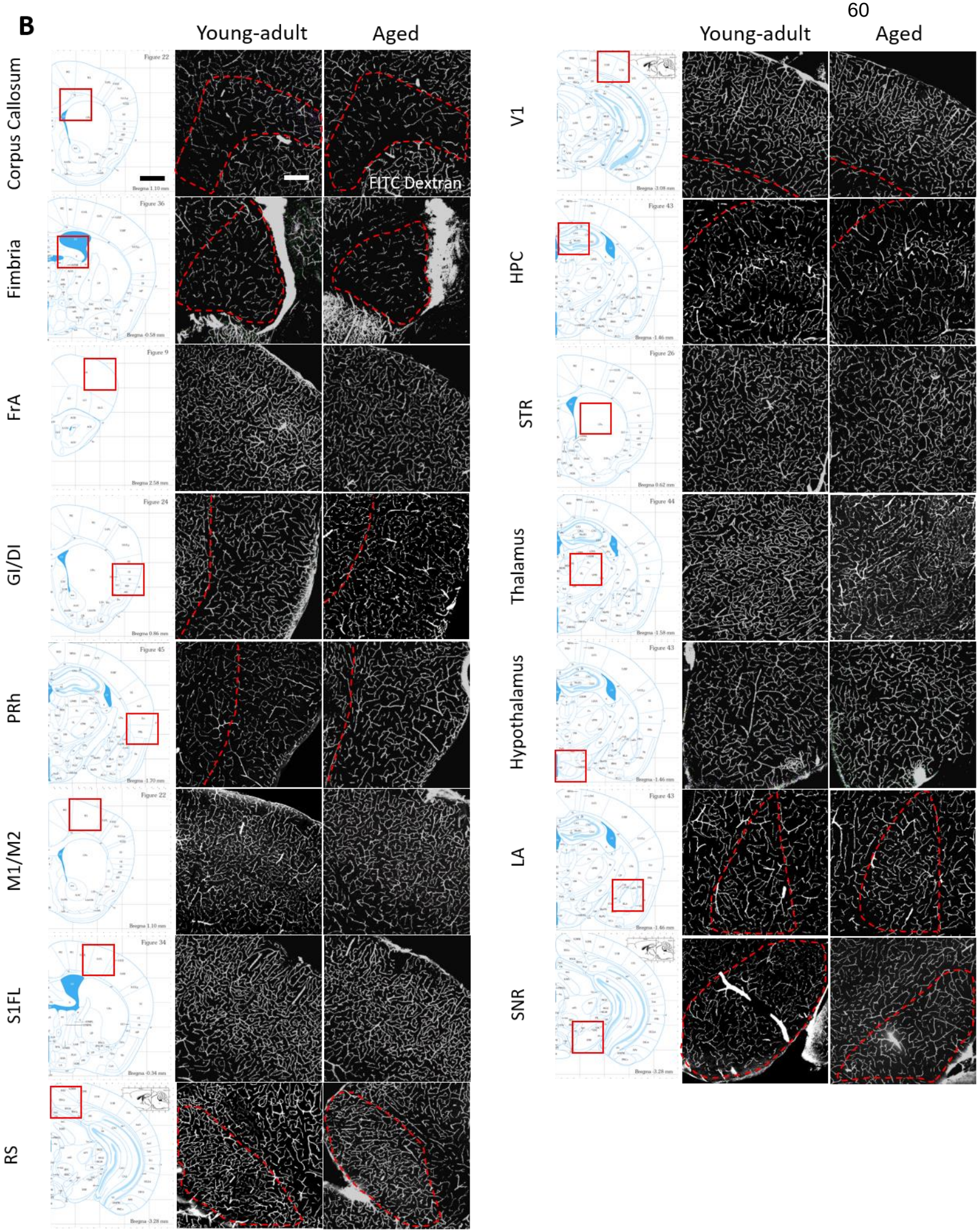
B
Young-adult
Aged
Young-adult
Aged
Corpus Callosum
Fimbria
FrA
GI/DI
PRh
M1/M2
S1FL
RS
V1
HPC
STR
Thalamus
Hypothalamus
LA
SNR
FITC Dextran

Figure 2.1. Sampling guide and representative images of the vasculature across different brain regions in young adult and aged mice. (**A**) Figure describes stereotaxic levels and bounds of sampling locations for each brain area. These bounds guided ROI locations for each area in microsphere analysis and determined bounds and possible stereotaxic levels for confocal microscopy of vascular density. (**B**) The location of each brain region analyzed is illustrated by the stereotaxic atlas image shown in the left pane. On the right are confocal image projections showing FITC labelled vessels in young adult (3-5.5-month-old) and aged mice (16.5-22-month-old). FrA: frontal association cortex; GI/DI: granular/dysgranular insular cortex; PRh/Ect: peri-rhinal cortex/Ecto-rhinal; M1/M2: primary/secondary motor cortex; S1FL: primary forelimb somatosensory cortex; RS: retrosplenial cortex; V1: primary visual cortex; HPC: hippocampus; STR: striatum; LA: lateral amygdaloid nucleus; SNR: substantia nigra reticulate. Image contrast was adjusted for the sake of clarity. Scale bar = 200μm.

Table 2.0. Summary of statistical comparisons between young adult and aged animals.

Young adult vs. Aged Comparisons					Density				Tortuosity				Diameter				Low Density Subsections				(Cortical) Thickness			
Abbreviation	Full name	Tissue Type	Arterial Territory	Territory Reference	Adjusted P	t	DF	% Change (Young adult-aged)	Adjusted P	t	DF	% Change (Young adult-aged)	Adjusted P	t	DF	% Change (Young adult-aged)	Adjusted P	t	DF	% Change (Young adult-aged)	Adjusted P	t	DF	% Change (Young adult-aged)
C. Callosum	Corpus Callosum	White matter	ACA	Images from (Endepols et	<0.0001	7.194	48.8	-26.83	0.4899	2.071	47.31	-0.68552	0.9995	0.852	50.02	1.444328	0.0002	4.844	55.44	126.6047	0.5714	1.612	44.87	6.885645
Fimbria	Fimbria	White matter	ACA	(Thomas et al., 2011)	0.0826	2.874	55.59	-11.63	0.8631	1.563	51.68	-0.59473	0.0008	4.427	48.23	7.930941	0.9757	1.244	49.64	30.28617				
FrA	Frontal Association Cortex	Cortical	ACA	Images from (Endepols et	0.0759	2.907	54.82	-7.824	0.0432	3.131	48.9	0.600343	0.6291	1.889	56.83	2.54152	0.9999	0.763	53.11	-36.7971				
GI/DI	Insular Cortex	Cortical	MCA	Images from (Rousselet et	0.9087	1.47	53.4	-3.289	0.2569	2.409	51.41	0.512821	0.0019	4.131	53.39	5.590513	>0.9999	0.0999	53.96	3.795893	0.002	3.856	58.62	-5.72391
PRh/Ect	Perirhinal/Ectorhinal Cortex	Cortical	MCA	Images from (Rousselet et	<0.0001	5.976	52.11	-16.04	0.7094	1.793	49	0.426621	0.0007	4.652	35.87	7.80759	0.591	1.944	47.09	53.73953	0.0014	3.978	58.5	-6.07073
M1/M2	Primary/Secondary Motor Cortex	Cortical	ACA	Images from (Endepols et	<0.0001	5.967	54.77	-10.01	0.1429	2.669	49.99	0.599829	0.1572	2.638	45.92	3.51972	0.8716	1.55	46.39	80.94824	0.0078	3.429	58.4	-5.62891
S1FL	Forelimb Primary Somatosensory	Cortical	MCA	Images from (Rousselet et	0.0013	4.207	61.17	-7.214	0.0889	2.854	52.17	0.515907	0.0207	3.395	47.56	4.828974	0.1792	2.569	52.68	95.3304	0.0024	3.802	59.82	-6.17733
RS	Retrosplenial Cortex	Cortical	PCA	Images from (Xiong et al.,	0.0089	3.659	51.35	-7.915	0.7957	1.674	49.98	0.429923	0.0003	4.781	42.62	8.438384	>0.9999	0.5952	44.66	-28.1231	0.0478	2.807	53.35	-4.02641
V1	Primary Visual Cortex	Cortical	PCA	(Pula & Yuen, 2017)	0.997	1.001	56.55	-2.144	0.0224	3.414	38.82	0.598802	>0.9999	0.3276	49.06	-0.41708	>0.9999	0.07711	46.38	-2.32558	0.0005	4.336	52.19	-5.51172
HPC	Dorsal Hippocampus	Subcortical	PCA	(Erdem et al., 1993)	0.0007	4.421	56.5	-9.855	0.0264	3.369	36.72	0.599315	<0.0001	5.883	41.21	9.084084	0.9982	0.954	52.99	28.09917				
STR	Striatum (Caudate/Putamen)	Subcortical	MCA	(Feekes & Cassell, 2006)	0.0582	3.002	56.56	-4.598	0.4014	2.19	45.83	0.427716	<0.0001	5.347	49.38	7.820513	0.9928	1.095	38.72	92.99641				
Thalamus	Thalamus	Subcortical	PCA	(Schmahmann, 2003)	0.2904	2.342	58.22	-4.266	0.5514	1.999	42.29	0.344828	<0.0001	6.603	46.72	10.07121	>0.9999	0.5395	43.47	38.53484				
Hypothalamus	Hypothalamus	Subcortical	PCA	(Daniel, 1966)	0.0096	3.613	56.57	-11.09	0.0505	3.106	40.79	0.684346	0.8696	1.552	49.67	2.735174	>0.9999	0.539	48.77	17.74222				
LA	Lateral Amygdala	Subcortical	MCA	(Merksz et al., 1978)	>0.9999	0.0201	41.76	-0.07518	0.0064	3.764	51.33	0.861326	0.9982	0.9538	52.4	1.921132	0.9996	0.8469	35.81	46.00688				
SNR	Substantia Nigra Pars Reticulata	Subcortical	MCA	(Sonne & Beato, 2019)	0.081	2.88	56.27	-7.34	0.0809	2.904	46.81	0.85034	0.9887	1.142	57.69	1.869631	0.001	4.535	34.42	169.4276				
ACA	Anterior Cerebral Artery				<0.0001	5.911	56.73	-12.8327									0.0228	2.769	54.9	56.45514				
MCA	Middle Cerebral Artery				0.0005	4.335	44.91	-7.73626									0.1087	2.134	51.46	43.79865				
PCA	Posterior Cerebral Artery				0.0007	4.125	59.73	-6.6942									0.1097	2.128	53.63	41.56311				
WM	White Matter				<0.0001	6.614	50.76	-22.4813									0.0007	3.962	51.86	84.23272				
CGM	Cortical Gray Matter				<0.0001	5.33	54.07	-8.65645									0.998	0.1599	45.06	-4.41696				
SGM	Subcortical Gray Matter				0.0008	4.125	54.6	-5.83602									0.0401	2.56	50.02	52.99632				

Table 2.0. Summary of statistical comparisons between young adult and aged animals. Table shows tissue class and arterial territory assignments, as well as abbreviations for each area surveyed. Post-hoc comparisons between young adult and aged animals in vessel density, vessel tortuosity, mean vessel diameter, and cortical thickness are shown for each region, tissue class or perfusion territory.

2.2.2 Capillary obstruction model and microsphere density analysis.

To assess region specific differences in susceptibility to capillary obstructions, we used male young adult C57BL/6J mice (3-4-month-old, mean=3.4, 30 minute: n=16, 3 day: n=15). Mice were briefly (<15 min) anesthetized with 2% isoflurane gas mixed in medical grade air with body temperature maintained at 37°C. As previously described (Reeson et al., 2018), we intravenously injected 100µL of 4µm diameter fluorescent microspheres (2% solids; Life Technologies FluoSpheres sulfate) to induce capillary obstructions. Red or green fluorescent microspheres (ThermoFisher catalog# F8858 and F8859) were injected 3 days or 30 minutes respectively prior to euthanasia to estimate transient and long-lived capillary obstructions. Mice recovered under a heat lamp immediately after injection before being returned to their home cage. Mice were killed from an overdose of sodium pentobarbital, the brain was immediately extracted, then bisected and each hemisphere immersed in 4% PFA overnight before being transferred to 0.1M PBS. We sectioned brains on a Leica vibratome (T1000) to make 100 or 50µm-thick coronal sections. Every 3rd section was mounted onto a gel-coated slide, and cover-slipped with Fluoromount G. Ultra-bright fluorescent microspheres were imaged on an upright wide-field Olympus BX51 microscope with a 2x Olympus Plan objective (NA=0.05, 228 pixels/mm) using GFP and Cy3 excitation/emission filter sets on an Olympus DP73 digital CCD camera using CellSens software. Images were taken from every 3rd section from approximately +2.7mm to -3.5mm from bregma (Franklin and Paxinos, 2008). Using a custom-built macro for FIJI, ROIs were manually drawn on each image over every present brain region, as shown in **Figure 2.1A** and guided by the Franklin and Paxinos Mouse Brain Atlas (Franklin and Paxinos, 2008), and

microspheres were automatically counted in each ROI using a threshold of 2/3 maximum pixel intensity. The density of obstructions within each brain region was expressed as # obstructions per metre length of capillary.

To test the hypothesis that regional microvascular obstruction rates would correlate with capillary diameter or the magnitude of region-specific vessel loss with aging, a linear regression was calculated, plotting mean vascular length loss or mean vessel diameter against microsphere density. Density values for each region were normalized within each animal and expressed as % difference relative to the mean microsphere density across all brain regions. The obstruction clearance rate was based on the difference between 30-minute and 3-day obstruction densities in each region.

To test whether there might be differences in obstruction rates in young adult and aged animals, we expressed aged obstruction densities and clearance rates as a value normalized to the young-adult means.

2.2.3 Cortical and callosal thickness analysis.

Cortical thickness was measured in FIJI by drawing straight lines perpendicular from the cortical surface to the white matter in 6 places: retrosplenial (drawn dorsally from the peak of the corpus callosum), visual, peri-rhinal, insular, motor and forelimb somatosensory cortex. Every 3rd section was sampled with one line drawn for each area. Callosal thickness was determined by dividing the pixel area for each corpus callosum ROI by the pixel width of the ROI along the cardinal x-axis, equivalent to taking the average of the height (y-distance) of the ROI at each pixel in the x-plane.

2.2.4 Code Accessibility.

Custom FIJI macros can be freely accessed on GitHub at https://github.com/bschager/Microvessel-Density-Analysis (Schager, 2019). Image classifier files are available from the authors on demand.

2.2.5 Statistics.

All statistical analyses were performed using GraphPad Prism 8 using an alpha value of 0.05. A multivariate mixed analysis was used where appropriate. For repeated measures data, two-way mixed ANOVA or one-way repeated measures ANOVA was used when there were no missing values, while a mixed model was fitted to the data (using Restricted Maximum Likelihood) when there were missing values in the dataset. Where the assumption of sphericity was not met, the Geisser-Greenhouse correction was used. Post-hoc comparisons were performed using Sidak's multiple comparisons test for multi-variate mixed-model analyses (where comparisons were not paired) and paired t-tests (with Bonferroni correction when >3 comparisons were made) for univariate repeated measures analyses. Repeated measures ANOVA was used to test for region-related differences in microsphere clearance rates. Data are presented as mean ± 95% confidence interval (CI), unless otherwise stated. Repeated measures data is acknowledged with connecting lines only when there are only two conditions or few enough lines to follow points through all conditions. **Table 2.0** provides detailed results of the post-hoc tests comparing young adult and aged animals.

Outliers were detected using Grubbs test, with an alpha value of 0.05. For example, 4/1298, 2/431, 2/848, and 1/122 data points were identified as outliers for

vessel density, cortical thickness, tortuosity, and callosal vessel density (**Fig. 2.4F**) respectively. When analyzing the relationship between vessel loss and obstruction rate, retrosplenial cortex was identified as an outlier at both 30-minute and 3-day time points and excluded from the linear regression analysis.

2.3 Results

2.3.0 Vessel loss with aging occurs in a region-specific manner

In order to determine the magnitude of vessel loss with aging and whether certain brain regions were more vulnerable than others, we intravenously injected young adult and aged mice (n=40 and 25, respectively) with fixation-compatible FITC dextran and then generated over 3,000 confocal image stacks of fluorescently labelled blood vessels in 15 different brain regions (**Fig. 2.1B**). To analyze this large data set, we generated an automated macro for estimating vessel length that very closely matched estimates produced by a blinded observer (**Fig. 2.0B,C**, r^2=0.964; mean difference of 0.08±3.74%). A mixed model two-way ANOVA revealed a significant main effect of age ($F_{(1,63)}$= 27.08, p<0.0001), brain region ($F_{(14,821)}$= 664.8, p<0.0001), and a significant age by region interaction ($F_{(14,821)}$= 3.870, p<0.0001). As shown in **Figure 2.2A,B** and **Table 2.0**, vessel loss (displayed as m/mm^3 and % vessel loss) with aging was not uniform across brain regions. Post-hoc analysis revealed significant loss of vessel length in 7 out of the 15 regions sampled. The area with the greatest magnitude of vessel loss was the corpus callosum, exhibiting a ~26% reduction in vascular density with age (**Fig. 2.2A,B**). In the cortex, the motor, peri-rhinal/ecto-rhinal, forelimb somatosensory and retrosplenial areas exhibited significant loss of vessel length (mean= 10.29%) and frontal cortex trended towards statistical significance (7.8%, $t_{(54.82)}$=2.907 p=0.0759), whereas the insular ($t_{(53.40)}$= 1.470, p=0.9087) and visual cortex ($t_{(56.55)}$= 1.001, p=0.9970) did not show any loss (**Fig. 2.2A,B**). Subcortically, loss of vessel length was also observed in the hippocampus and hypothalamus (**Fig. 2.2A,B**; mean= 10.47%), with striatum and substantia nigra trending toward statistical significance (Striatum:

4.6%, $t_{(55.56)}$= 3.002, p=0.0582; Substantia nigra: 7.3%, $t_{(56.27)}$= 2.880, p=0.0810), but not in the thalamus ($t_{(58.22)}$= 2.342, p=0.2904) or lateral amygdala ($t_{(41.76)}$= 0.201, p>0.9999).

Given our broad sampling of brain regions, we next attempted to determine if there were supra-regional patterns of age-related vessel loss. For example, white matter is known to be susceptible to degeneration with aging and is thought to be an important factor in cognitive decline (Bennett and Madden, 2014; Birdsill et al., 2014; de Groot et al., 2015; Bagi et al., 2018). Additionally, it is conceivable that vessel loss may vary as a function of vascular perfusion territory given inherent territorial differences in the incidence of stroke or collateral circulation (Ng et al., 2007; Menon et al., 2013). Therefore, we assigned each brain region area a classification based on tissue type (white matter vs cortical gray vs subcortical gray matter) or major supplying cerebral artery and assessed vascular loss. Classifications and references for assigning brain regions to a specific perfusion territory are detailed in **Table 2.0**. As shown in **Figure 2.2C**, vessel length was significantly lower in aged mice regardless of tissue class (Main effect of Age for Tissue Class: $F_{(1,63)}$= 30.63, p<0.0001) or arterial supply ($F_{(1,63)}$= 24.63, p<0.0001), reflective of the general trend for vessel density to decrease with age. However, comparing the percent vessel loss within these categories revealed differences. For tissue class (**Fig. 2.2D**), paired t-test revealed that vessel loss was significantly greater in white matter (WM) compared to cortical gray matter (CGM) ($t_{(24)}$= 11.64, p<0.0001) and subcortical gray matter (SGM) ($t_{(23)}$= 12.65, p<0.0001), while cortical gray matter vessel loss was greater than subcortical gray matter ($t_{(23)}$= 3.738, p=0.0011). For arterial territory (**Fig. 2.2D**), loss of vessel length was significantly greater for territories fed by the anterior cerebral artery (ACA) than for those supplied by

the middle (MCA; $t_{(23)}$= 4.324, p=0.0003) or posterior cerebral arteries (PCA; $t_{(24)}$= 6.744, p<0.0001). Lastly, we assessed cortical thickness in select cortical regions (n=6 regions) and found that cortical thickness was significantly reduced in aged mice (**Fig. 2.2E**, top panel; $t_{(60)}$= 3.562, p=0.0007). However, cortical thickness had no relationship with vessel length measurements (**Fig. 2.2E**, bottom panel), implying that slight shrinkage of the brain with age did not systematically influence our length measurements. Thickness reductions were uniform across the cortex (**Fig. 2.2F**, top panel), but we did not detect any changes in the thickness of the white matter that could have contributed to the large magnitude of vessel loss ($t_{(44.87)}$= 1.612, p=0.5714). Linear regression testing the relationship between vessel loss and changes in thickness revealed no relationship (after removal of clear outlier corpus callosum, r^2=0.08797) (**Fig. 2.2F**, bottom panel), further showing that thickness (and thus volume) reductions did not systematically influence length measurements. Collectively, these results show that the loss of vessel length with aging is a heterogeneous phenomenon with certain brain regions showing greater vulnerability than others.

Figure 2.2. Loss of vessel length with aging is brain region specific.

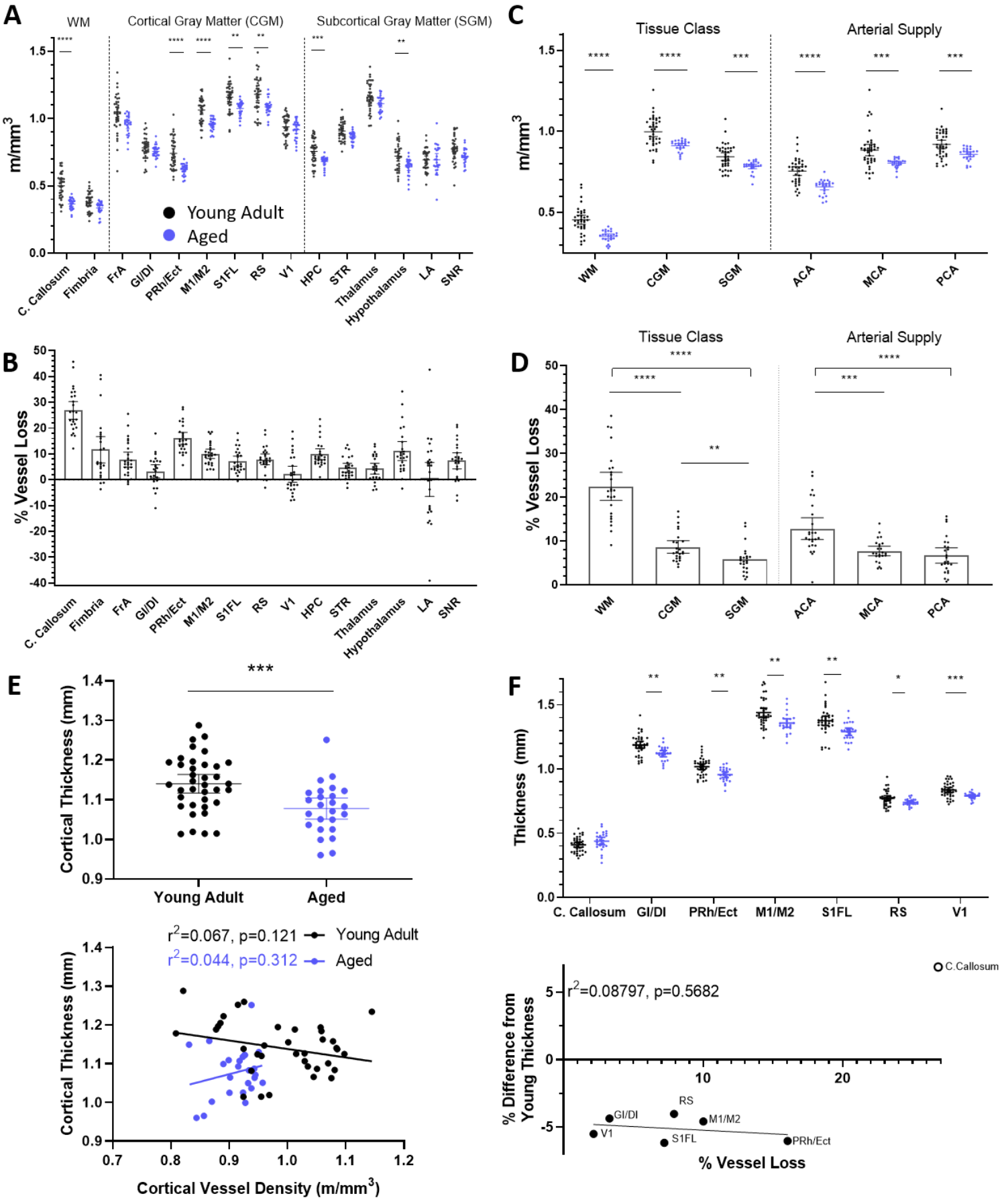

Figure 2.2. Loss of vessel length with aging is brain region specific. (**A**) Quantification of vessel length per cubic volume of tissue in each region in young adult (black dots; n=40 mice) and aged mice (red dots; n=25 mice). (**B**) Relative magnitude of age-related vessel loss in each brain region. (**C**) Graphs show vessel length changes in young adult and aged mice as a function of tissue class or arterial supply. (**D**) Age-related vessel loss binned according to tissue class or arterial supply. (**E**) Graph showing differences in average cortical thickness with aging (top panel) and linear regression analysis (bottom panel). Note no systematic relationship between cortical thickness and vessel length density measurements in young adult or aged mice. (**F**) Graph showing age related changes in cortical, but not callosal thickness. WM: white matter; CGM: cortical gray matter; SGM: subcortical gray matter. Data in A, C and F were analyzed by fitting a mixed model to approximate two-way mixed ANOVA followed by Sidak's multiple comparisons test. Data in D were analyzed by fitting a mixed model to approximate repeated measures ANOVA followed by post-hoc paired t-tests. Data in E were analyzed with an unpaired t-test. Error bars: mean ± 95%CI. ****$p < 0.0001$, ***$p < 0.001$, **$p<0.01$, *$p<0.05$.

2.3.1 Age-related changes in vessel tortuosity and diameter

Next, we wanted to determine if the loss of vessel length with aging could be explained or compensated for by changes in vessel structure such as tortuosity or width. We estimated mean vessel tortuosity, measured as the arc-chord ratio (**Fig. 2.0D**, increasing values indicate greater tortuosity), from 2-3 images in each region per animal. Tortuosity measurements generated from our custom macro were cross referenced and validated against tortuosity measurements generated through hand-traced images (**Fig. 2.0E,F**). We ensured that our tortuosity measurements would not be influenced by differences in vascular diameter by plotting the difference between macro-generated tortuosity and hand-measured tortuosity against mean vessel diameter (17 images) and by modelling a capillary increasing in diameter and measuring recorded tortuosity (**Fig. 2.0G,H**). Our analysis of tortuosity revealed a significant main effect of age ($F_{(1,59)}$= 15.19, p=0.0003), and brain region ($F_{(6.542,353.7)}$= 16.87, p<0.0001), and an age by region interaction ($F_{(14,757)}$= 4.383, p<0.0001). Specifically, tortuosity increased with age in frontal cortex, visual cortex, hippocampus, and amygdala (**Fig. 2.3A**). Next, we used a linear regression analysis to determine whether vessels in brain regions that were more prone to loss with aging were: a) more tortuous in young adult mice, or b) more likely to show a change in tortuosity with age (**Fig. 2.3C**). Our analysis revealed no significant systematic relationship between vessel loss and young adult tortuosity (**Fig. 2.3B**); however, we found a moderate relationship between areas that experience large magnitudes of vessel loss and areas that show a change in tortuosity with age (**Fig. 2.3C**), though this relationship may be skewed by the corpus callosum (with callosum: r^2=0.4659, without callosum: r^2=0.1195

). Vessel diameter also showed age and region specific changes (main effect of age: $F_{(1,59)}$= 28.72, p<0.0001; brain region: $F_{(3.053,165.5)}$= 22.97, p<0.0001; age by region interaction: $F_{(14,759)}$= 6.133, p<0.0001), with the general trend for vessel diameter to increase with age (**Fig. 2.3D**). We found only a weak relationship between vessel loss and vessel diameter in young animals (**Fig. 2.3E**), and we discovered no systematic relationship between regional vessel loss and changes in vessel diameter with aging (**Fig. 2.3F**). These findings reveal that vessel tortuosity and width vary between regions in young animals and change in a region-specific manner with aging, but that changes in tortuosity are very small, and neither variable possesses strong predictive value for the magnitude of vessel loss.

Figure 2.3. Age-related changes in vessel tortuosity and diameter.

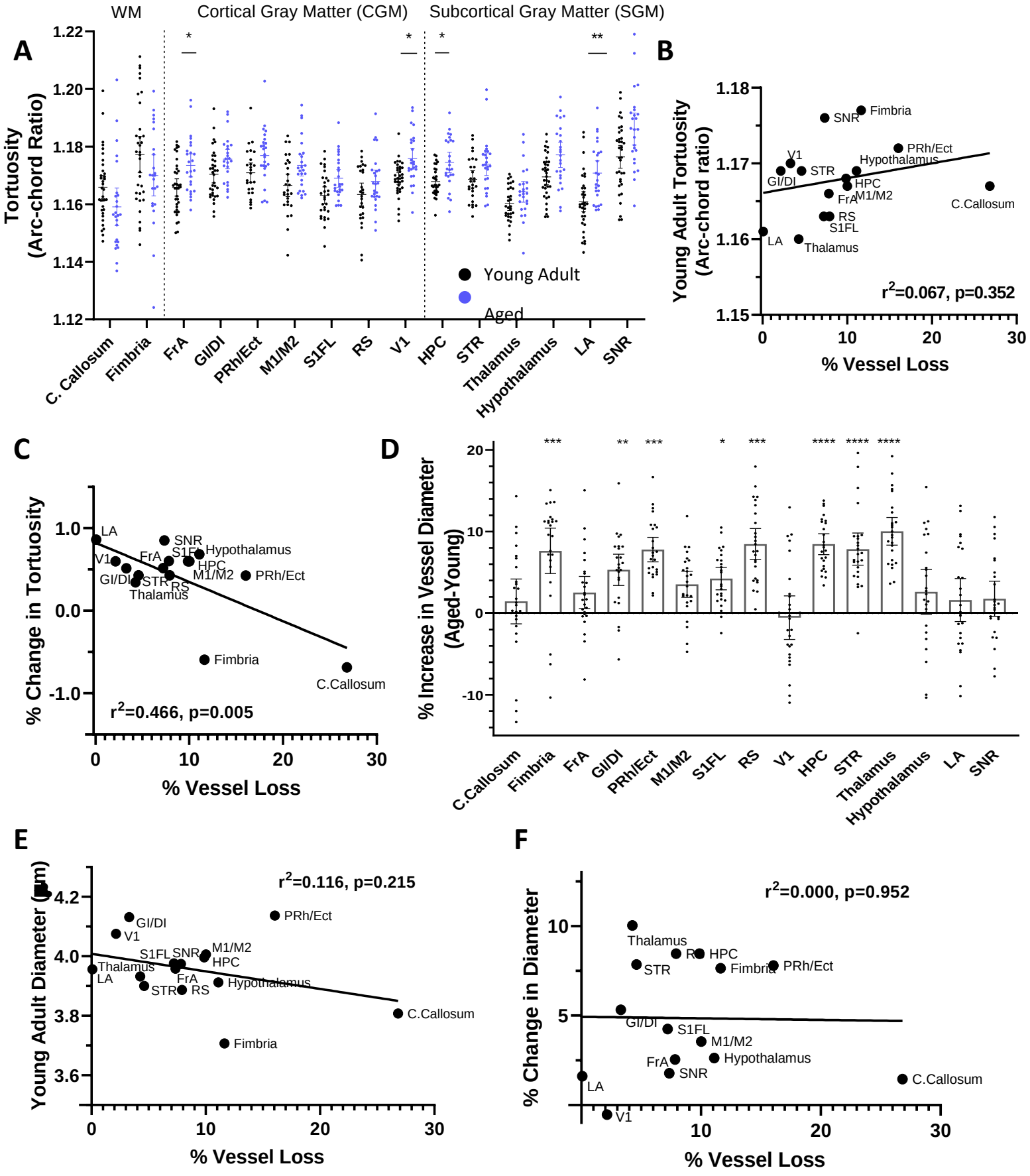

Figure 2.3. Age-related changes in vessel tortuosity and diameter. (**A**) Quantitative differences in tortuosity across different brain regions in young adult and aged mice. Regression analysis did not reveal any relationship between age-related vessel loss and the extent of tortuosity in specific brain regions of young adult mice, (**B**) but a moderate relationship was found in the % change with aging (**C**). (**D**) Graphs show age-related changes in vessel width in each brain region. There was a very weak relationship between regional vessel loss and diameter in young mice (**E**), and no relationship between regional vessel loss and changes in vessel width with aging (**F**). Data in A and D were analyzed by fitting a mixed model to approximate two-way mixed ANOVA followed by Sidak's multiple comparisons test. Error bars: mean ± 95%CI. ****p < 0.0001, ***p < 0.001, **p<0.01, *p<0.05.

2.3.2 Zones of vessel sparse regions increase with age

A recent oxygen imaging study found micro-pockets of hypoxic brain tissue (up to 200µm in size) in ~24-month-old mice (Moeini et al., 2018). One possible explanation for this local hypoxia is that aging may increase the likelihood of vessel sparse micro-zones, especially if vessel loss exhibits some degree of clustering. To test this, we subdivided vascular skeletons into 211x211µm grids and quantified the number of pockets that had less than 50% of the mean vascular density for the brain region examined (**Fig. 2.4A**). Our analysis revealed a significant main effect of age ($F_{(1,59)}$= 11.58, p=0.0012), brain region ($F_{(4.003,217.0)}$= 59.69, p<0.0001) and age by region interaction ($F_{(14,759)}$= 8.508, p<0.0001). As shown in **Figure 2.4B**, two areas in particular exhibited a significant increase in the frequency of vessel sparse zones: the corpus callosum ($t_{(55.44)}$= 4.844, p=0.0002) and the substantia nigra ($t_{(34.42)}$= 4.535, p=0.0010). When grouped by tissue class or arterial territory, white matter, subcortical gray matter, and ACA-supplied tissues showed a statistically significant age-related increase in the prevalence of vessel sparse pockets (WM: $t_{(51.86)}$= 3.962, p=0.0007; SGM: $t_{(50.02)}$= 2.560, p=0.0401; ACA: $t_{(54.90)}$= 2.769, p=0.0228) (**Fig. 2.4C**).

Given that the corpus callosum displays a large magnitude of vessel loss and displays a higher prevalence of vessel-sparse zones, we wondered whether structural differences or systematic differences in where vessels were lost could explain the large amount of loss. We found no difference in the thickness of the corpus callosum between young adult and aged mice (**Fig. 2.2F**) and no relationship between callosal vessel density and thickness in young adult or aged mice (**Fig. 2.4D**). Seeing as structural changes could not explain the large magnitude of vessel loss, we further looked for

regional patterns in vascular loss in the corpus callosum by classifying subregions as either ventral (sharing a border with the lateral ventricle or striatum) or dorsal (**Fig. 2.4E**). We discovered that areas along the ventral surface of the striatum showed a greater increase in the proportion of vessel sparse zones in aged animals than in young adult animals (**Fig. 2.4F;** unpaired t-test: $t_{(59)}$= 5.119, p<0.0001) and that areas along the ventral surface of the corpus callosum displayed a larger magnitude of vessel loss than dorsal areas (**Fig. 2.4G**; paired t-test: $t_{(24)}$= 5.193, p<0.0001). However, seeing as dorsal areas still experienced a very large magnitude of vessel loss (~25%), this sub-regional difference does little to explain why the corpus callosum loses so many more vessels with age than other brain areas.

Figure 2.4. Pockets of vessel sparse zones in the aged brain.

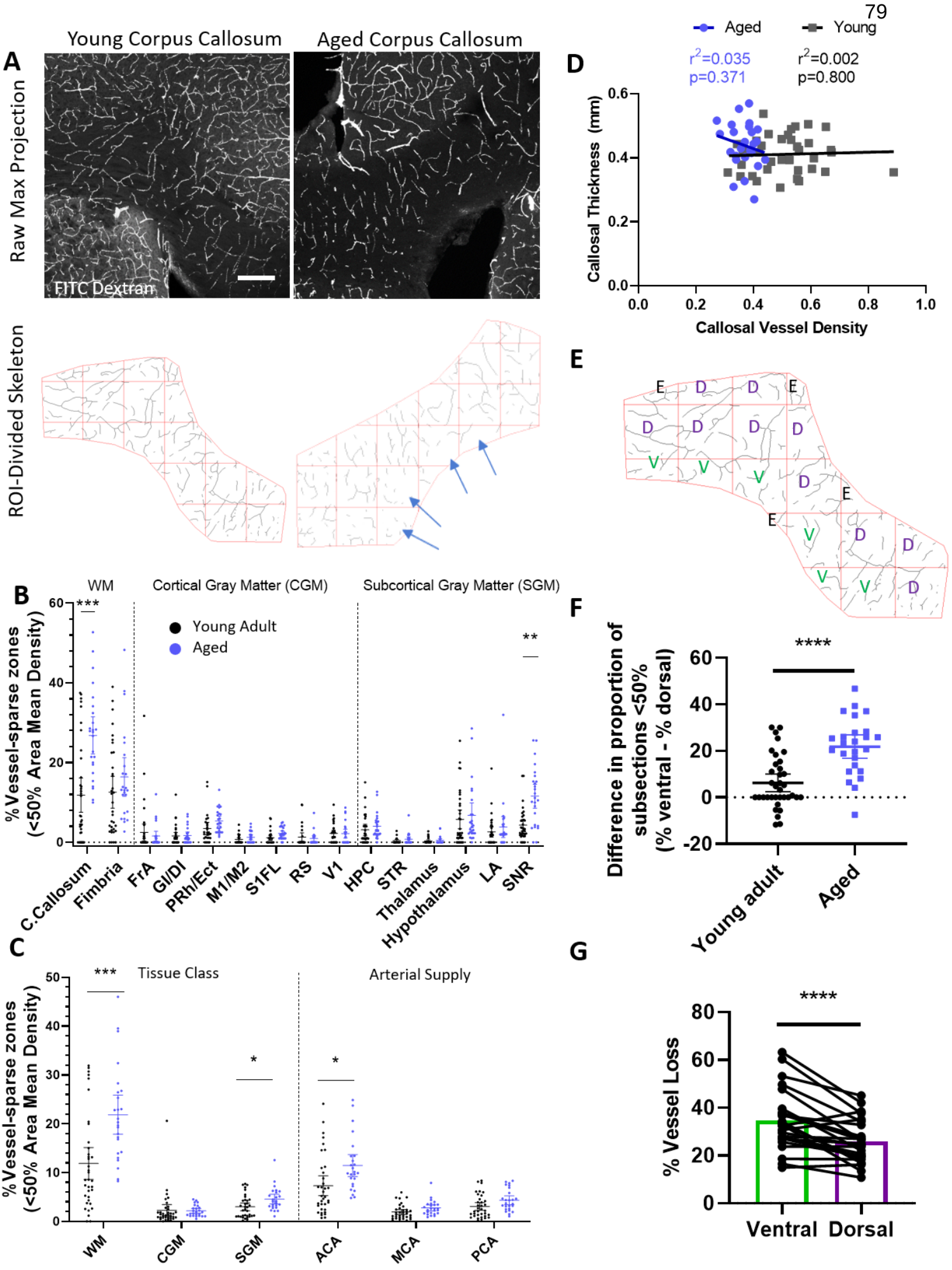

Figure 2.4. Pockets of vessel sparse zones in the aged brain. (**A**) Confocal image projections showing FITC labelled vasculature in the corpus callosum in young adult and aged mice (top row), and corresponding skeletonized images illustrating how vessel sparse micro-zones were analyzed (bottom panel). Scale bar = 200μm. Graphs show the % of vessel sparse zones in young adult and aged mice in each brain region (**B**) or according to tissue class or arterial supply (**C**). (**D**) Graph plots the relationship between callosal thickness and vessel density in young adult and aged animals, revealing no obvious effect of callosal size (and presumably shrinkage) on vessel density. (**E**) Example image of how we classified image subsections as along the ventral border (green V), dorsal from the ventral subsections (purple D), or excluded because the subsection did not meet the minimum area requirement of 1/3 the maximum subsection size (black E). (**F**) Graph showing the difference between the proportion of low-density ventral subsections and the proportion of low-density dorsal subsections. Note aged animals have more proportionally more low-density subsections in ventral areas than young adult animals. (**G**) Mean vessel density of subsections was calculated for both ventral and dorsal areas in both age groups. Aged vessel densities were normalized to the young adult means for that part of the corpus callosum. Graph shows a larger magnitude of vessel loss in ventral areas of corpus callosum than in dorsal areas. Data in B and C were analyzed by fitting a mixed model to approximate two-way mixed ANOVA followed by Sidak's multiple comparisons test. Linear regression was performed in D. Data in F was compared with an unpaired two-sample t-test. Data in G was compared with a paired t-test. Error bars: mean ± 95%CI. ****$p < 0.0001$, ***$p < 0.001$, **$p<0.01$, *$p<0.05$.

2.3.3 Vulnerability to long lasting capillary obstructions is predictive of vessel loss with aging

Previous work from our lab has shown that long-lasting naturally occurring or microsphere-induced capillary obstructions result in vessel pruning in ~30% of cases (Reeson et al., 2018). To help explain why some brain regions might show greater vessel loss with aging than others, we hypothesized that these vulnerable regions would be more susceptible to capillary obstructions. Therefore, we intravenously injected 4µm diameter red or green microspheres into young adult mice 30min and 3d before extracting the brain (**Fig. 2.5A**). We reasoned that the 30-minute time point would provide an estimate of short-lived obstructions whereas the 3d time point would reflect persistent, long lasting obstructions. **Figure 2.5B** demonstrates the presence of microspheres within cerebral vessels, obstructing the lumen of capillaries. We should note that microspheres did not lead to ruptured vessels as they were not found in extravascular spaces (**Fig. 2.5B**), nor were microglia aggregated around them (**Fig. 2.5C**) (Reeson et al., 2018). Quantification of microsphere density in different brain regions from 30-minute (green microspheres) and 3-day (red microspheres) time points revealed a heterogenous distribution (**Fig. 2.5D**; Repeated measures ANOVA of brain region at 30 minutes with RS: $F_{(4.035,60.52)}$= 19.54, p<0.0001 and 3 days: $F_{(4.235,59.29)}$= 3.7.890, p<0.0001). This distribution remained regionally heterogeneous even after excluding retrosplenial cortex from the analysis (Repeated measures ANOVA of brain region at 30 minutes without RS: $F_{(3.532,52.97)}$= 10.43, p<0.0001 and 3 days: $F_{(3.826,53.56)}$= 3.239, p=0.0202). As indicated in **Figure 2.5E**, the overwhelming majority of microspheres were cleared from the brain between 30 minutes and 3 days (~95% on

average across all regions). By calculating the % clearance rate (1 – 3 day density/30 minute density), one can note significant region-specific variability in clearance rates (**Fig. 2.5E;** Repeated measures ANOVA $F_{(4.265,59.71)}$= 3.840, p=0.0066). To determine whether obstruction density at 30min or 3d was predictive of region-specific vessel loss with aging, we performed linear regression analyses between the mean magnitude of vessel loss for each area and normalized obstruction rates in young adult animals (**Fig. 2.5F**). In addition, we performed a regression analysis for vessel loss and each region's clearance rate (**Fig. 2.5G**). Our analysis revealed a significant positive relationship between long lasting obstructions found in each region at 3 days (but not 30 minutes) and the degree of microvascular loss with aging (**Fig. 2.5F**, left panel). Similarly, brain regions that were better at clearing obstructions (indicated by higher clearance rates in **Fig. 2.5G**, left panel) were less susceptible to age-related vessel loss. Parsing out these relationships according to tissue class, we found stronger correlations for vessel loss in cortical gray and white matter regions (**Fig. 2.5F and G**, middle panel), than subcortical gray matter (**Fig. 2.5F and G**, right panel). These results indicate that brain regions with an increased susceptibility to long-lasting capillary obstructions (and those less able to clear them) are more likely to experience greater vessel loss with aging.

Though underpowered (30 min: n=6; 3 day: n=5), an analysis of obstruction rates in aged animals (21.8 months old) also revealed regional heterogeneity in the density of obstructions (**Fig. 2.6A**; Repeated measures ANOVA of brain region at 30 min: $F_{(1.809,9.043)}$= 25.23, p=0.0002 and 3 days: $F_{(3.081,12.32)}$= 3.907, p=0.0353), and trended toward statistical significance in recanalization rate (**Fig. 2.6B;** Repeated measures ANOVA $F_{(1.951,7.414)}$= 3.840, p=0.0724). However, no relationships were found between

region-specific vessel loss and obstruction or clearance rates in aged animals (**Fig. 2.6C and D**). This result implied that obstruction rates change with in a region-dependent manner. To further explore this possibility, we normalized the aged obstruction and clearance rates to the young adult means and looked for regional differences (**Fig. 2.6E**). One-way repeated measures ANOVA revealed a significant effect of brain region on relative (to young adult) obstruction rate at 30 minutes ($F_{(1.703,8.517)}$= 22.21, p=0.0005), and 3 days ($F_{(3.256,13.02)}$= 4.245, p=0.0249), and an effect on clearance rate trending toward statistical significance ($F_{(2.014,8.058)}$= 3.859, p=0.0666). Post-hoc paired t-tests for each region against the brain average obstruction rate (with Bonferroni correction) revealed significant differences in obstruction rates between young-adult and aged animals in the fimbria ($t_{(5)}$= 9.595, p=0.0054) and substantia nigra ($t_{(5)}$= 6.347, p=0.0199) at 30 minutes (**Fig. 2.6E**, left panel), and in the retrosplenial cortex ($t_{(4)}$= 10.65, p=0.0066) and somatosensory forelimb cortex ($t_{(4)}$= 6.408, p=0.0418) at 3 days (**Fig. 2.6E**, middle panel). Interestingly, we found no differences in the brain average obstruction rates between young-adult and aged animals. In summary, by comparing obstruction densities in young adult and aged mice, our analysis reveals that obstruction rates in some brain regions may change with age even if brain average obstruction rates do not.

Finally, to understand whether areas with smaller diameter capillaries would experience more obstructions or reduced recanalization rates, we plotted diameter against obstruction and clearance rates for young adult and aged animals and subsequently performed linear regression. We found a moderated relationship between 3-day obstruction rate and vessel diameter and between clearance rate and vessel

diameter in young adult animals (**Fig 2.6F and G**, left panel), but not in aged animals (**Fig. 2.6F and G**, right panel). This indicates that young-adult diameter plays some role in vessel obstruction and recanalization, but interestingly only weakly predicts vessel loss (**Fig. 2.3E**).

Figure 2.5. Regional vulnerability to capillary obstructions is predictive of vessel loss with aging.

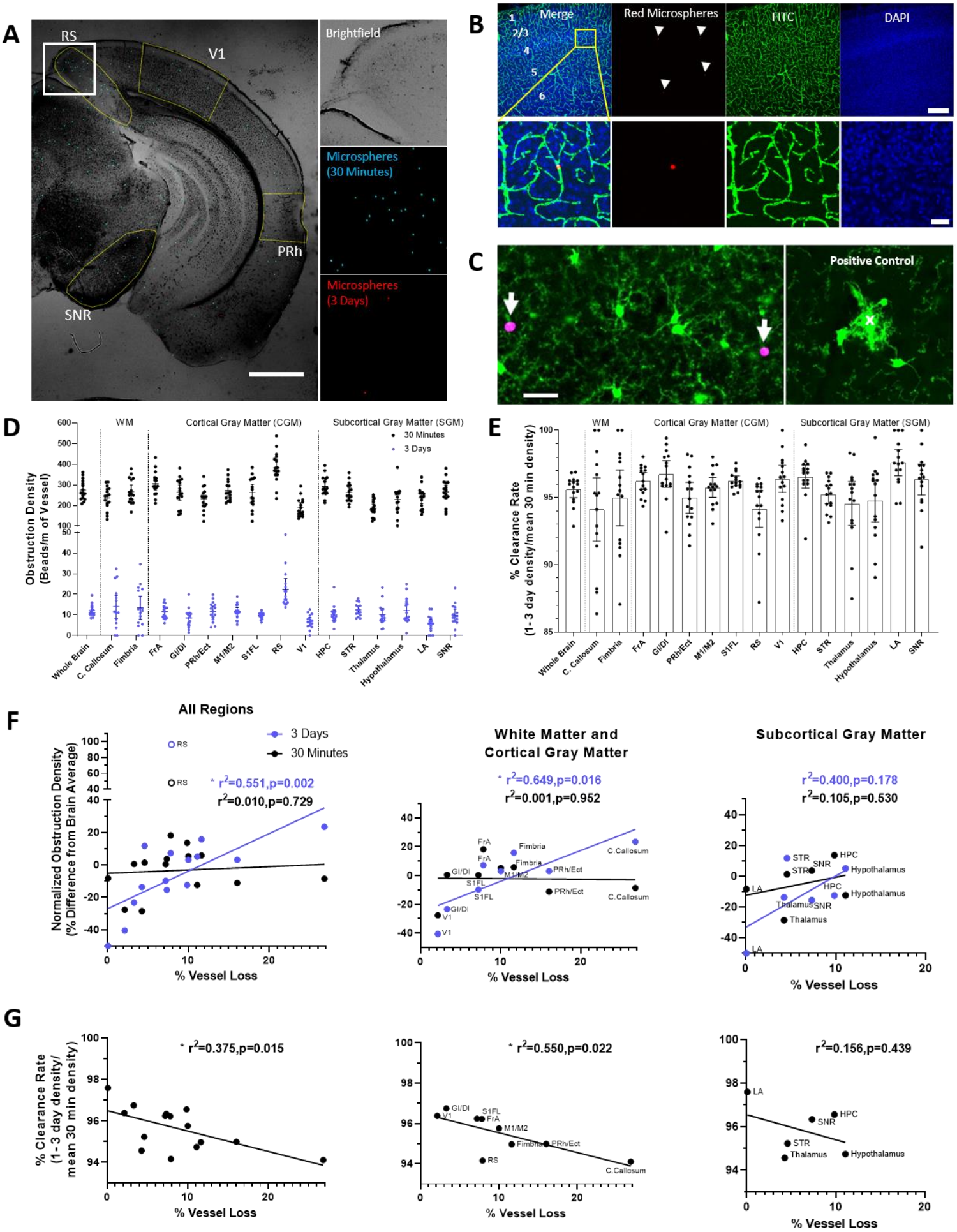

Figure 2.5. Regional vulnerability to capillary obstructions is predictive of vessel loss with aging. (**A**) Widefield images of coronal brain sections showing transient (blue colored microspheres) and long-lasting capillary obstructions (red colored microspheres) injected 30min or 3d, respectively, prior to brain extraction. Scale bar=1mm. (**B**) Images show red microspheres reside within FITC labelled capillaries in the forelimb somatosensory cortex. Scale bar=200µm (top row), 20µm (bottom row). (**C**) Confocal images show no preferential aggregation of GFP labelled microglia around microspheres, suggesting that microspheres do not cause local rupture of the blood brain barrier. As a positive control (right), we show microglia aggregation around a cortical capillary ruptured in vivo. Scale bar=20µm. (**D**) Graphs show the density of short (30min) or long-lived (3d) microsphere obstructions across each brain region in young adult mice (30 min: $F_{(4.035,60.52)}$= 19.54, p<0.0001 and 3 days: $F_{(4.235,59.29)}$= 3.7.890, p<0.0001). (**E**) Graphs plot the % clearance of obstructions (1- 3d/30min density) to illustrate significant variability across brain regions ($F_{(4.265,59.71)}$= 3.840, p=0.0066). (**F**) Regression analysis of short or long-lived obstruction density (30min vs 3d) for each brain region plotted as a function of vessel loss with aging. With the exception of the retrosplenial (RS) cortex, which was a clear outlier at both time points (identified by Grubbs test), the density of long-lived obstructions (3d) in each brain region was significantly related to the extent of vessel loss with aging. (**G**) Similarly, regression analysis indicated that those brain regions more adept at clearing obstructions (higher % clearance rate values), were less likely to show age-related vessel loss. Note that these relationships were stronger for white and cortical gray matter (middle panel in F and G) than for subcortical gray matter (right panel in F and G). Data presented in D

and E were analyzed using one-way repeated measures ANOVA. Error bars: mean ± 95%CI.

Figure 2.6. Differences in obstruction rates between young adult and aged animals and relationships between capillary obstruction and vessel width.

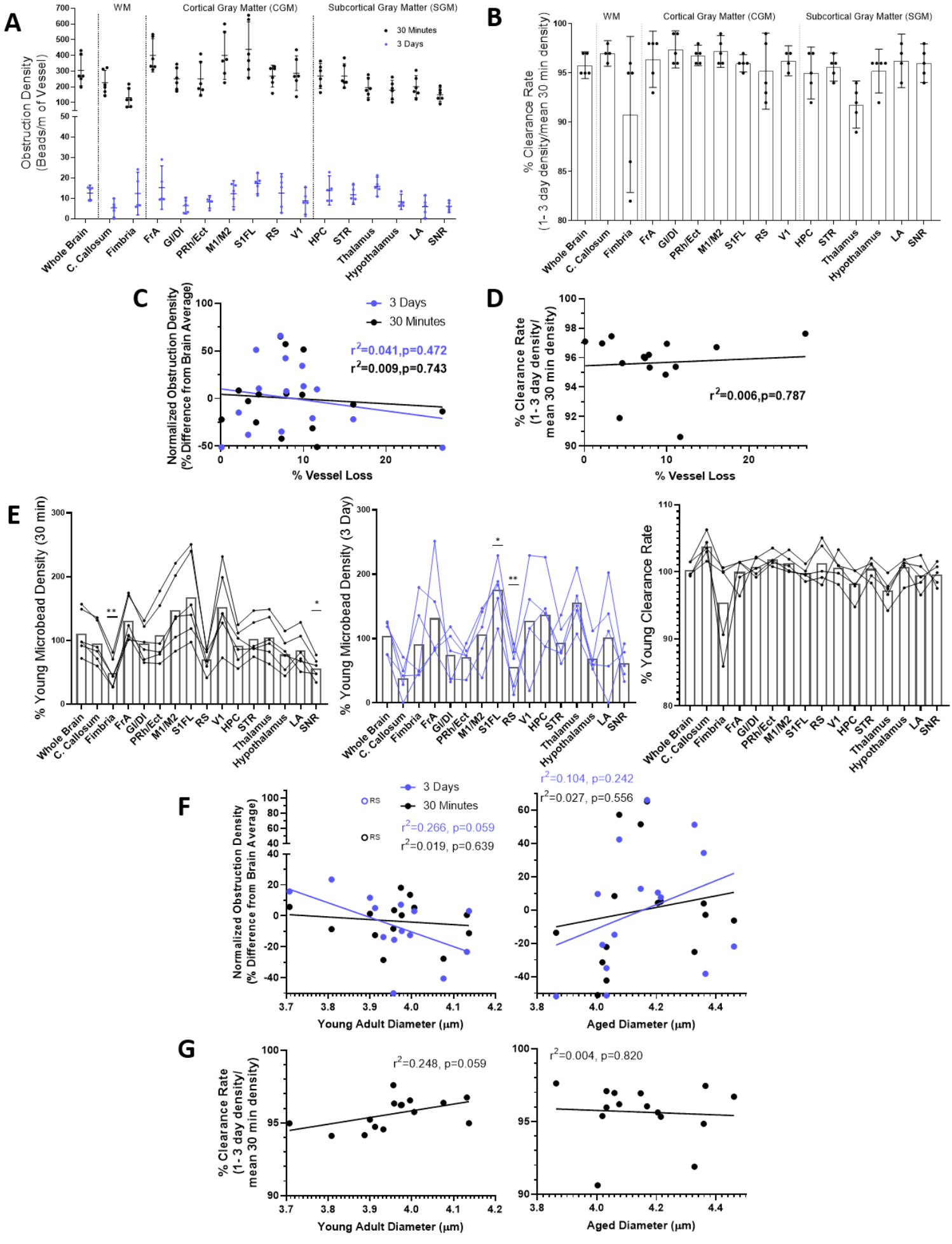

Figure 2.6. Differences in obstruction rates between young adult and aged animals and relationships between capillary obstruction and vessel width. (**A**) Graphs show the density of short (30min) or long-lived (3d) microsphere obstructions across each brain region in aged mice (30 min: $F_{(1.809,9.043)}$= 25.23, p=0.0002 and 3 days: $F_{(3.081,12.32)}$= 3.907, p=0.0353). (**B**) Graphs plot the % clearance of obstructions (1-3d/30min density) to illustrating no clear variability across brain regions (**C**) Regression analysis of short or long-lived obstruction density (30min vs 3d) or (**D**) clearance rate for each brain region plotted as a function of vessel loss with aging. No variable in aged mice was significantly related to the extent of vessel loss with aging. (**E**) Aged rates of obstruction at 30 minutes (left panel), 3 days (middle panel), and clearance rate (right panel) presented as a % of young adult mean values for each area. Post-hoc tests following one-way repeated measures ANOVA consisted of paired t-tests (with Bonferroni correction) comparing each area with the brain average. (**F**) Obstruction rate for each area at 30 minutes and 3 days in young adult (left) and aged (right) animals and (**G**) clearance rate in young adult (left) and aged (right animals plotted against mean vessel diameters in each age group. Note a moderate relationship between vessel diameter and both 3-day obstruction rate and clearance rate in young animals, suggesting that thinner vessels are less likely to recanalize and more likely to remain obstructed at 3 days. Data in A, B, and E were analyzed with one-way repeated measures ANOVA. Error bars: mean ± 95%CI. ****p < 0.0001, ***p < 0.001, **p<0.01, *p<0.05.

2.4 Discussion

The loss of brain microvessels with aging has been reported in several species including humans (see **Table 1.0**). However, to our knowledge, no previous study had examined this question in more than a couple brain regions (see **Table 1.0**) (Amenta et al., 1995b, 1995a; Murugesan et al., 2012), therefore a systematic assessment of brain region-specific vulnerability to vessel loss with aging was lacking. We believe this was an important question to address because if there are strong brain region specific patterns in vessel loss, it may help explain why certain cognitive and sensory-motor functions are more susceptible to aging than others. Here we assessed 15 different regions in the mouse brain and show that age-related microvascular loss occurs in a heterogeneous manner. Our data show that motor and somatosensory cortex, but not visual cortex, undergo significant vessel loss with aging, which agrees with previous studies in both mouse (Reeson et al., 2018) and rat (Amenta et al., 1995b, 1995a). In accordance with previous reports (Amenta et al., 1995b, 1995a; Murugesan et al., 2012), the hippocampus and white matter tracts of the corpus callosum show pronounced age-related vessel loss. By including previously unexplored limbic cortical or sub-cortical regions like the retrosplenial, insular, peri-rhinal cortex, amygdala, and thalamus in our study, our data reveal that limbic cortical areas (retrosplenial and peri-rhinal cortex) exhibit significant vessel loss, whereas subcortical regions such the thalamus, striatum and amygdala were more resilient. Despite the scant literature in sub-telencephalic regions, a *post-mortem* study examining the lateral geniculate nucleus of the thalamus also found very little change in vessel length or number with

aging (Villena et al., 2003). Collectively, these findings strongly support the idea that rarefaction of microvascular networks are differentially affected by aging.

Our findings also suggest regional differences in vascular loss based on tissue class and perfusion supply. Indeed, when vessel loss was grouped according to tissue class (white matter vs cortical vs subcortical gray matter), white matter was most vulnerable while subcortical gray matter was the least affected. Furthermore, white matter was one of the only regions studied to show pockets of vessel sparse zones. The finding that white matter is susceptible to vessel loss is perhaps not surprising since white matter atrophy is associated with aging, especially when compounded with dementia or vascular risk factors such as diabetes, hypertension and hypercholesterolemia (Iadecola, 2013; Bennett and Madden, 2014; Tong et al., 2019). The directionality of this relationship is not fully understood as white matter degeneration could lead to capillary rarefaction or the loss of capillaries could exacerbate white matter degeneration by reducing perfusion and increasing the risk of infarction, as capillary dysfunction is known to do (Østergaard et al., 2015). As noted by Brown and Thore (Brown and Thore, 2011), the blood supply for more anterior white matter tracts (similar to the location of corpus callosum analyzed in the present study) is more perilous as it arises from the distal ends of the anterior cerebral artery. A possible consequence is that capillary blood flow would be more susceptible to global perfusion changes (Li et al., 2019b) that could increase the risk of capillary stalls/obstructions (caused by blood cells, fibrin, cholesterol). In fact, the relative distance of each brain region to the proximal branches of a cerebral artery may partially explain why more distal perfusion regions like the somatosensory, motor, frontal and retrosplenial cortices

exhibited significant vessel loss with aging whereas more proximal subcortical regions such as the striatum and thalamus, did not.

Another related factor influencing vessel loss appears to be which cerebral artery supplies blood flow. When regions were grouped according to cerebral artery supply, we noted higher microvascular loss in regions supplied by the ACA than the MCA or PCA. It is possible that the ACA may have less redundancy or collateral flow then branches of the MCA and PCA. Indeed, a study using time resolved computed tomography angiography revealed weaker collateral connections between the MCA and ACA, and stronger ones connecting MCA with PCA (Menon et al., 2013). With reduced collateral circulation, regions supplied by the ACA may have less resilience to interruptions or changes in blood flow that can occur throughout life (Ma et al., 2019). Alternatively, the PCA does not appear to experience as large of an age-related drop in blood flow rates as the ACA or MCA (Zarrinkoob et al., 2015), which could conceivably change capillary plugging or recanalization rates in a region-dependent manner. An ACA-specific susceptibility to microvascular loss also would fit with the (debated) frontal lobe theory of aging (Greenwood, 2000; Pugh and Lipsitz, 2002; Nyberg et al., 2010), where reduced nutrient delivery due to low microvascular density could contribute to frontal dysfunction.

Even though our data agrees with past studies examining vessel loss in cortex and hippocampus, the magnitude of loss tended to be lower in our study (**Table 1.0**). The reason for this difference could be methodological in nature. The majority of previous studies used enzyme or immuno-histochemical approaches to label the vasculature. It is possible that the expression of these vascular proteins could be

affected by age and thus influence measurements. We opted to avoid this potential issue by injecting a fluorescent dye in vivo to label all perfused vessels and then collected the brain without intracardial perfusion. This approach was also compatible with our experiment assessing the regional distribution of fluorescent microspheres, which would have been disrupted if we employed a standard transcardial perfusion approach for immunohistochemistry. It is important to note that our method for labelling and quantifying vascular length yielded results (typically ~ 1m/mm^3 for sensory cortical areas) that closely match more recent estimates (Tsai et al., 2009; Murugesan et al., 2012; Lugo-Hernandez et al., 2017; Xiong et al., 2017).

Based on our previous work in the somatosensory cortex, we know that capillaries with long-lasting obstructions are pruned in ~30% of cases (Reeson et al., 2018). In order to better understand why certain brain regions were more vulnerable to vessel loss with aging than others, we hypothesized that those regions prone to long-lasting obstructions, ones evident 3 days after induction, would show greater vessel loss. Indeed, our data support this idea given that brain regions with higher rates of microsphere induced obstructions (and lower microsphere clearance rates) were also more likely to show greater vessel loss. However, this is an admittedly simplistic explanation of vessel loss, supported by modeling showing that the range of obstruction rates we witnessed can account for far less of a range in vascular density changes than we observed (**Fig. 2.7C**; predicted: ~6 to 12% vs observed: 26.8%), For explanation is that vessel loss may be compensated for by angiogenesis (Ndubuizu et al., 2010). While previous time lapse imaging experiments in somatosensory cortex, both from our lab and from others, report little and sometimes no compensatory vessel sprouting in

healthy adult animals (Mostany et al., 2010; Harb et al., 2013; Tennant and Brown, 2013; Masamoto et al., 2014; Cudmore et al., 2017; Reeson et al., 2018), other regions, particularly subcortical regions that did not show significant vessel loss, may balance capillary rarefaction with angiogenesis. Our study is also limited by the fact that we did not test regional differences in susceptibility to naturally occurring obstructions such as blood cells or lipids. However, given how infrequent these naturally occurring events are (more persistent natural obstructions affect <1% of all capillaries), as well the impossibility of estimating the duration of capillary obstruction without time lapse *in vivo* imaging in all 15 regions, we opted to study capillary plugging rates with microspheres. We should note that capillary pruning rates for microsphere induced obstructions are nearly identical to those that occur naturally (Reeson et al., 2018). Our study also did not examine regional differences in how capillaries clear obstructions. For example, engulfing and removing obstructions through the vessel wall (angiophagy) is a process that requires several days as opposed to embolus washout (Lam et al., 2010; Grutzendler et al., 2014; van der Wijk et al., 2019). It is conceivable that angiophagy may show regional differences which could explain why retrosplenial cortex exhibited unusually high obstruction rates at 30min and 3 days yet showed relatively normal vessel loss with aging. Future studies employing time lapse imaging in multiple regions, especially in deep tissues, would be helpful in resolving these issues.

Among the possibility that angiogenesis and differences in recanalization mechanisms may also differ based on brain region, it is possible that each of these traits could also change longitudinally with age. We discovered that, although there is a relationship between obstruction rate and vessel loss in young animals, such a

relationship was absent from aged mice. The lack of a relationship in aged mice may be simply explained by our small sample size or by the fact that obstruction rate in an aged brain is the end product of a life's worth of pruning events. For example, the capillaries in the corpus callosum that were most prone to being obstructed (and subsequently pruned) in the young adult brain might no longer exist when testing obstruction densities in the aged brain. Therefore, it is not necessarily surprising that the corpus callosum is no longer particularly vulnerable to obstructions in old age. However, it is worth noting that the significant decline in obstruction rate at 3 days in retrosplenial cortex in aged animals might also help to explain why that area does not experience far more vessel loss than predicted by its obstruction rate.

The functional significance of age and brain region-specific vessel loss remains an important question. Cognitive testing in humans and experimental animals has revealed that some functions, such as working memory, attention, executive functions, speed of information processing and sensory-motor function are particularly vulnerable to aging (Murman, 2015). Given the central role of the frontal cortex, hippocampus, corpus callosum and somatosensory-motor cortex in these functions, it is conceivable that progressive loss of microvascular structure in these regions may underlie some of these changes. Indeed, several studies show that microvascular pathology precedes or at least accompanies cognitive impairments that occur with aging or neurodegenerative disease (Bell and Zlokovic, 2009; Brown et al., 2009; Iadecola, 2013; Iturria-Medina et al., 2016; Østergaard et al., 2016). While the reasons for region specific vulnerabilities to vessel loss remain speculative, our findings suggest that susceptibility to capillary obstructions and/or inability to clear these obstructions represents at least one plausible

factor. We anticipate our study will provide key normative data for future studies, especially in brain regions not previously studied (e.g. retrosplenial, peri-rhinal cortex), to interpret vessel loss in premature aging or neuropathological conditions.

3. Chapter 2: *In vivo* two-photon microscopy reveals regional heterogeneity in angiogenesis and time course for recanalization of microvascular obstructions

3.0 Abstract

Vessel loss in the aging brain occurs in a regionally heterogeneous manner that is partially explained by differences in regional susceptibilities to capillary plugging using a model of microsphere-induced capillary obstructions. However, questions remain as to whether the microsphere model accurately predicts regional pruning rates in all areas, and whether there may also be compensatory vessel sprouting in some areas. Here we injected fluorescent microspheres to model capillary obstructions and used *in vivo* 2-photon microscopy to image microsphere-related and microsphere-independent changes in vascular architecture over 24 days in young adult mice. We imaged retrosplenial and visual cortex because they display different magnitudes of vessel loss and wildly different capillary obstruction rates. Surprisingly, our data indicate that there are no differences in the number of capillary pruning events between the two areas. Instead, we observed that brain region-specific differences in angiogenesis and the time course of capillary recanalization likely explain why retrosplenial cortex and visual cortex show different obstruction rates and magnitudes of vessel loss. These findings indicate that further research examining rates of angiogenesis in other areas of the brain will be required to more fully explain region-specific differences in age-related vessel loss.

3.1 Introduction

Plasticity is a hallmark of the cerebral vasculature — one that is critical to setting up vascular networks to meet ever changing brain energy demands, particularly in the case of acute vascular insults or advancing age. The loss of cerebral capillaries is one age-related challenge that the brain faces (Riddle et al., 2003; Brown and Thore, 2011). A decline in capillary density may result in reduced nutrient supply to brain tissue through 1. creation of low-oxygen pockets (Moeini et al., 2018), 2. reduction in the efficiency of oxygen delivery (by changing capillary spacing and transit times) (Lücker et al., 2018a, 2018b), and 3. contribution to age-related reductions in cerebral blood flow (CBF), all of which may negatively affect cognitive function (Nielsen et al., 2017; Cruz-Hernández et al., 2019). I argue in chapter 1 above that capillary loss occurs in a region-dependent manner and is driven by region-dependent rates in microcirculatory obstruction-induced pruning events (Reeson et al., 2018). However, the regional prevalence of these obstructions themselves is not sufficient to fully predict age-related changes in capillary density across different brain regions. For example, retrosplenial cortex experiences far less vessel loss than would be predicted by its obstruction rate. There is very little current data available that can explain variance in the relationship between vessel loss and obstruction rate. There are few, if any, reports of how other forms of vascular plasticity, such as angiogenesis and angiophagy, might differ between brain regions.

Our work in chapter 1 shows that no brain regions were completely bereft of microvascular obstructions. The fact that some areas experience almost no vessel loss at all might indicate that those areas either lose very few vessels as a result of those

obstructions, or that they still regularly lose vessels but that the decline in capillary density is counterbalanced by the sprouting of new capillaries. If capillary obstructions continue to occur but vessels are not being lost in some areas, then there must be some key brain region-specific differences in vascular plasticity. Reeson's model assumes that 30% of long-lasting obstructions result in pruning events; however capillary recanalization rates do not perfectly predict pruning rates. Reeson found that approximately half of pruning events occur after the vessel is first recanalized (Reeson et al., 2018). If the proportion of vessels that are recanalized before pruning can change between brain regions, then the number of microspheres left in the tissue at 3 days does not fully predict vessel loss. Capillaries may also be able to avoid pruning even if the natural embolus or microsphere remains near the obstruction. This is because some vessels can recanalize through a process called angiophagy, wherein the vessel is recanalized through endothelial envelopment of the embolus and subsequent extravasation of it (Lam et al., 2010; Grutzendler et al., 2014; van der Wijk et al., 2019). Reeson et al. (2018) reported its occurrence at a rate of only 2% in capillaries of the somatosensory cortex. However, if some areas have higher rates of angiophagy than others, then the presence of a microsphere in the tissue after 3 days cannot be assumed to uniformly represent a common pruning rate in all areas. We hypothesize that greater rates of angiophagy are associated with areas that have obstruction rates that predict greater-than-observed magnitudes of vessel loss.

Capillary pruning may be counterbalanced by the sprouting of new vessels in some brain regions, too. Consistent with this idea, there are reports of capillary density increasing over time through middle age (Hunziker et al., 1979; Meier-Ruge et al., 1980;

Wilkinson et al., 1981; Hinds and McNelly, 1982; Villena et al., 2003; Moeini et al., 2018), and reports of vessel sprouting or increasing capillary density in response to hypoxic conditions, stroke, and exercise (Isaacs et al., 1992; Shweiki et al., 1992; Kleim et al., 2002; Swain et al., 2003; Ding et al., 2006; Brown et al., 2007a; Ndubuizu et al., 2010; Harb et al., 2013; Gao et al., 2014; Masamoto et al., 2014; Morland et al., 2017). However, with the exception of one study that shows minor remodeling (Harb et al., 2013), direct evidence for vessel sprouting, through *in vivo* time-lapse imaging, is surprisingly lacking in healthy adult animals (>2-3 months of age) in normoxic conditions (Mostany et al., 2010; Tennant and Brown, 2013; Masamoto et al., 2014; Cudmore et al., 2017; Reeson et al., 2018). It is possible that angiogenesis is rare enough in adults that the sampling volumes were too low, and the search methods used were not exhaustive enough to detect its occurrence. For example, Reeson et al. (2018) only looked for angiogenesis near where pruning occurred. Moreover, most *in vivo* time-lapse studies tended to focus on somatosensory or motor cortex, and thus would have missed angiogenesis if it occurred at higher levels in other areas of the brain (Mostany et al., 2010; Harb et al., 2013; Tennant and Brown, 2013; Masamoto et al., 2014; Cudmore et al., 2017; Reeson et al., 2018). Unresolved issues therefore remain as to whether angiogenesis occurs at different rates in different brain areas, or even whether it occurs in healthy adult brains at all.

In this study we use longitudinal 2-photon imaging of cortical vascular networks in multiple regions in an attempt to determine whether other aspects of vascular plasticity — namely angiogenesis, pruning, angiophagy, and delayed recanalization — could help better predict brain region-specific vessel loss with aging. We installed

cranial windows on adult mice, injected 4 μm fluorescent microspheres along with a fluorescent dye intravenously to model microvascular obstructions and label patent vessels, and proceeded to image the same areas in retrosplenial, visual, and somatosensory barrel cortex over a course of 24 days, searching for differential rates of angiogenesis, angiophagy, pruning, or recanalization. Our experiments did not find compelling evidence for differences in pruning, angiophagy, or recanalization rates between brain areas; however, we identified longer recanalization times in retrosplenial cortex than in visual or barrel cortex which may explain why retrosplenial cortex shows higher obstruction densities than would be predicted by how much vessel loss it experiences. We were also the first to report time-lapse imaging evidence of regional differences in angiogenesis in the adult mouse cortex in the absence of vascular insult or challenge. Together, these findings indicate that plasticity in the adult mouse brain displays a regionally heterogeneous phenotype that must be considered to fully understand vascular aging processes.

3.2 Methods

3.2.0 Animals

We used young adult female mice (age at imaging start: 3.4-3.6 month-old; n=8) from the C57BL/6J strain and male (n=5) and female (n=2) mice (age at imaging start: 3.5-5.5 month-old) from the *Tek*-GFP (Tie-2 GFP) strain (The Jackson Laboratory, 003658). All mice were housed under a 12-hour light/dark cycle with *ad libitum* access to water and standard laboratory diet. All experiments were conducted according to the guidelines set by the Canadian Council of Animal Care and approved by the University of Victoria Animal Care Committee (protocol 2016-016). Reporting of this work complies with ARRIVE guidelines. Animal training certificate: #17-020-AC.

3.2.1 Cranial window surgeries

We anesthetized 2-month-old mice using isoflurane gas (2% initial, ~1.3% maintenance) in medical grade air and head-fixed into a custom-built surgical stage. Their body temperature was maintained at 37 degrees Celsius and mice were given both a 30 µL bolus of lidocaine subcutaneously under the scalp to reduce pain associated with an incision and a 30 µL bolus of dexamethasone intramuscularly to reduce inflammation associated with the procedure. A midline incision was made on the scalp, the scalp was retracted, and a custom circular metal ring (outer diameter 11.3 mm, inner 7.0 mm, height 1.5 mm) was attached to the skull using cyanoacrylate glue. A 4mm diameter craniotomy was performed over the visual and retrosplenial cortex (stretching just over the midline) using a high-speed dental drill, taking breaks to cool the animal’s head with chilled HEPES-buffered artificial cerebral spinal fluid to reduce

inflammation. We left the dura intact and positioned a 5mm circular glass coverslip over the craniotomy and secured the coverslip to the skull with glue and dental cement. The retracted skin was then glued to the ring and the mice were allowed to recover under a heat lamp before returning to their home cage. Mice that showed a marked drop in window clarity after a minimum of 4 weeks of recovery were excluded from imaging.

3.2.2 Intrinsic optical signal imaging

Intrinsic optical signal imaging (IOS) was used to map prospective imaging areas based on changes in cortical blood flow generated by sensory stimuli. Mice were anesthetized with isoflurane (2% induction, 1.2% maintenance), their head-rings were fixed to a custom-built stage, and their body temperature was maintained at 37 degrees Celsius using a temperature feedback regulator, rectal probe, and heating pad. Through the cranial window, the cortex was illuminated with a red LED (635nm) and sensory evoked changes in red light reflectance (changes that are thought to reflect increases in deoxyhemoglobin) were collected through a 2x objective on an upright microscope using a MiCAM02 CCD camera and Brainvision software (SciMedia). Intrinsic signals were recorded at 100 Hz with a 10ms exposure for each image. Each sensory stimulus trial consisted of recording intrinsic signals for 3 seconds total with one second of baseline before a 1 second block of sensory stimulation. Each stimulus trial was followed by an identical trial without a sensory stimulus. Each imaging set consisted of 12 stimulus/no stimulus trials with a 12 second interval between trials. All 12 trials were mean filtered (pixel radius=3), and trials were averaged together. Stimulus trials were then normalized to an average intensity projection of pre-stimulus images to generate a measure of change in reflectance relative to baseline. Finally, an average intensity

projection of post-stimulus normalized responses was generated, thresholded in image J, and superimposed onto a surface image of the brain. To generate visual cortical responses, green light (LED centered at 532nm) was presented for 1 second directed below the mouse's eye. To generate barrel cortex responses, one second of vibro-tactile stimulation, consisting of 3ms biphasic pulses generated at 40ms intervals (25Hz), was applied to the contralateral C1 whisker using a pencil lead attached to a piezo electric element.

3.2.3 Longitudinal 2-photon imaging

Mice were anesthetized with isoflurane (2% induction, 1.3% maintenance), their head-rings were fixed to a custom-built stage, and their body temperature was maintained at 37 degrees Celsius using a temperature feedback regulator, rectal probe, and heating pad. On the first imaging timepoint, mice were injected intravenously with 100µL of 4µm diameter red fluorescent microspheres (2% solids; actual size: 3.7µm; peak emission 605nm; Life Technologies FluoSpheres sulfate; ThermoFisher catalog # F8858) to model capillary obstructions and either FITC-dextran (100µL; 3% w/v in 0.9% saline; Sigma; molecular weight 70kDa, #46945), Rhodamine B dextran (100µL; 4% w/v in 0.9% saline; Sigma; molecular weight 70kDa, #R9379), or lysine fixable Texas Red dextran (for final imaging timepoint only; 100µL; 2% w/v in 0.9% saline; ThermoFisher, molecular weight 70kDa, D1864) to label patent capillaries. We acquired image stacks of the cerebral vasculature 30 minutes, 3 days, 10 days, and 24 days following microsphere injection in all mice, adding a 1-day timepoint for C57BL/6 mice. Two to three imaging areas were selected for visual cortex (located within the IOS response area), and retrosplenial cortex (as close to the midline as possible) in each animal. One

to two imaging areas were chosen in somatosensory barrel cortex in C57BL/6 mice, window clarity permitting.

The cerebral vasculature was imaged through the cranial window with a multiphoton laser scanning microscope (Olympus FV1000MPE) and a mode-locked Ti:Sapphire laser (Spectral Physics). The laser was tuned to 800nm for FITC, 900nm for the combination of GFP and Rhodamine B, or 850nm for Texas Red. Laser power measured at the back aperture or the objective typically ranged between 15 and 150mW depending on imaging depth and window clarity. Emitted light was separated by a dichroic mirror and directed through bandpass filters (495–540nm and 558–706nm). Image stacks were collected using a 20x Olympus XLUPlanFl water-immersion objective (NA = 0.95, 0.62µm/pixel) in 2µm z-steps up to a depth of 200µm in Tie-2 GFP animals and 400µm in C57BL/6 animals with Olympus Fluoview FV10-ASW software. Images were acquired with a pixel dwell time of 2µs/pixel and the image size was 1024x1024 pixels.

Following the final imaging timepoint, we induced microbleeds in each imaging area so that we could precisely relate the location of each area to stereotaxic brain coordinates. This was done by scanning a small clipped circle (diameter of just smaller than the vessel diameter) for 400 frames at a pixel dwell time of 100µs/pixel and with 100% laser power until a plume of fixable Texas Red was observed in the extravascular space. Mice were killed from an overdose of sodium pentobarbital and transcardially perfused with 0.1M PBS and then with 4% PFA. The brain was extracted, immersed in 4% PFA overnight, transferred into 0.1M PBS, and then sectioned on a Leica vibratome (T1000) to make 50µm-thick coronal sections. Every second slice was mounted and

microbleeds were found to verify imaging area locations using a Cy3 filter set on an Olympus BX51 microscope.

Four C57BL/6 mice were imaged longitudinally for 24 days without microspheres before three of them received microsphere injections and were subsequently imaged for an additional 24 days. This was done to determine whether angiogenesis would occur without a vascular insult. In these animals, we only looked for natural angiogenic and pruning events for the first 24 days.

3.2.4 Collagen IV immunohistochemistry

Every 2nd 50µm-thick coronal section from 5 of the C57BL/6 animals above, containing microspheres 24 days after injection, was first washed for 10 minutes in 0.1M PBS, then antigen retrieval was completed by bathing slices in sodium citrate buffer (10mM, pH=6.0) for 40 minutes in a 75-degree water bath. Slices were then incubated for 90 minutes in 0.1M PBS+0.2% TX-100 and 2% BSA, then incubated in polyclonal goat anti Collagen 4 primary antibody (1:100 stock concentration; Millipore, AB769) in 0.1M PBS with 0.1% TX-100 for 40-48 hours at 4 degrees on a shaker. Next slices were washed three times (5 minutes each) in 0.1M PBS and incubated with a 488-conjugated IgG anti-goat secondary antibody (1:500 stock concentration) in 0.1M PBS for 4 hours at room temperature. Slices were finally washed three more times (5 minutes each) in 0.1M PBS before being mounted onto a gel-coated slide and cover-slipped with Fluoromount G (ThermoFisher, 00-4958-02). Collagen IV was visualized using a 488nm laser (emitted light passed through 505-540nm emitter filter) and microspheres were excited with a 561nm laser (575-620nm emitter filter) on an Olympus confocal microscope with a 40x objective (NA 0.95). Images were collected at a resolution of

0.155μm/pixel with 1μm z-steps. We acquired image stacks of all microspheres within the bounds of retrosplenial cortex and all those within the bounds of somatosensory forelimb cortex, as determined by **Figure 2.1A** in chapter 1, for a total of 29 microspheres sampled in the retrosplenial cortex and 36 sampled in somatosensory cortex. Microspheres were classified by a blinded observer into three categories. They were determined to be associated with a string vessel if the microsphere was found adjacent to a collapsed capillary no wider than 2μm in diameter. If microspheres were not associated with string vessels, they were further classified as still blocking the vessel if the microsphere appeared in contact with both edges of the capillary's Collagen IV staining, and as a possible instance of angiophagy if there was a visible space between the microsphere and the border of the Collagen IV staining.

3.2.5 Analysis of obstruction, recanalization, pruning, and angiogenic events.

Data on microsphere density *in vivo* was determined as the sum of all subsurface microspheres per sampled volume at a given timepoint, normalized to the approximate vascular length for that area determined in chapter 1. Barrel cortex density was estimated with forelimb somatosensory cortex density from chapter 1. Vessels in some portions of an imaging area could be difficult to visualize due to window degradation or light scattering by large pial vessels. Microspheres were counted regardless of whether they could be clearly localized to a vessel. Recanalization was defined as the disappearance of a microsphere that was previously lodged in a given subsurface capillary. If the microsphere was not clearly localized to a visible capillary, the disappearance of a microsphere from the area where it previously resided was

classified as recanalization. Recanalization rates for microspheres was calculated for all microspheres that were present within an image stack at any timepoint before day 24. Recanalization rates were also assessed separately for microspheres that were present only at day 0 and recanalized by 3, 10, and 24 days. If there was doubt about whether a microsphere was present or not, due to changes in the window conditions, that microsphere was excluded from analysis for that timepoint. A proportion of microspheres never washed out. We broke down the fate of these no-washout events, classifying them by whether they pruned or not. Those that never washed out but also never pruned were considered evidence for angiophagy. If the vessel and its surroundings could not be visualized at the final timepoint and no clear pruning event occurred prior to the final timepoint, we classified that event in a third category, which we called “Unknown”.

Any vessel obstructed by a microsphere was followed through subsequent imaging timepoints. This was done to determine whether the proportion of obstructed vessels that resulted in a pruning event could be different in separate brain areas. If a vessel was visible at one timepoint but disappeared (i.e. no evidence of blood plasma filling the lumen as indicated by intravascular fluorescent dextran presence) at any subsequent timepoint and never reappeared, that vessel was considered to have been pruned. For the pruning analysis, we only considered vessels in portions of the imaging window that remained clear for all 24 days or until a pruning event took place. In addition to measuring the proportion of obstructed vessels that were pruned, we also measured the number of obstruction-related pruning events, normalized to the vascular density (m/mm^3), to occur over 24 days. This metric is sensitive to differences in both

obstruction and pruning rates, and therefore is most predictive of a change in vessel density with age. Finally, we broke down all pruning events by whether they occurred before microsphere washout, or whether pruning occurred before washout was possible. If the microsphere and vessel disappeared between the same two imaging timepoints, we classified the pruning event as “Unknown”.

We also conducted a survey for pruning and angiogenic events that were not associated with microspheres. This was done by comparing each vessel in an imaging stack at the second post-injection day to that same vessel at the final imaging timepoint, and vice versa. If a vessel existed at the first timepoint but not at the last one, it was considered a pruned vessel. Conversely, if a vessel existed at the final timepoint but not the first one, it was considered an angiogenic event. To facilitate analysis, image stacks were binned in the z-dimension by maximally projecting 20 images (40µm bins). Sampling volume was limited to an ROI that encompassed all vessels that were visible at both timepoints. Instances of pruning and sprouting were counted and normalized to the sampled volume and vascular density in each area (m/mm^3). For each pruning/angiogenic event, we measured the two-dimensional vessel length, the depth below the surface of each vessel endpoint, and whether the vessel was flowing at any timepoint. 3-dimensional length was approximated by modeling the capillary length as a vector with the vertical component consisting of the z-axis difference between the capillary endpoints, and the horizontal component consisting of the measured 2-dimensional vessel length. The capillary depth was calculated as the depth below the surface of the midpoint between each capillary endpoint. Pruning or angiogenic vessels that had streaking RBCs in the capillary lumen at any time, indicated by changes in

fluorescent-negative space, would have been classified as “flowing”. Pruning events that started with, or angiogenic events that ended with, a vessel filled with dye that was attached at both endpoints but lacking streaking RBCs was classified as “unsure”. If pruning events did not start with, or angiogenic events did not end with, vessels attached at both endpoints to other vessels, the event was classified as “incomplete”.

Topographic heat maps were constructed using a custom macro built for FIJI (ImageJ). Briefly, rectangles with shades corresponding to event prevalence for each imaging area (for C57BL/6 mice only) were overlaid onto a single model brain. Where overlap existed between imaging areas, the shaded area value was determined by calculating the average event prevalence for all overlapping imaging areas.

3.2.6 Statistics

All statistical analyses were performed using GraphPad Prism 8 using an alpha value of 0.05. Since microsphere obstruction in each capillary is a semi-random event and given our limitations on how much volume we can sample in 2-photon imaging, sampling of microspheres tended to be highly variable between animals and imaging timepoints. Since values of 0 were common and proportions for many values were based on sampling very few microspheres in an animal (sometimes 0, depending on the timepoint), the sampling distribution for variables is often not normally distributed and there was too much variance on an animal to animal basis to draw meaningful trends from the data. To optimize erratic and low sampling of microspheres, we treated each microsphere obstruction event as an independent event, pooled the events in each brain from all animals, and compared proportions between areas using Chi-squared

analyses. These data are either presented as pooled (with no variance), and as connected points showing variance between animals.

For instances of angiogenesis and pruning separate from microspheres, data showed more of a normal distribution. For repeated measures data, two-way mixed ANOVA or one-way repeated measures ANOVA was used when there were no missing values, while a mixed model was fitted to the data (using Restricted Maximum Likelihood) when there were missing values in the dataset. Where the assumption of sphericity was not met, the Geisser-Greenhouse correction was used. Post-hoc comparisons were performed using paired t-tests for repeated measures analyses. Data are presented as connected points when multiple points represent the same animal, and as mean ± 95% confidence interval (CI) for depth and length measurements in **Figure 3.5**.

3.3 Results

3.3.0 Capillary obstruction rates are higher in retrosplenial and barrel cortex than visual cortex 3 days post-microsphere-injection

To examine the possibility that there might be region-specific differences in the time course of recanalization and pruning following micro-circulatory obstruction, we chose to compare vascular networks *in vivo* in two cortical areas that showed different profiles of microvascular obstruction and vessel loss in chapter 1: visual cortex and retrosplenial cortex. The visual cortex was of interest because it showed virtually no vessel loss with aging. By contrast, the retrosplenial cortex showed an unusually high propensity for capillary obstructions, yet experienced modest vessel loss with aging. First, we installed cranial windows on young adult mice, mapped out visual cortex using IOS imaging (**Fig. 3.0B**), and intravenously injected 4µm diameter red microspheres to model capillary obstructions (Reeson et al., 2018). We proceeded to use high resolution 2-photon microscopy to image large volumes (**Fig. 3.0C**) of vasculature in each of those two areas, and in barrel cortex where possible, over the course of 24 days (**Fig. 3.0A**). Microbleeds were subsequently used to find imaging areas *post-mortem* (**Fig. 3.0D**). Finally, we verified that dysgranular retrosplenial cortex, the part of retrosplenial cortex that we were able to image, displayed similar histological trends (in vessel loss, obstruction, and clearance rates) to granular retrosplenial cortex, reported in chapter 1 (**Fig. 3.0E**).

Since retrosplenial cortex was shown in chapter 1 to experience an abnormally high number of microvascular obstructions than visual cortex, we counted the number of

microspheres in each imaging area at each timepoint (see white arrows in **Fig. 3.1A**), and normalized to the microvascular density (m/mm^3) for each area (**Fig. 3.1B,D**). We found that when we used each animal's *in vivo* obstruction data to run a mixed statistical analysis (2-Way RM-ANOVA, timepoint and area both within-subject variables), there was no area-related preference for obstruction density at any timepoint (**Fig. 3.1C**; Mixed model two-way RM-ANOVA, main effect of Area: $F_{(1.949, 25.34)}=0.8507$, $p=0.4364$); Area-time interaction $F_{(1.944, 10.69)}=0.4882$, $p=0.6217$). However, since we were able to sample very few obstructions (especially after the 30-minute timepoint) in some animals, which greatly exaggerated between animal variances, we decided to group obstructions in all animals together to look for trends (**Fig. 3.1E**). For this reason, I will continue to report animal averages, but statistics will be restricted to analysis of proportions (i.e. compare between areas, using a chi-square analysis, the proportion of all vessels that are obstructed, or proportion of all obstructions that are recanalized or pruned). We estimated the number of vessels sampled in each area using the volume and the vascular density from **Figure 3.1D**, and assuming an average capillary length of 60µm, supported by unpublished data from our lab. A test of the proportion of all vessels that were plugged by a microsphere revealed higher obstruction rates in retrosplenial cortex and barrel cortex than in visual cortex (referred to as RS, S1B, and V1, respectively in **Fig. 3.1E**), but only at the 3-day timepoint (retrosplenial: $\chi^2_{(1)}=12.38$, $p=0.0004$; barrel: $\chi^2_{(1)}=5.315$, $p=0.0211$). Retrosplenial cortex and barrel cortex were also more likely than visual cortex to experience obstructions that stayed in the same capillary for more than one timepoint (see "multiple timepoints" in **Fig. 3.1E**; retrosplenial: $\chi^2_{(1)}=7.096$, $p=0.0077$; barrel: $\chi^2_{(1)}=4.253$, $p=0.0392$). As shown by the

topographical heat maps in **Figure 3.1F**, there are region and time point-specific changes in obstruction densities. These data indicate a preference for capillary obstruction in retrosplenial and barrel cortex at 3 days, but not at 30 minutes. Visual examination, but not chi-squared analyses, indicates that the preference for stalling may continue to a lesser extent 10 and 24 days after microsphere injection in retrosplenial cortex, barrel cortex, and anterior areas of visual cortex.

Figure 3.0. Timeline and methodology of 2-photon imaging experiment.

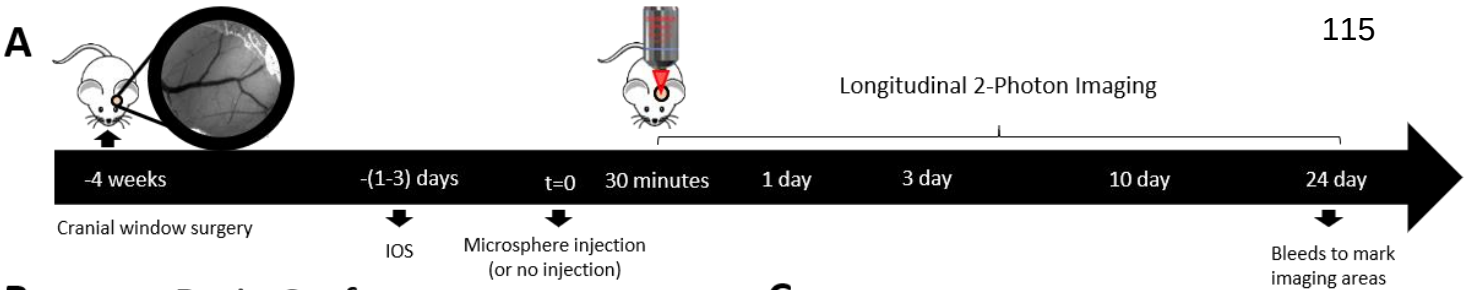

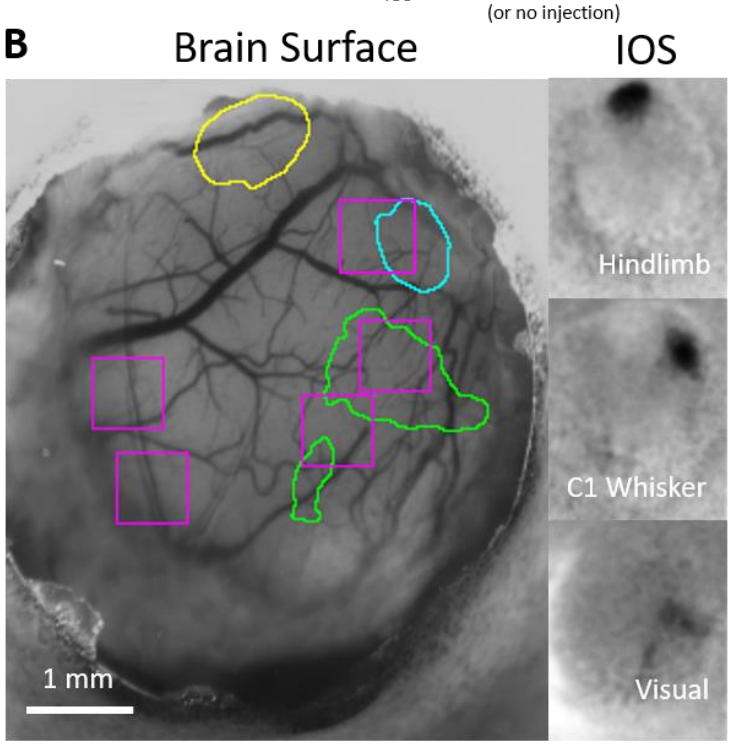

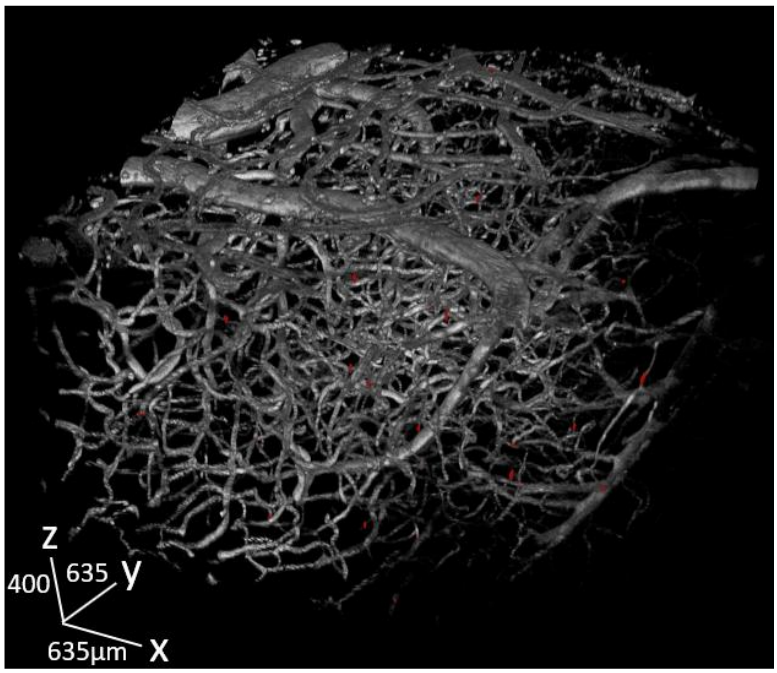

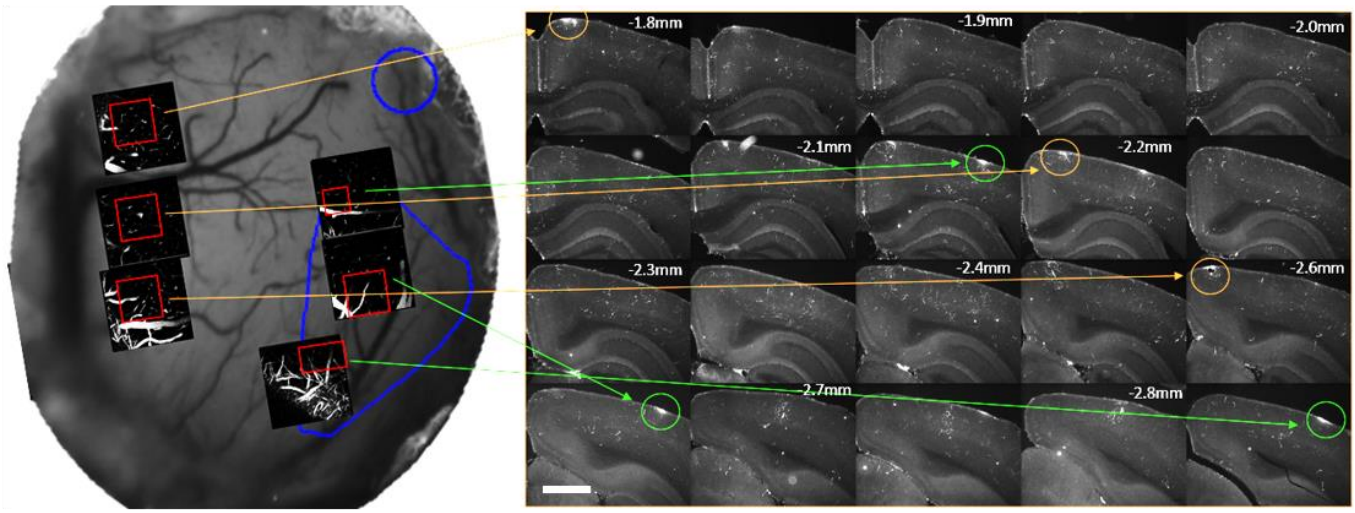

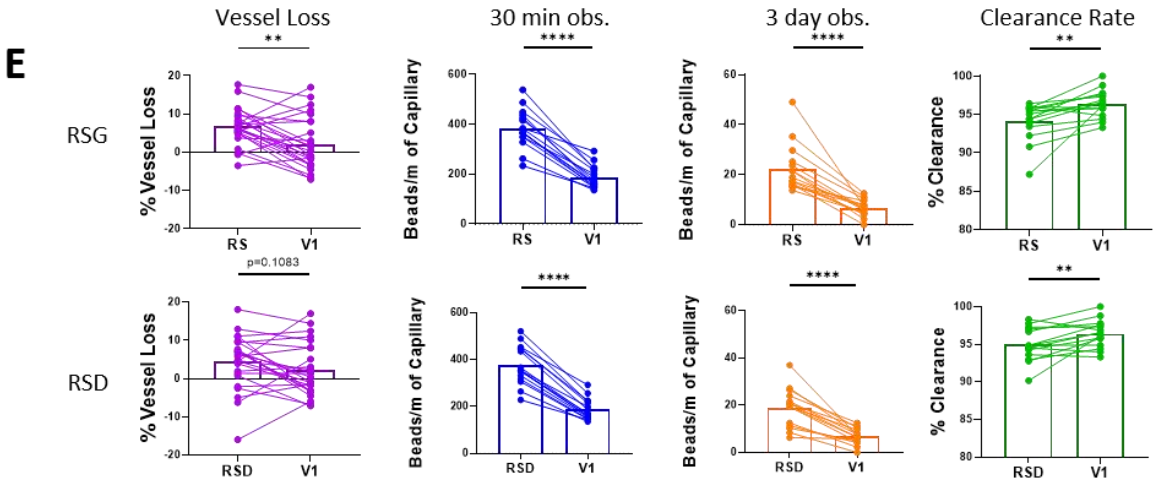

Figure 3.0. Timeline and methodology of 2-photon imaging experiment. (**A**) Timeline for imaging experiments, including imaging timepoints. (**B**) Example of intrinsic optical signal (IOS) responses following sensory stimulation and examples of how those responses guide the choosing of imaging areas. (**C**) 3-dimensional reconstruction of a typical imaging area with FITC dextran marking plasma. Imaging volumes measured approximately 636x636x400µm. (**D**) Example of how we used Lysine-fixable Texas Red dextran to find imaging areas *post-mortem*. Stereotaxic levels were approximated based on visual similarity to Franklin and Paxinos brain atlas (Franklin and Paxinos, 2008). (**E**) Comparison between visual cortex and either granular (RSG) or dysgranular (RSD) retrosplenial cortex for histological measures of vessel loss, obstruction rates, and clearance rate. Note that RSD shows similar trends in all histological measures as RSG. ****$p < 0.0001$, ***$p < 0.001$, **$p<0.01$, *$p<0.05$.

Figure 3.1. Preference for microsphere obstruction in retrosplenial cortex after 3 days, but not 30 minutes.

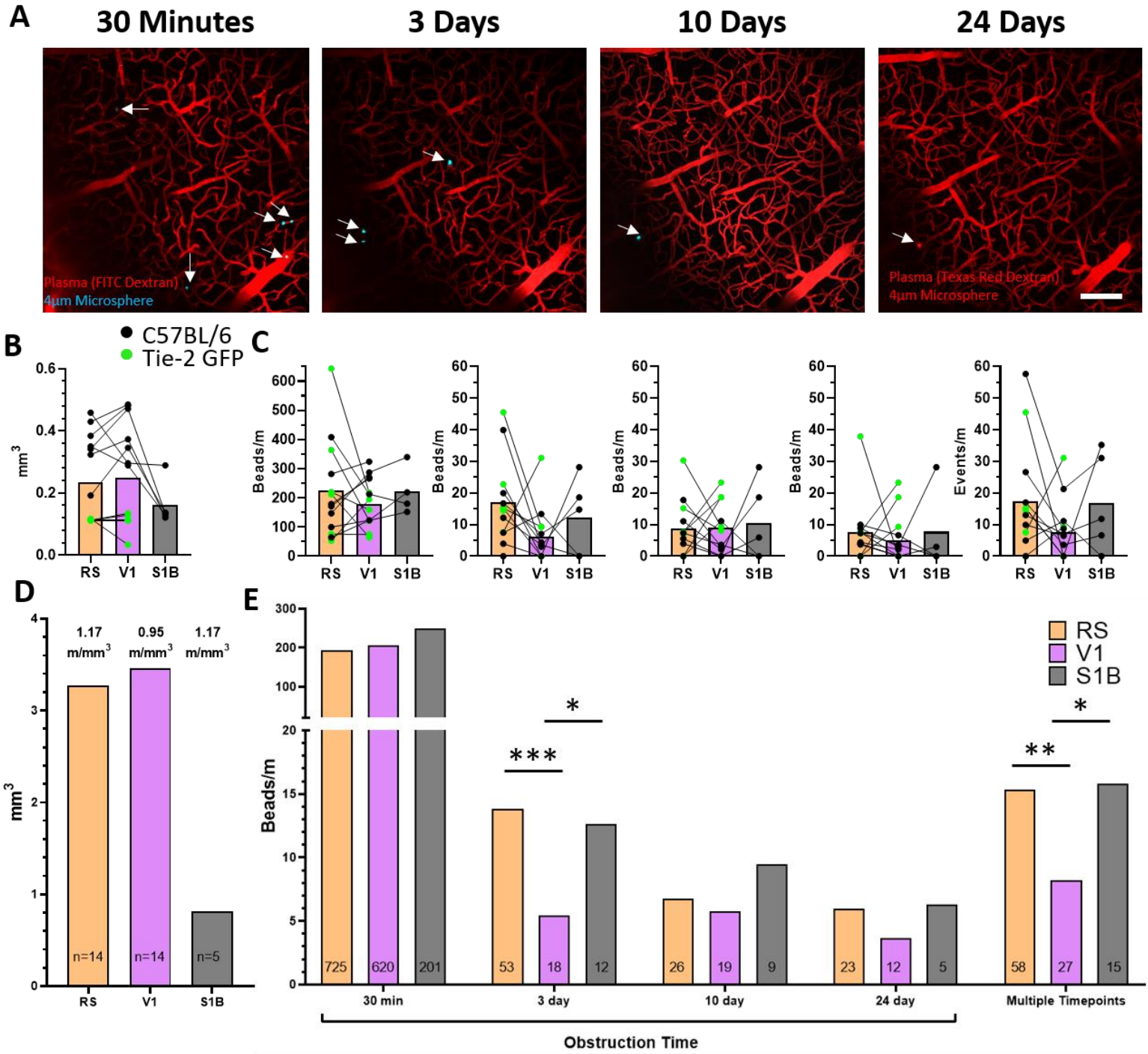

Figure 3.1. Preference for microsphere obstruction in retrosplenial cortex after 3 days, but not 30 minutes. (**A**) Example 100µm maximum z-projections showing microspheres in capillaries at each time point. Each white arrow points to a microsphere. (**B**) and (**D**) show animal totals and pooled total, respectively, of the volume sampled to determine obstruction, recanalization, and pruning rates involving microspheres. (**C**) Animals totals and (**E**) pooled totals of the number of obstructions in each area at any given timepoint, expressed as number of microspheres per metre of vasculature. Writing in the bars notes the total number of microspheres sampled. Green points are Tie-2 GFP (*Tek*-GFP) animals and black points are C57BL/6 animals. Three comparisons for each time point were carried out using Chi-squared tests comparing proportions. For tests of proportion of obstructed vessels, total number of vessels was estimated using the sampled volume, vascular densities of 1.17 and 0.95 for retrosplenial/barrel and visual cortex, respectively, and an average capillary length of 60µm. For a vessel to be counted in the multiple timepoints comparison, it had to be obstructed with a microsphere for at least two consecutive imaging timepoints. (**F**) Topographical heat maps of microsphere density. Density for every area was overlaid on a single model brain and average values were calculated where overlap existed. Scale bar in A: 100µm. Scale bar in F: 1mm. ****$p < 0.0001$, ***$p < 0.001$, **$p<0.01$, *$p<0.05$.

3.3.1 Obstructions in retrosplenial cortex take longer to recanalize than those in visual cortex

A plausible explanation for why retrosplenial cortex shows more obstruction events at three days than visual cortex, but that obstruction preference weakens thereafter, is that obstructions may simply take longer to recanalize in retrosplenial cortex. To answer the question of whether recanalization could differ between areas, we looked at the time-course for recanalization of capillaries that were obstructed at day 0. Although we found no difference between absolute recanalization rates between areas (i.e. they all had similar proportions of capillaries that never recanalized after obstruction) (See “any time” in **Fig. 3.2A,B**), we found that a higher proportion of capillaries, initially obstructed at 30 minutes, recanalized by 3 days in visual cortex than retrosplenial cortex (**Fig. 3.2B**; $\chi^2_{(1)}=4.227$, $p=0.0398$). However, this preference was abolished by 10 ($\chi^2_{(1)}=0.6529$, $p=0.4191$) or 24 days ($\chi^2_{(1)}=0.1604$, $p=0.6888$). These results suggest that capillaries in some areas, such as in retrosplenial cortex, may take longer to recanalize than in others, which may help explain why a region with an exceptionally high obstruction density (at 3 days) would not also necessarily show unusually high vessel loss with aging.

Figure 3.2. Little evidence for differences in angiophagy, but capillaries in retrosplenial cortex take longer to recanalize than those in visual cortex.

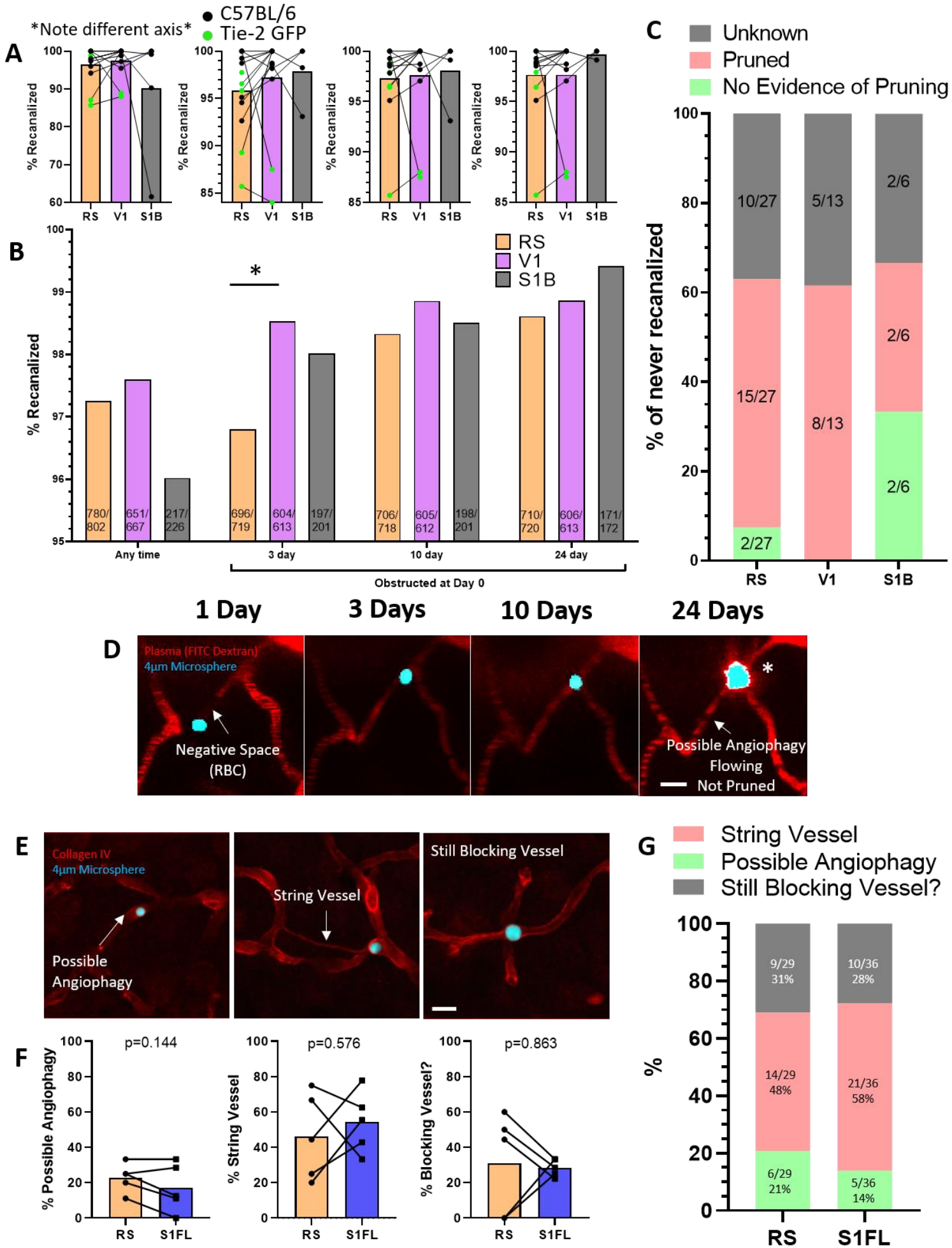

Figure 3.2. Little evidence for differences in angiophagy, but capillaries in retrosplenial cortex take longer to recanalize than those in visual cortex. (**A**) Animal totals and (**B**) pooled totals of the proportion of obstructions that occurred at any time point and subsequently recanalized (left) and the proportion of microspheres obstructed at 30-minutes that recanalized by 3 days, 10 days and 24 days post-injection. Writing in the bars notes the total number of microspheres recanalized and the total number sampled. Green points are Tie-2 GFP (*Tek*-GFP) animals and black points are C57BL/6 animals. (**C**) Breakdown of the fates of all microspheres that were never washed back into circulation. Microspheres were classified as Unknown if no clear pruning event occurred and the vessel could not be visualized well on day-24. (**D**) ~50µm maximum z-projection of a capillary with a microsphere that never washed out, but that regained flow, as evidenced by streaking RBCs (white arrow in right panel). (**E**) ~10µm maximum z-projections from Collagen IV immunostaining (red) around microspheres (blue). Left panel (white arrow) shows an example of space between the microsphere and basement membrane, leading to the classification of possible angiophagy. Middle panel white arrow points to a string vessel associated with the microsphere. Right panel contains an example of the microsphere touching the basement membrane on both sides, leading to a classification of potentially still blocking the vessel. (**F**) Animal totals comparing forelimb somatosensory cortex with retrosplenial cortex for each possible classification. (**G**) Breakdown of the classification of all microspheres in both areas. Only the proportion of string vessels was compared between areas. Chi-squared tests comparing proportions were used in A, C, and G. Paired t-tests were used in F. Scale bar in D and E: 10µm. ****$p < 0.0001$, ***$p < 0.001$,

**p<0.01, *p<0.05. White asterisk in images (*) shows when a microsphere that was originally in another channel was pseudo-coloured blue for the sake of clarity

3.3.2 No strong evidence for regional heterogeneity in angiophagy-like events in capillaries

Differing rates of angiophagy between brain areas might help to explain why there is not a perfect relationship between vessel loss and obstruction rate. Nowhere is the disconnect between those two variables as great as it is in retrosplenial cortex. Somatosensory cortex is known to have very low rates of angiophagy in capillaries (~2% of obstruction events recanalized by angiophagy) (Reeson et al., 2018), but perhaps retrosplenial cortex has a higher incidence of these events than other brain regions. To determine whether there were differences in the rates of angiophagy between brain areas, we examined the fate of obstructions that were never recanalized in our 2-photon imaging. While most capillaries that never washed out (i.e. the microsphere was still present at day 24 or until the pruning event took place) were pruned, a small proportion never experienced a pruning event. As shown previously by Reeson *et al*., instances where capillaries were never recanalized (i.e. the microsphere was still present) but also not pruned were rare (4/29 obstructed capillaries that were visible for all 24 days; **Fig. 3.2C**). Though there may be a trend for more of these events (that could be attributable to angiophagy) occurring in barrel cortex, too few instances of capillary recanalization failure were observed to determine whether differences exist between areas (**Fig. 3.2C**). It should be noted that we did not have the z-resolution to determine whether these microspheres were located outside of the capillary lumen, but given that flow was regained in the capillaries (see white arrow identifying streaking in **Fig. 3.2D**) and that pruning never took place, the most likely explanation is that these microspheres had been engulfed and extravasated.

In an effort to increase sampling of microspheres that were never washed out, we also used Collagen IV immunohistochemistry to look for possible cases of angiophagy *post-mortem*. Since Reeson et al. (2018) showed that angiophagy was rare in somatosensory cortex and since somatosensory cortex experiences a similar magnitude of vessel loss but different obstruction rates than retrosplenial cortex, we hypothesized that there would be more angiophagy in retrosplenial cortex than somatosensory cortex. We decided to look at somatosensory cortex, and not visual cortex, because somatosensory cortex has a similar magnitude of vessel loss as retrosplenial cortex, but just experiences fewer obstructions. Although we could not find evidence of microspheres completely outside of the capillary lumen, we instead compared the fraction of microspheres in each area that were associated with a string vessel (**Fig. 3.2E**, middle panel), where a string of collapsed basement membrane remains following a pruning event. We further classified microspheres that were not associated with a string vessel as “possible angiophagy” if there was some evidence of space between the microsphere and the vessel basement membrane (**Fig. 3.2E**, left panel), or “still blocking vessel?” if no clear space existed between the microsphere and the basement membrane (**Fig. 3.2E**, right panel). We reasoned that if there were differences in angiophagy rates, there should be a difference in the proportion of microspheres associated with string vessels. However, neither animal totals (**Fig. 3.2F**) or total proportions of event frequency across all animals (**Fig. 3.2G**) indicate large between-area differences in either the proportion of possible angiophagy events or the proportion of instances where a microsphere was associated with a string vessel. This suggests that somatosensory and retrosplenial cortex likely do not exhibit differences in

the rates of angiophagy or pruning events in microspheres that never wash out. Although these results do not discount the possibility that there may be region-specific differences in angiophagy rates elsewhere in the brain, they also provide no strong evidence for a large number of them in retrosplenial cortex, where we might have expected to see more.

3.3.3 Area-specific pruning rates do not explain previously reported differences in vessel loss between visual and retrosplenial cortex

In chapter 1, we found that the magnitude of vessel loss was greater in the retrosplenial cortex than the visual cortex. The simplest explanation, and the one we proposed in chapter 1, is that the retrosplenial cortex experiences more obstructions, and thus more pruning events, than the visual cortex. However, two findings above could complicate that hypothesis. First, we found that capillaries in retrosplenial cortex take longer to recanalize than in visual cortex. And second, we found that there are no clear differences between microsphere densities in those areas at 10 or 24 days. If visual and retrosplenial cortex have similar microsphere densities at 10 and 24 days, then it is still unclear as to why retrosplenial cortex displays a larger magnitude of vessel loss than visual cortex. We have shown above that these two areas show similar rates of pruning for vessels that never wash out after microsphere obstruction; however, it is important to note that previous work from our lab has shown that if a capillary becomes obstructed and later recanalizes and regains flow, it is still at risk of being pruned at a later timepoint. If the proportion of capillaries that prune after recanalization can differ between regions, it might explain why we observed differences in vessel loss despite

our observations concerning recanalization times and obstruction density at 10 and 24 days.

In order to more fully address this possibility, we assessed the fraction of all obstruction events that lead to a pruning event (including both vessels that recanalized first, and never recanalized), and then broke pruning events down by whether they recanalized first or not. Also, to predict vessel loss, you need to consider obstruction rates as well as the proportion of obstructions that prune; therefore, we also quantified the number of pruning events in each brain region that result from our dose of microspheres, which is a metric that accounts for both factors. We did not find any statistically significant differences between areas in the proportion of all obstructions (occurring at any timepoint) that resulted in a pruning event (**Fig. 3.3A,B**, leftmost comparison). Although the presence of a microsphere at later timepoints was (not surprisingly) correlated with higher probabilities of vessel pruning, we also found no differences between areas in the proportion of vessels pruned that were obstructed at 30 minutes, 3 days, 10 days, or in those vessels obstructed for multiple imaging timepoints (**Fig. 3.3A,B**). Even if there are no differences in pruning rates detectible using our methods, it's still possible that slight differences in obstruction rates might result in more pruning events in retrosplenial cortex than in visual cortex. We therefore compared the number of pruning events in each brain region resulting from our injection of microspheres. We found a trend for more pruning events in retrosplenial and barrel cortex than in visual cortex. However, this trend did not reach statistical significance in either area when compared with visual cortex (**Fig. 3.3C,D**; retrosplenial cortex: $\chi^2_{(1)}=2.126$, $p=0.1448$; barrel cortex: $\chi^2_{(1)}=0.1883$, $p=0.6643$). Consistent with a trend for

more pruning events in retrosplenial and barrel cortex than visual cortex, a topographical heat map of the total number of pruning events reveals a trend for posterior areas of visual cortex to show fewer microsphere-triggered pruning events (darker shades of gray and black) relative to more anterior and medial areas of cortex (**Fig. 3.3E**).

Further analysis of animal averages revealed a possible strain-effect. Specifically, Tie-2 GFP mice showed a higher proportion of obstructions that result in pruning events (**Fig. 3.3A**) and a higher total number of pruning events resulting from a dose of microspheres (**Fig. 3.3C**). There does not, however, appear to be clear interaction between strain and brain region affecting proportion of obstructions pruned (2-way mixed ANOVA mixed model; main effect of strain: $F_{(1, 22)}=9.173$, $p=0.0062$; interaction: $F_{(1, 22)}=1.457$, $p=0.2402$) or total pruning events (2-way mixed ANOVA mixed model; main effect of strain: $F_{(1, 22)}=4.582$, $p=0.0436$; interaction: $F_{(1, 22)}=0.4108$, $p=0.5282$).

We examined capillaries that had been pruned to determine whether there were region-specific differences in the proportion of pruned capillaries that were never recanalized before pruning (**Fig. 3.3F**, middle panel) or those that were recanalized before pruning (**Fig. 3.3F**, bottom panel). Of note, we were unable to determine whether recanalization happened before pruning in a subset of vessels (**Fig. 3.3F**, top panel). We found no evidence for region-specific differences in the proportion of vessels that are recanalized before pruning in the regions of cortex that we were able to sample (**Fig. 3.3G**). Collectively, these results do not reveal a clear brain-region specific difference in the number of pruning events. However, it is important to recognize that

the low frequency of these pruning events and wide variability in pruning frequency between animals greatly reduced our power for detecting significant differences between brain regions.

Figure 3.3. Frequency of pruning events and proportion of vessels pruned after recanalization does not differ between areas.

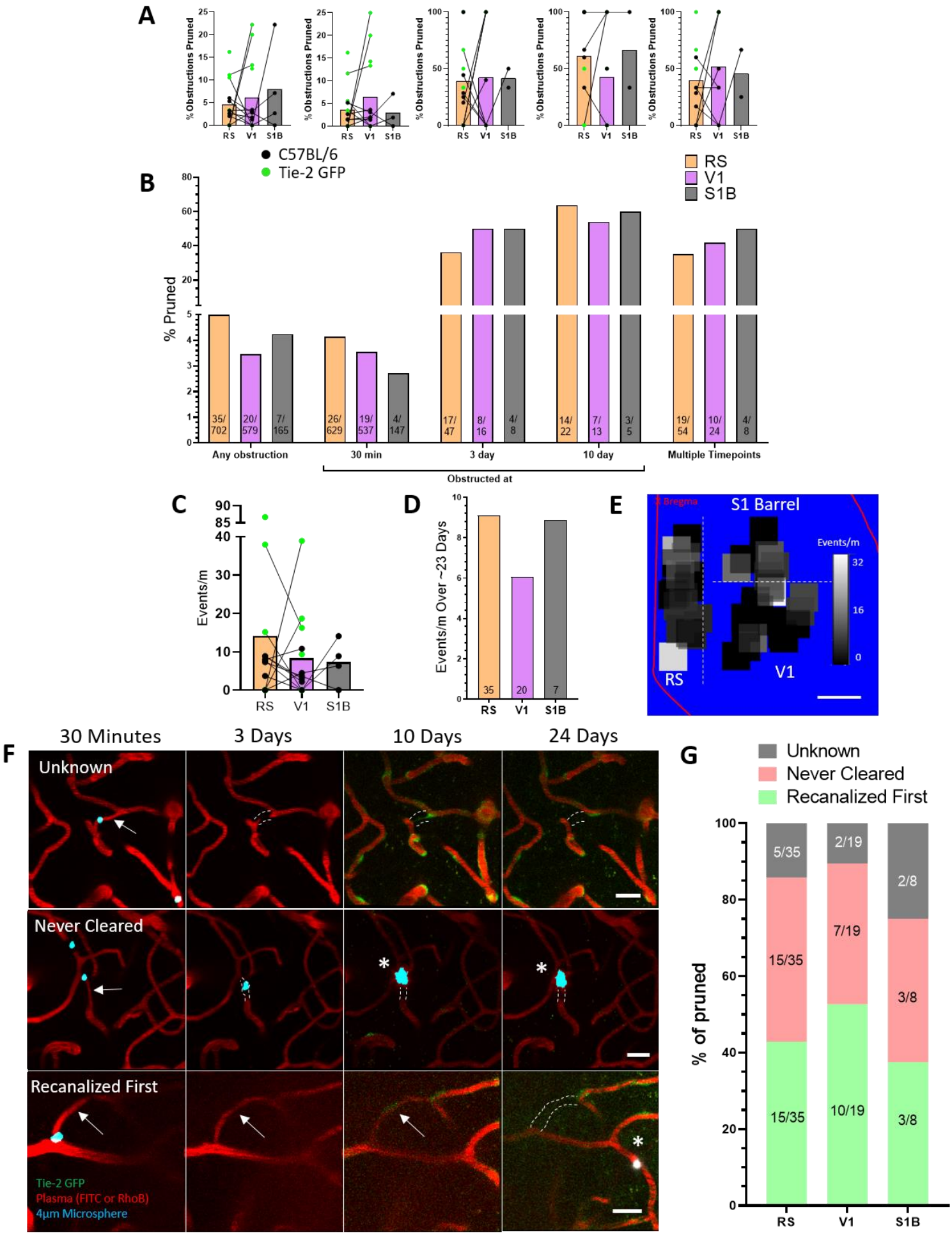

Figure 3.3. Frequency of pruning events and proportion of vessels pruned after recanalization does not differ between areas. (**A**) and (**B**) show animal totals and pooled total, respectively, of the fraction of microsphere obstruction events that resulted in pruning of a vessel. From right to left, microsphere-containing vessels were categorized as obstructed at any time point (except 24 days), obstructed at 30 minutes, obstructed at 3 days, obstructed at 10 days, and obstructed for a minimum of 2 consecutive time points. (**C**) Animal totals and (**D**) pooled total of number of microsphere-related pruning events resulting from a single microsphere injection. Values expressed as number of pruning events per metre of vasculature. Green points are Tie-2 GFP (*Tek*-GFP) animals and black points are C57BL/6 animals. Values written in bars in C show number of total pruning events. (**E**) Topographical heat maps of microsphere density. Density for every area was overlaid on a single model brain and average values were calculated where overlap existed. Note possible trend for darker values in visual cortex (lateral and posterior areas). (**F**) ~50µm maximum z-projections of pruning capillaries in 3 conditions. Bottom panel shows capillary pruned after recanalization (see white arrow and dashed lines to see vessel). Middle panel shows capillary that was never recanalized being pruned (see white arrow and dashed lines to see vessel). Top panel shows an example of an Unknown classification, as it is unclear whether pruning of the vessel (white arrow and dashed lines) started before or after recanalization. (**G**) Figure shows proportions of all pruning events that were recanalized (or not) before pruning. Chi-squared analyses of proportions were used for A, C, and G. For C, pruned proportion of total number of vessels was estimated using the sampled volume, vascular densities of 1.17 and 0.95 for retrosplenial/barrel and visual cortex,

respectively, and an average capillary length of 60μm. Scale bar in E: 1mm. Scale bars in F: 20μm. White asterisk in images (*) shows when a microsphere that was originally in another channel was pseudo-coloured blue for the sake of clarity.

3.3.4 Visual cortex exhibits more angiogenesis than retrosplenial or barrel cortex

Thus far, we have not found a clear difference in pruning rates between retrosplenial and visual cortex that wold explain why the former (retrosplenial) region shows moderate vessel loss with aging whereas the latter region (visual) does not. The simplest explanation for why visual cortex might experiences less microvascular loss is that it experiences higher rates of sprouting angiogenesis than retrosplenial cortex. To test this hypothesis, we carefully examined large volumes of cortical vasculature in different brain regions in the Tie-2 GFP mice with microsphere injections and C57BL/6 mice that had received (n=4) or had not received (n=4) microsphere injections. We found clear instances of angiogenesis in the cortex over 21 (Tie-2 GFP) and 23 (C57BL/6) days of imaging (**Fig. 3.4A**). **Figure 3.4B** shows the topographic organization of these angiogenic events and the sampling frequencies for imaging areas in C57BL/6 mice (left panel). When the number of angiogenic events was normalized to the sampled volume (right panel), we discovered that angiogenesis occurs in a medial to lateral (low-high) gradient in the posterior part of the cortex. Natural pruning events, those not associated with microspheres, were also observed. When we binned the events by brain region, we found no differences between areas in the density of pruning events (**Fig. 3.4C,D**; Mixed model equivalent of one-way repeated measures ANOVA in C57BL/6 mice: $F_{(1.015, 5.074)}=0.9415$, $p=0.3775$; paired t-test in Tie-2 GFP mice: $t_{(4)}= 0.2308$, $p=0.8288$). However, consistent with the topographic map of angiogenesis, we found a significant effect of brain region on density of angiogenic events in C57BL/6 mice (**Fig. 3.4C**; Mixed model equivalent of one-way repeated measures ANOVA:

$F_{(1.865, 9.326)}$=8.949, p=0.0073), though not in Tie-2 GFP mice (**Fig. 3.4D**; paired t-test: $t_{(4)}$= 1.000, p=0.3739). Post-hoc paired t-tests in C57BL/6 mice revealed a significantly higher rate of angiogenesis in visual cortex than retrosplenial cortex ($t_{(6)}$= 3.706, p=0.0100). A comparison of the angiogenic rates in barrel cortex and visual cortex also trended toward statistical significance (visual > barrel: $t_{(3)}$= 3.173, p=0.0504). Microsphere injection had no detectable effect on rates of pruning (Mixed model equivalent of two-way repeated measures ANOVA; main effect of microspheres: $F_{(1, 6)}$=0.1143, p=0.7469; microsphere-area interaction: $F_{(1, 5)}$=1.174, p=0.3280) or angiogenesis (Mixed model equivalent of two-way repeated measures ANOVA; main effect of microspheres: $F_{(1, 6)}$=0.6844, p=0.4397; microsphere-area interaction: $F_{(1, 5)}$=0.5405, p=0.4953) in C57BL/6 mice. These results indicate that region-specific differences in rates of angiogenesis may affect changes in vascular density with age.

Figure 3.4. Angiogenesis in visual cortex predicts increases in vascular density over time.

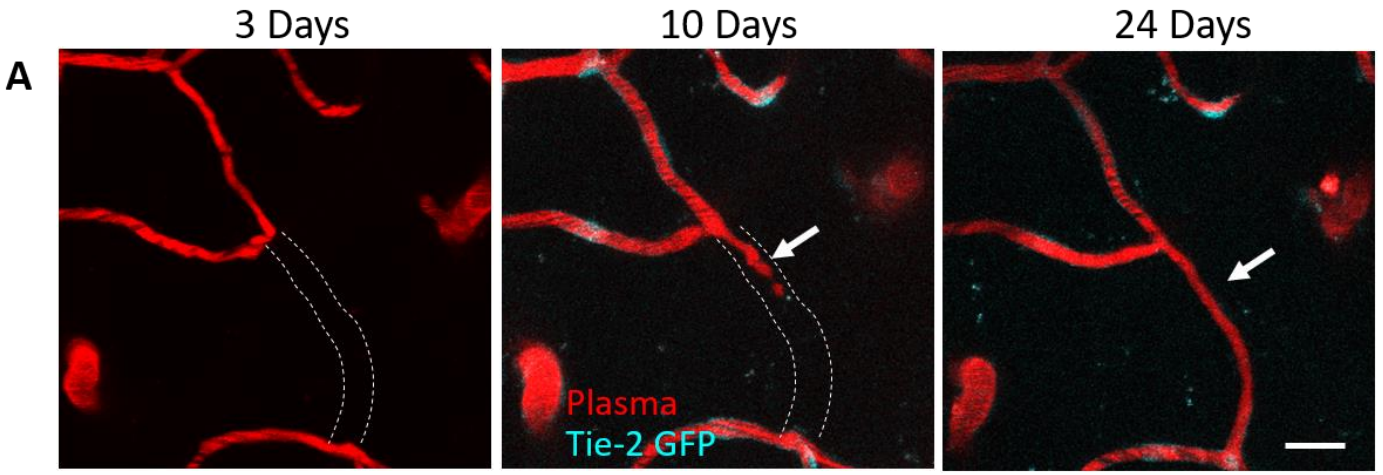

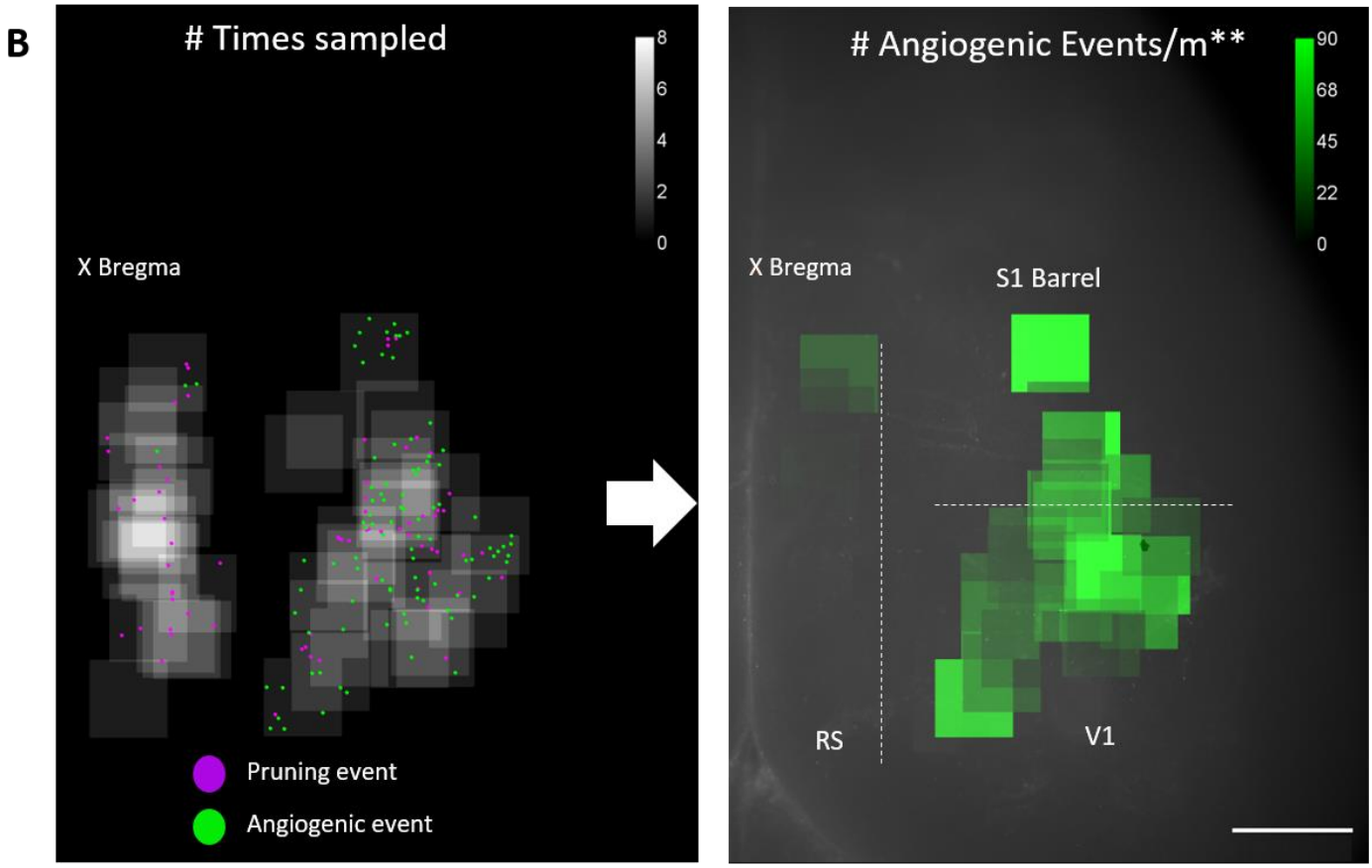

*All areas (n=47) in 7 animals sampled

**mean of animals where sampling overlap exists

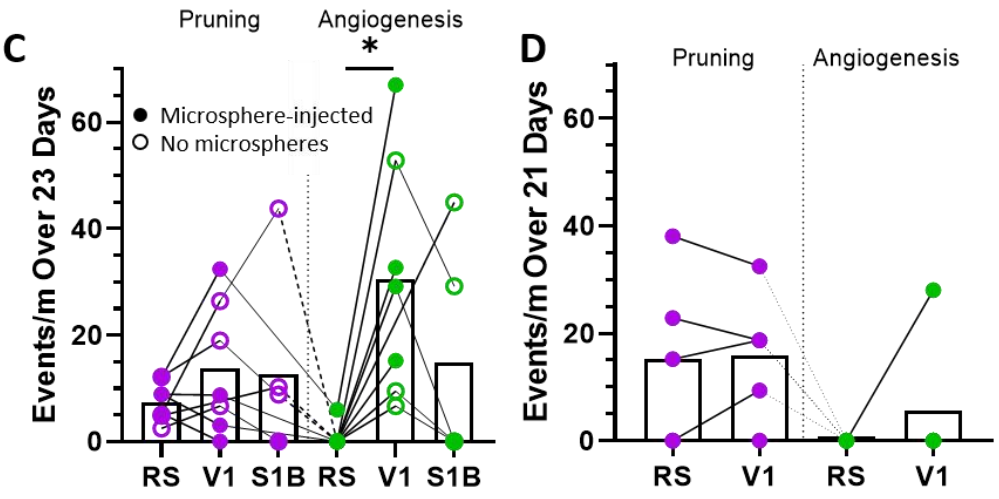

Figure 3.4. Angiogenesis in visual cortex predicts increases in vascular density over time. (**A**) Example of a sprouting vessel in a Tie-2 GFP animal. Images are ~50µm maximum z-projections. Note the lack of any Tie-2 GFP signal (blue) before the capillary starts to sprout. (**B**) Left panel shows the topographical location of all angiogenic events (green dots) and pruning events (purple dots) overlaid on a heat map showing how many times each area was sampled. Right panel shows a topographic heat map of the frequency of angiogenic events in each imaging area. Where overlap exists, values were averaged. (**C**) and (**D**) show the frequency of pruning events (purple) and the frequency of angiogenic events (green) in C57BL/6 and Tie-2 GFP animals, respectively. Open circles in C show animals that did not receive a microsphere injection. Paired t-tests were used to compare data in C and D. Scale bar in A: 20µm. Scale bar in B: 1mm. ****$p < 0.0001$, ***$p < 0.001$, **$p<0.01$, *$p<0.05$.

3.3.5 Characterization of angiogenesis in the cortex

In order to understand the full impact that angiogenesis could have on age-related changes in vascular density, we first asked whether there were differences in the lengths of the vessels that were pruning and those that were sprouting, and then we asked whether the observed vascular plasticity was happening at all accessible cortical depths. The two-dimensional (2-D) lengths of all capillaries involved in pruning or sprouting events were measured by drawing a segmented line along a maximum projection of each vessel (**Fig. 3.5A**, left panel). Three-dimensional (3-D) lengths were estimated by treating the 3-D length as a vector consisting of the 2-D length and the difference between vessel endpoints along the z-axis. Unpaired t-test between the 3-D length of angiogenic vessels and pruned vessels (pooled for all animals and areas) revealed that sprouted vessels were much longer than pruned vessels (**Fig. 3.5A**, right panel; mean difference: 44.28µm; $t_{(160)}$= 10.99, $p<0.0001$), a trend that did not change when averaged by animal and area (**Fig. 3.5B**).

We also measured the distance below the pial surface and found that both angiogenesis and pruning events tended to cluster within ~250µm of the pial surface (**Fig. 3.5C,D**). Instances of angiogenesis were especially rare further than 250µm from the pial surface (3/94 events) (**Fig. 3.5C**). Finally, we classified pruning and angiogenic events as flowing if they started or ended with evidence of streaking RBCs, respectively. Since our imaging timepoints are just a snapshot in time, some cases of pruning or new vessel formation were only partially completed at day 0 or day 24 (**Fig. 3.5E**, bottom panel). Events that did not start (in the case of pruning) or end (in the case of angiogenesis) with an attached or flowing capillary were classified as “Incomplete”, and

those that started or ended with a connected vessel that could not be confirmed to be flowing were classified as “Unsure”. Although we could not be sure of the permanence of the angiogenic events beyond 24 days, a very large proportion of angiogenic events ended with a flowing capillary (~80%), with a further ~10% connected to other vessels at each endpoint (**Fig. 3.5E**). Together this data shows that most angiogenic vessels in adult mice are rather long, occur close to the pial surface, and end in a patent capillary.

Figure 3.5. Characterization of angiogenic events.

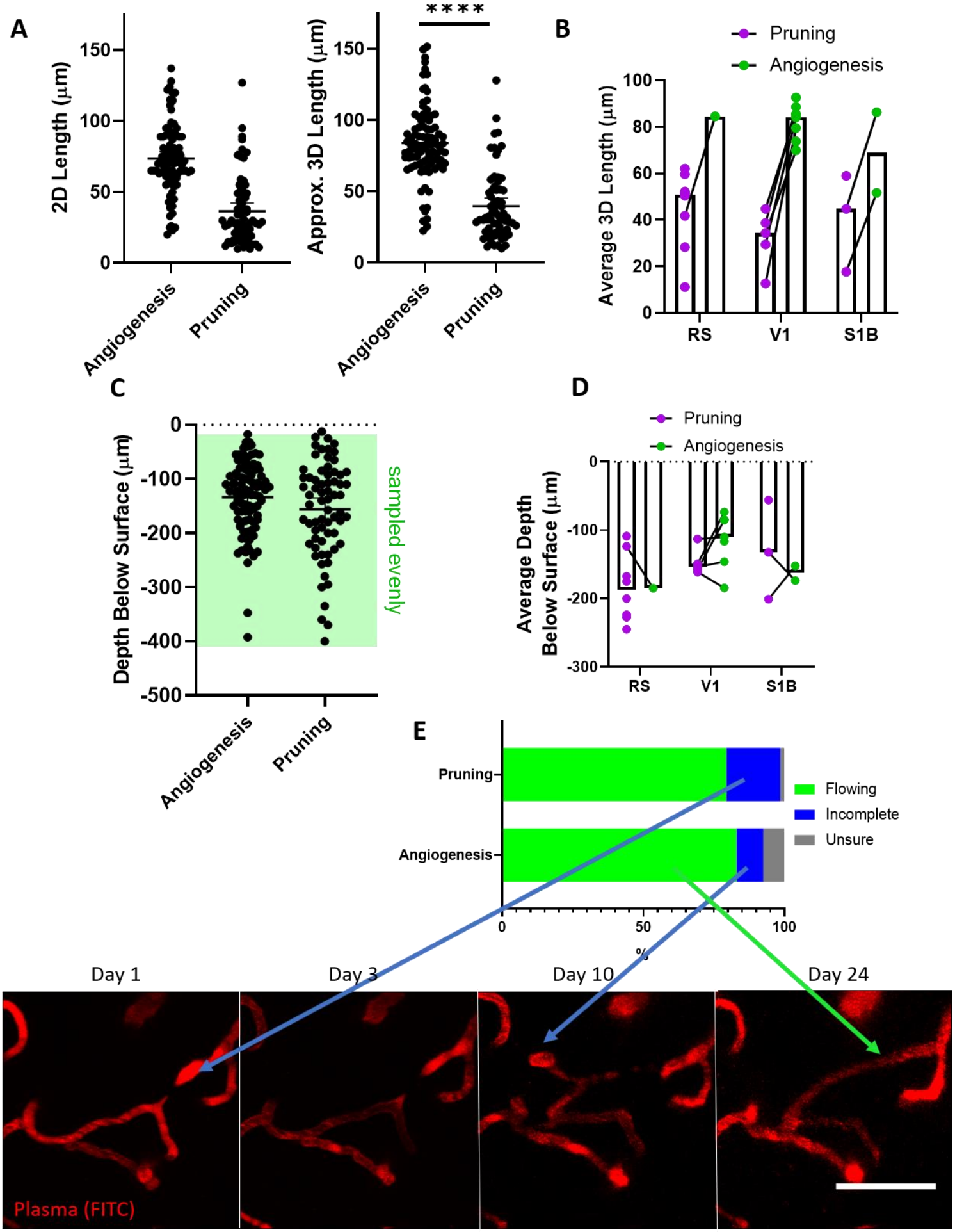

Figure 3.5. Characterization of angiogenic events. (A) 2-dimensional traced length of each plastic event over a maximum projection of the vessel (left) and 3-dimensional length estimated as the hypotenuse of a right triangle with sides consisting of the 2-dimensional length and the z-axis distance between the vessel endpoints. (B) Animal average length of plastic events in each area. Note the absence of differences between areas. (C) Depth below the surface of the midpoint for each plastic event. (D) Animal averages for depth of plastic events broken up by sampling area. (E) (Top panel) Classification of all plastic events as flowing (if angiogenic events ended in a flowing vessel or pruning events started with a flowing vessel), incomplete (if angiogenic events ended in a vessel unattached at one endpoint or pruning events started with one endpoint unattached), or unsure (if angiogenic events ended up attached at both endpoints or if pruning events started attached at both endpoints, but it RBC streaks were never obvious). Bottom panel shows examples of incomplete and flowing vessels. Note RBC streaks at day 24 as evidence of blood glow, denoted by the green arrow. Scale bar in E: 50μm. Data in A compared with unpaired two-sample t-test. ***p < 0.0001, ***p < 0.001, **p<0.01, *p<0.05.

3.4 Discussion

Age-related capillary loss shows region-specific differences in magnitude. We previously showed a relationship between microsphere-induced capillary obstructions and vessel loss, but *post-mortem* evidence of microsphere obstruction rates was insufficient to explain the full range of changes in vascular density that we observed. It also failed to explain the occurrence of one clear regional outlier, namely the retrosplenial cortex, in the relationship between capillary obstruction rates and vessel loss. These knowledge gaps were important to address as they open the possibility of previously unidentified regional heterogeneity in other forms of vascular plasticity. Specifically, we might have suspected between-area differences in angiophagy, the process of embolus extravasation (Lam et al., 2010), and angiogenesis, the process of vessel sprouting. Reeson et al. (2018) reported that approximately half of pruning events took place after vessel recanalization. It is also possible that we might have expected different post-recanalization pruning rates between areas, too. All of these other factors could provide a better explanation for region specific vessel loss and therefore we systematically assessed each one.

The retrosplenial cortex was far more prone to microsphere-induced obstructions but yet showed normal rates of vessel loss with aging. Therefore, it is possible that this area would show higher rates of angiophagy, or lower rates of post-recanalization pruning, than other areas. Either possibility could help to explain the presence of many microcirculatory obstructions in the area at 3-days, but a lower-than-anticipated magnitude of vessel loss. Here we used longitudinal 2-photon imaging to monitor recanalization rates of microspheres and follow the fates of previously obstructed

capillaries. When a microsphere never washed out, but no pruning event ensued, we called that event a possible case of angiophagy. Please note that recanalization rates differed from those reported by Reeson et al. (2018). This may be because we monitored recanalization rates of any microsphere present at 30 minutes, many of which may have been very transiently stalled, whereas Reeson required all microspheres to have been stuck for a minimum of 20 minutes. We report some evidence of angiophagy in retrosplenial and barrel cortex, but not in visual cortex. That said, the rate of possible angiophagy was low enough (2/629 obstructions from day 0 that could be tracked for 24 days in retrosplenial cortex) that the rates between areas were not markedly different. On the whole, these events occurred at a similar frequency in vessels that never washed out (~14%) as the frequency reported by Reeson (~12%) (Reeson et al., 2018). It is possible that we did not see area-specific differences because synthetic microspheres may experience different rates of angiophagy from natural emboli. However, recent work with 15µm diameter microspheres shows very high rates of angiophagy in slightly larger vessels (van der Wijk et al., 2019). Thus, it is likely that angiophagy rates differ more based on vessel caliber than on embolus composition. Although we found low rates of possible angiophagy events in capillaries and no evidence for large differences in angiophagy rates in retrosplenial cortex, future work that uses more natural emboli, samples a larger number of emboli, and samples more brain regions may be needed to ensure that area-specific differences in angiophagy rates do not exist.

While we did not find regional differences in the rates of angiophagy, we did discover that capillaries in retrosplenial cortex take longer to recanalize (remove

obstructions) than capillaries in visual cortex. Correspondingly, we found a preference for microsphere accumulation in retrosplenial cortex at 3 days, but the difference in microsphere density between retrosplenial cortex and visual cortex declined after 10 and 24 days. This finding is consistent with data shown in the only other published study that uses microspheres to model obstructions in capillaries. Reeson et al. (2018) quantified the number of microspheres that occurred in dorsal areas of mouse cortex at different stereotaxic levels along the anterior-posterior axis. Although they did not consider the medial-lateral position of the microspheres or sample as far posterior as we did 4 days after microsphere injection, they still showed a slight trend towards larger densities of microspheres aggregating in more posterior areas of cortex 4 days after microsphere injection (Reeson et al., 2018). As would be expected with delayed recanalization in retrosplenial cortex, they show that trend disappearing by 10 and 31 days (Reeson et al., 2018). The discovery of differences in capillary recanalization times between brain regions is a novel finding that helps to explain why retrosplenial cortex does not experience a greater magnitude of vessel loss with age, despite being prone to microsphere induced obstructions.

With our *in vivo* approach, we were able to replicate the preference for stalling in retrosplenial cortex that we saw in histology at 3 days, but not at 30 minutes. Several factors could have contributed to this result. The first and most obvious possibility is that the cranial window itself may have influenced microsphere-induced capillary obstructions. First, we have pilot data from a separate unpublished study showing that fewer microspheres accumulate in the cortex of the cortical hemisphere over which the cranial window is installed (mean=0.68±0.21 of contralateral density, one-sample t-test

against 1: $t_{(15)}$= 6.122, p<0.0001). Perhaps the magnitude of this effect changes depending on where you sample in the brain in relation to the window. Second, 2-photon imaging with water immersion objectives results in slight changes in brain temperature and blood flow (Roche et al., 2019). It is possible that these hemodynamic changes could affect obstruction rates in the brain. Finally, in the histology experiments, we sampled a slightly different part of retrosplenial cortex than was accessible for 2-photon imaging. For chapter 1, we sampled primarily in granular retrosplenial cortex, which is much deeper than dysgranular retrosplenial cortex and therefore could not be accessed in 2-photon imaging. However, we did verify that vessel loss and obstruction patterns were similar in granular and dysgranular retrosplenial cortex, so it is unlikely that the slight change in sampling area created the absence of stalling preference at 30 minutes.

Perhaps most importantly, and unexpectedly, here we provide the first strong evidence for regional patterns of angiogenesis in the healthy adult mouse cortex, occurring primarily in the primary visual cortex. As discussed in the introduction to this chapter, many studies report changes in vascular density with age, exercise, and vascular challenge that imply the existence of angiogenesis (Hunziker et al., 1979; Meier-Ruge et al., 1980; Wilkinson et al., 1981; Hinds and McNelly, 1982; Isaacs et al., 1992; Shweiki et al., 1992; Szpak et al., 1999; Kleim et al., 2002; Swain et al., 2003; Villena et al., 2003; Ding et al., 2006; Brown et al., 2007a; Ndubuizu et al., 2010; Harb et al., 2013; Gao et al., 2014; Masamoto et al., 2014; Morland et al., 2017; Moeini et al., 2018). Although some measurements based on fractional volume of vessels may inflate these reports of angiogenesis, it is still surprising that *in vivo* time-lapse imaging studies

have generally failed to replicate these findings in adult rodents in the absence of stroke or hypoxic challenge (Brown et al., 2007a; Mostany et al., 2010; Tennant and Brown, 2013; Masamoto et al., 2014; Cudmore et al., 2017; Reeson et al., 2018). The one exception is Harb et al. (2013), who demonstrated low-level vessel turnover in healthy adult mice. In fact, even in cases of substantial vascular challenge, such as extended periods of hypoxia or stroke, these *in vivo* imaging studies report modest quantities of vessel sprouting, at the most (Brown et al., 2007a; Harb et al., 2013; Masamoto et al., 2014), and sometimes no evidence at all (Mostany et al., 2010; Tennant and Brown, 2013; Reeson et al., 2018). For example, Masamoto et al. (2014) only found 45 angiogenic sprouts in 11 animals after 7-14 days of hypoxia (8-9% oxygen). Further, Harb et al. (2013) showed that 15% oxygen was insufficient to stimulate any angiogenesis, and that one month of hypoxia (10% oxygen; note oxygen is normally 20%) produced rates of angiogenesis of ~1% (% of total branch points over 1 month) in young adult mice (and was not different from the rate in normoxic conditions), and no angiogenesis in aged mice.

Several possible explanations exist for why time-lapse imaging fails to yield evidence of angiogenesis. It is possible that the process of the imaging preparation, whether that be thinning the skull or removing a piece of the cranium, might restrict the ability for the brain to elicit angiogenesis. Or perhaps animals simply do not show angiogenesis because they are usually housed in deprived (non-enriched) environments. This is countered, however, by time-lapse imaging data showing that exercise-induced angiogenesis is very scarce (Cudmore et al., 2017; Dorr et al., 2017). Our results suggest an additional possibility that these other studies might have missed.

First, these studies all examined microvascular structure in somatosensory and motor areas of cortex. Perhaps these are areas where angiogenesis may not occur. Our results suggest that if these studies had taken place in visual cortex, they may have seen more instances of angiogenesis. Second, we also demonstrate that there may be strain differences in the capacity for pruning and angiogenesis. All C57BL/6 mice sampled (n=8) showed some degree of angiogenesis in visual cortex; however, only one of seven Tie-2 GFP mice displayed any evidence of angiogenesis. Tie-2 GFP mice, the primary strain of mice used by Reeson et al. (2018), also exhibited more microcirculatory obstructions and pruning events than C57BL/6 mice. This may contribute to why we reported a lower magnitude of vessel loss and higher recanalization rates than Reeson's study.

We report that vascular plasticity, especially angiogenesis, occurs primarily in the superior ~250μm below the pial surface in the cortex. Similarly, Masamoto et al. (2014) report that angiogenesis resulting from hypoxia also primarily occurs in the top ~200μm of cortex, having sampled between 300 and 800μm below the cortical surface, depending on the animal. Anecdotally, we sometimes see substantial vascular remodeling along the pial surface of the brain under a cranial window. It is interesting to note also that some pro-angiogenic factors are much more highly expressed along the pial surface, such as the lactate receptor HCAR1 (Morland et al., 2017). It may be that subsurface angiogenesis is driven by a gradient of pro-angiogenic factors emanating from the pial surface. Masamoto et al. (2014) also report that angiogenesis tends to happen in the capillary-sparse zone surrounding penetrating vessels. We did not produce data in the present study that could answer whether that was also true in the

visual cortex in the absence of hypoxia. This question should be considered for future research.

Another interesting feature that we observed was that sprouted vessels tend to be much longer than pruned vessels. While angiogenic vessels tend to be ~70-80μm long, similar to the average capillary length that we observe (sample of 30 vessels in retrosplenial and barrel cortex mean±SD: 59.1±26.2μm), and that reported by others (Blinder et al., 2013; Reeson et al., 2018), pruned vessels tend to be much shorter (~40μm) and therefore may be primarily short collateral vessels. As such, the difference in the number of remodelling events is not sufficient to explain changes in vascular length on its own and vessel length must also be considered.

There are several limitations to the present study that should be considered when interpreting the results. First, the one major limitation of this study relates to the variability in microsphere sampling. Even though many microspheres were sampled at the first imaging timepoint, very high recanalization rates left very few obstructions in the cortex even at three days, allowing us to sample only ~80 microspheres at 3 days and 40 microspheres at 24 days across 3 areas in 14 animals. By pooling these microspheres together, we do not consider the variance in capillary stalling between animals. Next, we are limited in the volume and timepoints we can sample with 2-photon imaging. We assumed that if a capillary was obstructed at consecutive time points, then the microsphere was the same at both timepoints. However, it is possible that in some cases the capillary recanalized but was subsequently re-obstructed. To support that possibility, previous work has shown that capillaries that experience microvascular obstructions and recanalize are more likely to be stalled again at a later

time (Reeson et al., 2018). The imaging technique we used also prevented us from sampling more volume and deeper areas of cortex. As such, we could only draw conclusions about the superior 400µm of cortex. This is significant because there are reports of increases in vessel density in layer 5 of motor cortex following exercise (Kleim et al., 2002), but we could only image up to layer 4. Finally, finding examples of remodelling events in large volumes of vasculature is probably subject to substantial human error, leading to underestimation of the frequency of these events. Development of automated tools designed to identify changes in vascular structure would be very helpful to the future study of angiogenesis.

4. General Discussion

In this thesis, I began by describing the complex energy demands of the brain and the features of the cerebral vasculature that make it possible to meet that demand. Regional heterogeneity in the structure and function of the vasculature was discussed as an important feature of meeting those demands. I outlined some existing research that identified vascular differences between cortical layers and between brain regions, including differences in vascular density and cerebral blood flow. Finally, I also underlined the importance of further research characterizing the regional heterogeneity of these and other vascular features, such as the capacity for vascular plasticity. Specifically, I decided that it was important to identify how those features change with age in white matter and in both cortical and subcortical gray matter. These questions were addressed by testing the hypothesis that vessel loss with aging occurs in a region-specific manner, and then subsequently by asking what factors contribute to that region-specific decline. We've replicated and expanded studies that show regional heterogeneity in vascular density, and added novel data showing regional heterogeneity in mean microvascular diameter, tortuosity, susceptibility to microcirculatory obstruction, obstruction recanalization rates and times, and finally rates of angiogenesis. We also reported age-related changes in vascular density, diameter, tortuosity, and susceptibility to microcirculatory obstruction that also differ by brain region. Moreover, by sampling many of these variables in 15 different regions, including subcortical areas, we were able to expand the characterization of the vasculature while probing possible relationships between these features. For these reasons, this thesis constitutes valuable

foundational work for further research probing how these region-specific differences come to be and what consequences they may have over time/with age.

Perhaps the primary lesson to be learned from this work is that there is a lot of complexity underlying any of the physiological changes that happen with advanced aged. Ultimately, behaviour is affected not only by changes in neuronal circuits, but also by changes in the glial and vascular networks that support them. Here, we've shown that not only are there numerous vascular changes that happen with age, but that these changes do not present homogeneously in the brain. And, understanding the causes of even a single one of those changes is highly complex. For example, we show that changes in vessel density cannot be accurately predicted without understanding the rates of pruning events and angiogenic events in the brain. Further, we cannot predict differences in pruning rates without understanding that there is regional heterogeneity in susceptibility to microcirculatory obstruction, which in turn depends on more than just the average vessel width in each brain region. Finally, forms of plasticity, those that drive changes in vascular density, undergo age-related and brain region-specific changes. Unfortunately, we have only presented point-estimates of these parameters. We know that obstruction rates can change with age, but we do not know when or how those changes happen. Similarly, the balance of angiogenesis and pruning that we observed in visual cortex would predict an increase in vascular density, yet we observed a 2% decrease with age. It is therefore clear that angiogenic rates must also change with age, something that has been previously reported in the literature (Black et al., 1989; Harb et al., 2013; Tang et al., 2016). As such, further characterization of how, why, and where the vasculature changes with age (e.g. in middle age) will be required

to understand age-related changes in nervous system function and resulting behaviour. Obviously, characterizing these changes offers little therapeutic potential on its own. That is why the greatest questions that come from my work surround why we see these differences in vascular plasticity between brain regions.

We observed brain region-specific changes in capillary obstruction rates and in angiogenesis. Unfortunately, there is very little existing data that would explain why we saw angiogenesis in visual cortex but not retrosplenial cortex, or why an area like the amygdala experiences few microcirculatory obstructions. As a result, a review of the possible mechanisms that underlie these phenomena will be speculative in nature. To start, let's consider why we observe differences in capillary obstruction rates. The first obvious explanations for this phenomenon are mechanical. As capillaries are small tubes that need to pass relatively large debris through them, it would make sense that smaller vessels would be more likely to get stuck. As predicted, we showed that in young animals, mean vessel diameter was moderately predictive of obstruction rate. We might also predict that capillaries with lower pressure or lower flow rates would be more easily obstructed. If we relate Ohm's law to fluid dynamics, the change in pressure is equal to the flow multiplied by the resistance. We know that the length of vessels, blood viscosity, number of parallel paths, and flow turbulence can all affect vessel resistance (Klabunde, 2011). Moreover, we know that vascular differences that affect resistance can exist between parts of the brain. For example, we know that hematocrit, which affects viscosity, is greater in deeper cortical layers (Hartung et al., 2018) and there is a unequal distribution of RBCs at every capillary bifurcation, favouring more RBCs in wider daughter branches (Gould and Linninger, 2015). We also know that individual

capillary flow rates are highly heterogeneous and that there are preferred paths for RBCs through capillary networks (Schmid et al., 2017b). Perhaps the higher resistance paths that experience larger pressure drops are more likely to experience capillary obstructions. And, perhaps some brain regions, like those in watershed areas that are supplied by the distal ends of major arteries, are richer in low-pressure capillaries. In fact, one study notes that blood pressure in the small arterioles in the posterior parietal arterial bed is far lower than pressure in the small arterioles of the lenticulostriate bed (59/38 vs. 91/58) (Blanco et al., 2017; Spence, 2019). While this may help to roughly explain higher obstruction rates in some cortical areas, a larger study that estimates pressure in a large number of brain regions might be needed to shed more light on our vessel obstruction patterns. Another possibility is that vascular density, which can also affect resistance to flow, could affect obstruction rates. However, we saw no relationship between capillary density and obstruction rate at 30 minutes (r^2=0.013) or 3 days (r^2=0.057).

Chemical factors can equally affect obstruction rates. Many emboli, such as white blood cells, might plug a capillary partially due to the interactions between adhesion molecules and their ligands on the luminal endothelium (Schmidt et al., 2013; Talahalli et al., 2013). In fact, white blood cells tend to become stickier in various disease states that experience large numbers of microvascular obstructions. For example, a model of sickle cell disease displays a large number of capillary stalling events (Hyacinth et al., 2017), which correlates with the presentation of higher white blood cell counts and increased expression of l-selectin and αMβ integrin in patients (Okpala et al., 2002). These same patients show symptomatic improvements with

treatments that reduce leukocyte adhesion molecule expression (Okpala et al., 2002). Additionally, sticky white blood cells are thought to play an important role in a mouse model of Alzheimer's and in diabetic retinopathy (Noda et al., 2012; Cruz-Hernández et al., 2019). So clearly expression of integrins and adhesion molecules can influence obstruction rates, and there's evidence that cell adhesion molecule expression can change with age (Merat et al., 2000; Richter et al., 2003), but the question of whether differential expression of these molecules can influence regional obstruction rates remains unanswered. Expression of adhesion molecules has been shown to be regionally-heterogeneous in the development of chickens (Chuong and Edelman, 1984, 1985). However, further work examining differential expression of these proteins across brain regions of adult animals, as well as research on the associations of these proteins with various types of emboli, will be needed to answer why we see differences in obstruction rates between brain regions.

There are also many plausible explanations for brain region specific differences in angiogenesis, but there is very little research to pinpoint a specific mechanism. Typically, angiogenesis in development is driven by extracellular gradients of vascular endothelial growth factor (VEGF) that are generally secreted from astrocytes and progenitor cells in the subventricular zone (Gerhardt, 2013; Milner, 2014). VEGF expression in the context of angiogenesis can be driven by multiple pathways, including through hypoxia via hypoxia-inducible factor (HIF-1) expression and HIF-1 independent routes in the case of exercise (Ndubuizu et al., 2010; Gerhardt, 2013; Masamoto et al., 2014; Morland et al., 2017). In the end, the reason for angiogenesis may involve greater expression of pro-angiogenic molecules, such as VEGF-A or Angiopoietin-2 (Milner,

2014), in visual cortex than retrosplenial cortex. Or conversely, there might be fewer anti-angiogenic molecules in visual cortex. Molecules such as Nogo-A and Angiopoietin-1 are known to be important negative regulators of vascular remodeling and angiogenesis (Lacoste and Gu, 2015; Wälchli et al., 2017). Whether these proteins are expressed in a regional gradient is unknown. It is possible that angiogenesis in young adult visual cortex is part of a residual developmental chemical gradient involved in late remodelling of vascular networks. Or maybe something about the activity patterns of neurons (or networks) in the visual cortex affects the expression of pro or anti-angiogenic molecules, given that neural activity is known to be important for vessel patterning (Lacoste et al., 2014). Alternatively, angiogenic rates may depend on capillary density. According to our measurements, visual cortex has ~20% less vascular density than retrosplenial cortex. Still, visual cortex has more vessels than many other areas, so it is hard to imagine that even micro-pockets of hypoxic signals would exist there. Moreover, we show that angiogenesis happens more in superficial layers of cortex, and although those layers tend to have slightly lower vascular density (Tsai et al., 2009), they also tend to be well oxygenated (Devor et al., 2011).

Finally, its possible that the angiogenesis we observe (or do not observe, depending on the brain region) may be an artifact of the surgical cranial window procedure. Revascularization of the surface might happen, as bone and connective tissue can grow back under the window, particularly near the edges. It is possible that some of the signaling molecules that are responsible for this process may produce (or maybe inhibit) angiogenesis underneath the cortical surface depending on what part of the cortical window you look at. However, this explanation is unlikely. Visual cortex

tends to be in a fairly central part of the cranial window in our animals and exhibits angiogenesis. If angiogenesis was occurring in the centre of imaging windows, we would have expected studies that image in somatosensory cortex to also show angiogenesis in central areas of the cranial window, which they do not (Tennant and Brown, 2013; Reeson et al., 2018). Unfortunately, I have been unable to find supporting evidence for any of these possible explanations. Further research will have to start by determining whether there is clear differential expression of pro or anti-angiogenic molecules between visual and retrosplenial cortex, and then build from there.

According to a recent editorial on aging studies in the Journal of Neuroscience, our study of microcirculatory aging had strengths, but also a number of important weaknesses. This editorial pinpoints the inclusion of sex differences, unaffected phenotypes, multiple time points, and driving mechanisms as important considerations for an aging study (Society for Neuroscience, 2019). By sampling many areas and showing that some do not change with age, we were able to show that the changes we observed were not attributable to general trends. We were also able to identify capillary obstructions and angiogenic rates as mechanisms that drive age-related changes in vascular density. On the other hand, the largest weaknesses of the current work are the exclusion of sex differences and the lack of a middle age group. Sex differences are common in brain aging. They include many things, such as differences in regional brain volume reductions and associations with vascular risk factors, such as hypertension, just to name a couple (Armstrong et al., 2019). Our study was unable to probe the question of whether sex differences influence vascular density, diameter, and tortuosity changes with age due to limitations in the number of aged females in our colony. To

keep our comparisons fair, we chose not to include females in the assessment of these parameters in young adult animals. And since we wondered if capillary obstruction rates might predict vessel loss, we did not assess whether there were sex-differences in those rates, either. Because of these decisions, we missed out on collecting data on young adult females that would have been interesting in its own right. It is also worth noting that in chapter 2 we used primarily female mice. We reported a difference in obstruction rates at 30 minutes in our *in vivo* imaging that did not align with our finding from chapter 1. Namely, we saw more obstructions in retrosplenial cortex than visual cortex at 30 minutes. This conceivably could have been partially explained by sex differences. Moreover, even though evidence for angiogenesis in the brains of healthy adult mice was scant in the literature, we observed angiogenesis in female C57BL/6 mice. It is of the utmost importance to replicate this finding in male mice to determine whether a sex difference underlies this phenomenon, and perhaps why it has not been previously described in the literature.

Next, our study was limited in that we did not include a middle age group. The determination of when things change is also an important consideration for what those changes could mean. For example, a recent study reported a change in vascular diameter between middle age and old animals, but not between young and middle age animals (Moeini et al., 2018). The timing of these changes lining up with concomitant declines in vascular density between middle age and old animal, which led them to speculate that capillary dilation was helping to counteract increases in vascular resistance caused by the loss of vessels, thereby helping to keep blood flow from dropping too low (Moeini et al., 2018). Our study would have benefitted from the

inclusion of such a group in a couple ways. A number of studies indicate that vascular density does not decline much between young and middle age (Hunziker et al., 1979; Meier-Ruge et al., 1980; Wilkinson et al., 1981; Hinds and McNelly, 1982; Moeini et al., 2018). This non-linear change in vessel density would not fit with the gradual loss of vessels from capillary obstructions proposed by Reeson et al. (2018) and expanded by us in chapter 1. However, we could not comment on this possibility because we did not include a middle age group for vessel density or microsphere distribution. We also propose that changes in obstruction rates could partially explain why retrosplenial cortex is an outlier in the relationship between vessel loss and obstruction rate. While we see obstruction rates drop in that area in old age, we do not know when that change happens and therefore cannot predict the full effect of each of those obstruction rates on vessel pruning rates.

Finally, as discussed above in section 2.4, the functional significance of this work for cognitive and behavioural age-related changes remains speculative. There is still no existing research that definitively shows that declines in vascular density (of a physiological magnitude), are sufficient to cause behavioural deficits in the absence of other age or disease-related changes. Although a study that tested animal behaviour after reducing capillary density in young animals would be helpful, a negative result would not necessarily demonstrate that capillary density does not affect cognitive performance. Physiological changes in vessel density may only influence cognition in the absence of compensatory mechanisms that may also be lost with age. Not to mention, designing a study that reduced capillary density in a region-dependent manner would be an extremely difficult task. Alternatively, given the established relationship

between CBF and cognitive performance, demonstrating a causative relationship between reductions in capillary density and reductions in CBF would certainly help to determine the effect of vessel loss on cognition. By showing that greater vessel loss occurs in tissues that also experience age-related declines in CBF (i.e. white matter and cortical gray matter), we have contributed additional correlative evidence for this relationship. Moreover, computer modeling has already demonstrated that modest declines in the number of viable capillaries can, theoretically, decrease CBF (Cruz-Hernández et al., 2019). However, experimental evidence of direct causation is still lacking. Finally, it still remains to be established whether *regional* changes in CBF can selectively impair certain behavioural traits.

5. Conclusion

The cerebral vasculature is essential for maintaining an environment that permits optimal neural communication, which is in turn needed for optimal cognitive and behavioural function. Here, we have shown that the microvasculature declines in a region-dependent manner with age, with the greatest reductions occurring in white matter, followed by cortical gray matter, and finally subcortical gray matter. Mechanistically, we have shown using fluorescent microspheres that susceptibility to long-lasting microcirculatory obstruction can partially explain the regional patterns of vessel loss. However, we have also shown that the microcirculatory obstruction rate (in young adult animals after 3 days) in a brain region is insufficient to fully predict vessel loss on its own. Therefore, we used a histological assessment of microsphere density in aged animals and employed longitudinal 2-photon imaging to discover region-specific differences in rates of angiogenesis, pruning, the time course for capillary recanalization, and changes in susceptibility to obstruction with age. Based on these findings, we can explain why a region that is highly prone to obstructions, like the retrosplenial cortex, experiences modest vessel loss with aging. The answer resides in one of two possibilities, namely: a) capillaries in this region take longer to recanalize and therefore can reduce their chances of being pruned and/or b) the enhanced susceptibility to capillary obstructions that is present in young adult mice is lost with aging. Conversely, we showed that regional differences in angiogenesis might explain why some areas, such as visual cortex, experience very little vessel loss with age. Collectively, this work has demonstrated that regional differences in vessel loss with

aging is influenced, and can be partially explained, by factors such as susceptibility to capillary plugging, angiogenesis, vessel pruning and recanalization strategies.

6. References

Abernethy WB, Bell MA, Morris M, Moody DM (1993) Microvascular Density of the Human Paraventricular Nucleus Decreases with Aging but Not Hypertension. Exp Neurol 121:270–274.

Alexander GE, Ryan L, Bowers D, Foster TC, Bizon JL, Geldmacher DS, Glisky EL (2012) Characterizing cognitive aging in humans with links to animal models. Front Aging Neurosci 4:21.

Amenta F, Cavallotti D, Del Valle M, Mancini M, Naves FJ, Vega JA, Zeng YC (1995a) Age-related changes in brain microanatomy: sensitivity to treatment with the dihydropyridine calcium channel blocker darodipine (PY 108-068). Brain Res Bull 36:453–460.

Amenta F, Ferrante F, Mancini M, Sabbatini M, Vega JA, Zaccheo D (1995b) Effect of long-term treatment with the dihydropyridine-type calcium channel blocker darodipine (PY 108-068) on the cerebral capillary network in aged rats. Mech Ageing Dev 78:27–37.

Arganda-Carreras I, Kaynig V, Rueden C, Eliceiri KW, Schindelin J, Cardona A, Sebastian Seung H (2017) Trainable Weka Segmentation: a machine learning tool for microscopy pixel classification. Bioinformatics 33:2424–2426.

Armstrong NM, An Y, Beason-Held L, Doshi J, Erus G, Ferrucci L, Davatzikos C, Resnick SM (2019) Sex differences in brain aging and predictors of

neurodegeneration in cognitively healthy older adults. Neurobiol Aging 81:146–156.

Attwell D, Buchan AM, Charpak S, Lauritzen M, MacVicar BA, Newman EA (2010) Glial and neuronal control of brain blood flow. Nature 468:232–243.

Attwell D, Laughlin SB (2001) An Energy Budget for Signaling in the Grey Matter of the Brain. J Cereb Blood Flow Metab 21:1133–1145.

Attwell D, Mishra A, Hall CN, O'Farrell FM, Dalkara T (2016) What is a pericyte? J Cereb Blood Flow Metab 36:451–455.

Badhwar A, Brown R, Stanimirovic DB, Haqqani AS, Hamel E (2017) Proteomic differences in brain vessels of Alzheimer's disease mice: Normalization by PPARγ agonist pioglitazone. J Cereb Blood Flow Metab 37:1120–1136.

Bagi Z, Brandner DD, Le P, McNeal DW, Gong X, Dou H, Fulton DJ, Beller A, Ngyuen T, Larson EB, Montine TJ, Keene CD, Back SA (2018) Vasodilator dysfunction and oligodendrocyte dysmaturation in aging white matter. Ann Neurol 83:142–152.

Bangen KJ, Werhane ML, Weigand AJ, Edmonds EC, Delano-Wood L, Thomas KR, Nation DA, Evangelista ND, Clark AL, Liu TT, Bondi MW (2018) Reduced Regional Cerebral Blood Flow Relates to Poorer Cognition in Older Adults With Type 2 Diabetes. Front Aging Neurosci 10 Available at: https://www.frontiersin.org/articles/10.3389/fnagi.2018.00270/full [Accessed October 19, 2019].

Bär T (1978) Morphometric evaluation of capillaries in different laminae of rat cerebral cortex by automatic image analysis: changes during development and aging. Adv Neurol 20:1–9.

Bazargani N, Attwell D (2016) Astrocyte calcium signaling: the third wave. Nat Neurosci 19:182–189.

Bell MA, Ball MJ (1981) Morphometric comparison of hippocampal microvasculature in ageing and demented people: Diameters and densities. Acta Neuropathol (Berl) 53:299–318.

Bell MA, Ball MJ (1990) Neuritic plaques and vessels of visual cortex in aging and Alzheimer's dementia. Neurobiol Aging 11:359–370.

Bell RD, Zlokovic BV (2009) Neurovascular mechanisms and blood-brain barrier disorder in Alzheimer's disease. Acta Neuropathol (Berl) 118:103–113.

Bennett IJ, Madden DJ (2014) Disconnected aging: Cerebral white matter integrity and age-related differences in cognition. Neuroscience 276:187–205.

Berthiaume A-A, Hartmann DA, Majesky MW, Bhat NR, Shih AY (2018) Pericyte Structural Remodeling in Cerebrovascular Health and Homeostasis. Front Aging Neurosci 10 Available at: https://www.ncbi.nlm.nih.gov/pmc/articles/PMC6057109/ [Accessed July 24, 2019].

Birdsill AC, Koscik RL, Jonaitis EM, Johnson SC, Okonkwo OC, Hermann BP, LaRue A, Sager MA, Bendlin BB (2014) Regional white matter hyperintensities: aging, Alzheimer's disease risk, and cognitive function. Neurobiol Aging 35:769–776.

Black JE, Polinsky M, Greenough WT (1989) Progressive failure of cerebral angiogenesis supporting neural plasticity in aging rats. Neurobiol Aging 10:353–358.

Blanco PJ, Müller LO, Spence JD (2017) Blood pressure gradients in cerebral arteries: a clue to pathogenesis of cerebral small vessel disease. Stroke Vasc Neurol 2:108–117.

Blinder P, Tsai PS, Kaufhold JP, Knutsen PM, Suhl H, Kleinfeld D (2013) The cortical angiome: an interconnected vascular network with noncolumnar patterns of blood flow. Nat Neurosci 16:889–897.

Bollu T, Cornelius NR, Sunwoo J, Nishimura N, Schaffer CB, Doerschuk PC (2018) Experimentally constrained circuit model of cortical arteriole networks for understanding flow redistribution due to occlusion and neural activation. J Cereb Blood Flow Metab 38:38–44.

Brown CE, Li P, Boyd JD, Delaney KR, Murphy TH (2007a) Extensive turnover of dendritic spines and vascular remodeling in cortical tissues recovering from stroke. J Neurosci Off J Soc Neurosci 27:4101–4109.

Brown WR, Moody DM, Thore CR, Anstrom JA, Challa VR (2009) Microvascular changes in the white mater in dementia. J Neurol Sci 283:28–31.

Brown WR, Moody DM, Thore CR, Challa VR, Anstrom JA (2007b) Vascular dementia in leukoaraiosis may be a consequence of capillary loss not only in the lesions, but in normal-appearing white matter and cortex as well. J Neurol Sci 257:62–66.

Brown WR, Thore CR (2011) Review: Cerebral microvascular pathology in ageing and neurodegeneration. Neuropathol Appl Neurobiol 37:56–74.

Buchweitz-Milton E, Weiss HR (1987) Perfused capillary morphometry in the senescent brain. Neurobiol Aging 8:271–276.

Buée L, Hof PR, Bouras C, Delacourte A, Perl DP, Morrison JH, Fillit HM (1994) Pathological alterations of the cerebral microvasculature in Alzheimer's disease and related dementing disorders. Acta Neuropathol (Berl) 87:469–480.

Burns EM, Kruckeberg TW, Gaetano PK (1981) Changes with age in cerebral capillary morphology. Neurobiol Aging 2:283–291.

Casey MA, Feldman ML (1985) Aging in the rat medial nucleus of the trapezoid body. III. Alterations in capillaries. Neurobiol Aging 6:39–46.

Cavaglia M, Dombrowski SM, Drazba J, Vasanji A, Bokesch PM, Janigro D (2001) Regional variation in brain capillary density and vascular response to ischemia. Brain Res 910:81–93.

Chen JJ, Rosas HD, Salat DH (2011) Age-Associated Reductions in Cerebral Blood Flow Are Independent from Regional Atrophy. NeuroImage 55:468–478.

Chen Q, Jiang L, Li C, Hu D, Bu J, Cai D, Du J (2012) Haemodynamics-Driven Developmental Pruning of Brain Vasculature in Zebrafish. PLOS Biol 10:e1001374.

Choi I-Y, Seaquist ER, Gruetter R (2003) Effect of Hypoglycemia on Brain Glycogen Metabolism In Vivo. J Neurosci Res 72:25–32.

Chuong CM, Edelman GM (1984) Alterations in neural cell adhesion molecules during development of different regions of the nervous system. J Neurosci 4:2354–2368.

Chuong CM, Edelman GM (1985) Expression of cell-adhesion molecules in embryonic induction. I. Morphogenesis of nestling feathers. J Cell Biol 101:1009–1026.

Cipolla MJ (2009) The Cerebral Circulation. San Rafael (CA): Morgan & Claypool Life Sciences. Available at: https://www.ncbi.nlm.nih.gov/books/NBK53086/ [Accessed June 19, 2019].

Craigie EH (1945) The Architecture of the Cerebral Capillary Bed. Biol Rev 20:133–146.

Cruz-Hernández JC et al. (2019) Neutrophil adhesion in brain capillaries reduces cortical blood flow and impairs memory function in Alzheimer's disease mouse models. Nat Neurosci 22:413.

Cudmore RH, Dougherty SE, Linden DJ (2017) Cerebral vascular structure in the motor cortex of adult mice is stable and is not altered by voluntary exercise. J Cereb Blood Flow Metab 37:3725–3743.

Daneman R, Prat A (2015) The Blood–Brain Barrier. Cold Spring Harb Perspect Biol 7 Available at: https://www.ncbi.nlm.nih.gov/pmc/articles/PMC4292164/ [Accessed September 4, 2019].

de Groot M, Ikram MA, Akoudad S, Krestin GP, Hofman A, van der Lugt A, Niessen WJ, Vernooij MW (2015) Tract-specific white matter degeneration in aging: The Rotterdam Study. Alzheimers Dement 11:321–330.

de la Torre JC (2002) Alzheimer disease as a vascular disorder: nosological evidence. Stroke 33:1152–1162.

Desjardins M, Berti R, Lefebvre J, Dubeau S, Lesage F (2014) Aging-related differences in cerebral capillary blood flow in anesthetized rats. Neurobiol Aging 35:1947–1955.

Devonshire IM, Papadakis NG, Port M, Berwick J, Kennerley AJ, Mayhew JEW, Overton PG (2012) Neurovascular coupling is brain region-dependent. NeuroImage 59:1997–2006.

Devor A, Sakadžić S, Saisan PA, Yaseen MA, Roussakis E, Srinivasan VJ, Vinogradov SA, Rosen BR, Buxton RB, Dale AM, Boas DA (2011) “Overshoot” of O2 Is Required to Maintain Baseline Tissue Oxygenation at Locations Distal to Blood Vessels. J Neurosci 31:13676–13681.

Ding Y-H, Li J, Zhou Y, Rafols JA, Ding JCC and Y (2006) Cerebral Angiogenesis and Expression of Angiogenic Factors in Aging Rats after Exercise. Curr Neurovasc

Res Available at: http://www.eurekaselect.com/55263/article [Accessed July 8, 2019].

Dorr A, Thomason LA, Koletar MM, Joo IL, Steinman J, Cahill LS, Sled JG, Stefanovic B (2017) Effects of voluntary exercise on structure and function of cortical microvasculature. J Cereb Blood Flow Metab Off J Int Soc Cereb Blood Flow Metab 37:1046–1059.

El-Khoury N, Braun A, Hu F, Pandey M, Nedergaard M, Lagamma EF, Ballabh P (2006) Astrocyte End-Feet in Germinal Matrix, Cerebral Cortex, and White Matter in Developing Infants. Pediatr Res 59:673–679.

Erdener ŞE, Tang J, Sajjadi A, Kılıç K, Kura S, Schaffer CB, Boas DA (2017) Spatio-temporal dynamics of cerebral capillary segments with stalling red blood cells. J Cereb Blood Flow Metab 39:886–900.

Fabiani M, Gordon BA, Maclin EL, Pearson MA, Brumback-Peltz CR, Low KA, McAuley E, Sutton BP, Kramer AF, Gratton G (2014) Neurovascular coupling in normal aging: a combined optical, ERP and fMRI study. NeuroImage 85 Pt 1:592–607.

Farkas E, de Vos RAI, Donka G, Jansen Steur EN, Mihály A, Luiten PGM (2006) Age-related microvascular degeneration in the human cerebral periventricular white matter. Acta Neuropathol (Berl) 111:150–157.

Fernández-Klett F, Offenhauser N, Dirnagl U, Priller J, Lindauer U (2010) Pericytes in capillaries are contractile in vivo, but arterioles mediate functional hyperemia in the mouse brain. Proc Natl Acad Sci 107:22290–22295.

Filosa JA, Morrison HW, Iddings JA, Du W, Kim KJ (2016) Beyond neurovascular coupling, role of astrocytes in the regulation of vascular tone. Neuroscience 323:96–109.

Forde A, Constien R, Gröne H-J, Hämmerling G, Arnold B (2002) Temporal Cre-mediated recombination exclusively in endothelial cells using Tie2 regulatory elements. genesis 33:191–197.

Fox PT, Raichle ME (1986) Focal physiological uncoupling of cerebral blood flow and oxidative metabolism during somatosensory stimulation in human subjects. Proc Natl Acad Sci U S A 83:1140–1144.

Franklin K, Paxinos G (2008) The Mouse Brain in Stereotaxic Coordinates, 3rd ed. New York, NY: Academic Press.

Gao Y, Zhao Y, Pan J, Yang L, Huang T, Feng X, Li C, Liang S, Zhou D, Liu C, Tu F, Tao C, Chen X (2014) Treadmill exercise promotes angiogenesis in the ischemic penumbra of rat brains through caveolin-1/VEGF signaling pathways. Brain Res 1585:83–90.

Gerhardt H (2013) VEGF and Endothelial Guidance in Angiogenic Sprouting. Landes Bioscience. Available at: https://www.ncbi.nlm.nih.gov/books/NBK6141/ [Accessed November 5, 2019].

Gjedde A, Diemer NH (1985) Double-Tracer Study of the Fine Regional Blood—Brain Glucose Transfer in the Rat by Computer-Assisted Autoradiography. J Cereb Blood Flow Metab 5:282–289.

Göbel U, Theilen H, Kuschinsky W (1990) Congruence of total and perfused capillary network in rat brains. Circ Res 66:271–281.

Gold BT, Powell DK, Xuan L, Jicha GA, Smith CD (2010) Age-related slowing of task switching is associated with decreased integrity of frontoparietal white matter. Neurobiol Aging 31:512–522.

Gordon GRJ, Howarth C, MacVicar BA (2016) Bidirectional Control of Blood Flow by Astrocytes: A Role for Tissue Oxygen and Other Metabolic Factors. Adv Exp Med Biol 903:209–219.

Gould IG, Linninger AA (2015) Hematocrit Distribution and Tissue Oxygenation in Large Microcirculatory Networks. Microcirculation 22:1–18.

Gould IG, Tsai P, Kleinfeld D, Linninger A (2017) The capillary bed offers the largest hemodynamic resistance to the cortical blood supply. J Cereb Blood Flow Metab 37:52–68.

Greenwood PM (2000) The frontal aging hypothesis evaluated. J Int Neuropsychol Soc JINS 6:705–726.

Gruetter R (2003) Glycogen: The forgotten cerebral energy store. J Neurosci Res 74:179–183.

Grutzendler J, Murikinati S, Hiner B, Ji L, Lam CK, Yoo T, Gupta S, Hafler BP, Adelman RA, Yuan P, Rodriguez G (2014) Angiophagy Prevents Early Embolus Washout

But Recanalizes Microvessels Through Embolus Extravasation. Sci Transl Med 6:226ra31-226ra31.

Guan J, Pavlovic D, Dalkie N, Waldvogel HJ, O'Carroll SJ, Green CR, Nicholson LFB (2013) Vascular degeneration in Parkinson's disease. Brain Pathol Zurich Switz 23:154–164.

Gunning-Dixon FM, Raz N (2000) The cognitive correlates of white matter abnormalities in normal aging: A quantitative review. Neuropsychology 14:224–232.

Gutiérrez-Jiménez E, Cai C, Mikkelsen IK, Rasmussen PM, Angleys H, Merrild M, Mouridsen K, Jespersen SN, Lee J, Iversen NK, Sakadzic S, Østergaard L (2016) Effect of electrical forepaw stimulation on capillary transit-time heterogeneity (CTH). J Cereb Blood Flow Metab 36:2072–2086.

Hagstadius S, Risberg J (1989) Regional cerebral blood flow characteristics and variations with age in resting normal subjects. Brain Cogn 10:28–43.

Hall CN, Reynell C, Gesslein B, Hamilton NB, Mishra A, Sutherland BA, O'Farrell FM, Buchan AM, Lauritzen M, Attwell D (2014) Capillary pericytes regulate cerebral blood flow in health and disease. Nature 508:55–60.

Harb R, Whiteus C, Freitas C, Grutzendler J (2013) In vivo imaging of cerebral microvascular plasticity from birth to death. J Cereb Blood Flow Metab Off J Int Soc Cereb Blood Flow Metab 33:146–156.

Hartmann DA, Hyacinth HI, Liao F-F, Shih AY (2018) Does pathology of small venules contribute to cerebral microinfarcts and dementia? J Neurochem 144:517–526.

Hartmann P, Ramseier A, Gudat F, Mihatsch MJ, Polasek W (1994) Normal weight of the brain in adults in relation to age, sex, body height and weight. Pathol 15:165–170.

Hartung G, Vesel C, Morley R, Alaraj A, Sled J, Kleinfeld D, Linninger A (2018) Simulations of blood as a suspension predicts a depth dependent hematocrit in the circulation throughout the cerebral cortex. PLOS Comput Biol 14:e1006549.

Hicks P, Rolsten C, Brizzee D, Samorajski T (1983) Age-related changes in rat brain capillaries. Neurobiol Aging 4:69–75.

Hill RA, Tong L, Yuan P, Murikinati S, Gupta S, Grutzendler J (2015) Regional Blood Flow in the Normal and Ischemic Brain Is Controlled by Arteriolar Smooth Muscle Cell Contractility and Not by Capillary Pericytes. Neuron 87:95–110.

Hinds JW, McNelly NA (1982) Capillaries in aging rat olfactory bulb: a quantitative light and electron microscopic analysis. Neurobiol Aging 3:197–207.

Hogan-Cann AD, Lu P, Anderson CM (2019) Endothelial NMDA receptors mediate activity-dependent brain hemodynamic responses in mice. Proc Natl Acad Sci 116:10229–10231.

Hooper AT, Butler JM, Nolan DJ, Kranz A, Iida K, Kobayashi M, Kopp H-G, Shido K, Petit I, Yanger K, James D, Witte L, Zhu Z, Wu Y, Pytowski B, Rosenwaks Z,

Mittal V, Sato TN, Rafii S (2009) Engraftment and Reconstitution of Hematopoiesis Is Dependent on VEGFR2-Mediated Regeneration of Sinusoidal Endothelial Cells. Cell Stem Cell 4:263–274.

Hughes CCW, Lantos PL (1987) A morphometric study of blood vessel, neuron and glial cell distribution in young and old rat brain. J Neurol Sci 79:101–110.

Hunziker O, Abdel'Al S, Schulz U (1979) The aging human cerebral cortex: a stereological characterization of changes in the capillary net. J Gerontol 34:345–350.

Hyacinth HI, Sugihara CL, Spencer TL, Archer DR, Shih AY (2017) Higher prevalence of spontaneous cerebral vasculopathy and cerebral infarcts in a mouse model of sickle cell disease. J Cereb Blood Flow Metab 39:342–351.

Hyder F, Herman P, Bailey CJ, Møller A, Globinsky R, Fulbright RK, Rothman DL, Gjedde A (2016) Uniform distributions of glucose oxidation and oxygen extraction in gray matter of normal human brain: No evidence of regional differences of aerobic glycolysis. J Cereb Blood Flow Metab Off J Int Soc Cereb Blood Flow Metab 36:903–916.

Iadecola C (2013) The Pathobiology of Vascular Dementia. Neuron 80:844–866.

Iadecola C (2017) The Neurovascular Unit Coming of Age: A Journey through Neurovascular Coupling in Health and Disease. Neuron 96:17–42.

Institoris A, Tran CHT, Rosenegger D, Peringod G, Gordon GR (2019) Neurons and astrocytes control local brain blood flow on distinct timescales. In. Toronto, ON, Canada: Unpublished.

Isaacs KR, Anderson BJ, Alcantara AA, Black JE, Greenough WT (1992) Exercise and the brain: angiogenesis in the adult rat cerebellum after vigorous physical activity and motor skill learning. J Cereb Blood Flow Metab Off J Int Soc Cereb Blood Flow Metab 12:110–119.

Iturria-Medina Y et al. (2016) Early role of vascular dysregulation on late-onset Alzheimer's disease based on multifactorial data-driven analysis. Nat Commun 7:11934.

Jespersen SN, Østergaard L (2012) The Roles of Cerebral Blood Flow, Capillary Transit Time Heterogeneity, and Oxygen Tension in Brain Oxygenation and Metabolism. J Cereb Blood Flow Metab 32:264–277.

Joo IL, Lai AY, Bazzigaluppi P, Koletar MM, Dorr A, Brown ME, Thomason LAM, Sled JG, McLaurin J, Stefanovic B (2017) Early neurovascular dysfunction in a transgenic rat model of Alzheimer's disease. Sci Rep 7:46427.

Jucker M, Bättig K, Meier-Ruge W (1990) Effects of aging and vincamine derivatives on pericapillary microenvironment: stereological characterization of the cerebral capillary network. Neurobiol Aging 11:39–46.

Jucker M, Meier-Ruge W (1989) Effects of brovincamine on stereological capillary parameters in adult and old Fischer-344 rats. Microvasc Res 37:298–307.

Jung S, Wiest R, Gralla J, McKinley R, Mattle H, Liebeskind D (2017) Relevance of the cerebral collateral circulation in ischaemic stroke: time is brain, but collaterals set the pace. Swiss Med Wkly 147 Available at: https://smw.ch/en/article/doi/smw.2017.14538/ [Accessed September 3, 2019].

Kandel ER, Schwartz JH, Jessell TM, Siegelbaum SA, Hudspeth AJ (2012) Principles of Neural Science (Hudspeth AJ, ed)., Fifth. McGraw-Hill Education.

Kennedy KM, Raz N (2009) Aging white matter and cognition: Differential effects of regional variations in diffusion properties on memory, executive functions, and speed. Neuropsychologia 47:916–927.

Khennouf L, Gesslein B, Brazhe A, Octeau JC, Kutuzov N, Khakh BS, Lauritzen M (2018) Active role of capillary pericytes during stimulation-induced activity and spreading depolarization. Brain 141:2032–2046.

Kisler K, Nelson AR, Montagne A, Zlokovic BV (2017a) Cerebral blood flow regulation and neurovascular dysfunction in Alzheimer disease. Nat Rev Neurosci 18:419–434.

Kisler K, Nelson AR, Rege SV, Ramanathan A, Wang Y, Ahuja A, Lazic D, Tsai PS, Zhao Z, Zhou Y, Boas DA, Sakadžić S, Zlokovic BV (2017b) Pericyte degeneration leads to neurovascular uncoupling and limits oxygen supply to brain. Nat Neurosci 20:406–416.

Klabunde RE (2011) Cardiovascular Physiology Concepts, Second edition. Philadelphia, PA: LWW.

Kleim JA, Cooper NR, VandenBerg PM (2002) Exercise induces angiogenesis but does not alter movement representations within rat motor cortex. Brain Res 934:1–6.

Klein AW, Michel ME (1977) A morphometric study of the neocortex of young adult and old maze-differentiated rats. Mech Ageing Dev 6:441–452.

Kleinfeld D, Mitra PP, Helmchen F, Denk W (1998) Fluctuations and stimulus-induced changes in blood flow observed in individual capillaries in layers 2 through 4 of rat neocortex. Proc Natl Acad Sci 95:15741–15746.

Knox CA, Oliveira A (1980) Brain aging in normotensive and hypertensive strains of rats. III. A quantitative study of cerebrovasculature. Acta Neuropathol (Berl) 52:17–25.

Krejza J, Mariak Z, Walecki J, Szydlik P, Lewko J, Ustymowicz A (1999) Transcranial color Doppler sonography of basal cerebral arteries in 182 healthy subjects: age and sex variability and normal reference values for blood flow parameters. AJR Am J Roentgenol 172:213–218.

Kuzawa CW, Chugani HT, Grossman LI, Lipovich L, Muzik O, Hof PR, Wildman DE, Sherwood CC, Leonard WR, Lange N (2014) Metabolic costs and evolutionary implications of human brain development. Proc Natl Acad Sci U S A 111:13010–13015.

Lacoste B, Comin CH, Ben-Zvi A, Kaeser PS, Xu X, Costa L da F, Gu C (2014) Sensory-related neural activity regulates the structure of vascular networks in the cerebral cortex. Neuron 83:1117–1130.

Lacoste B, Gu C (2015) Control of cerebrovascular patterning by neural activity during postnatal development. Mech Dev 138 Pt 1:43–49.

Lam CK, Yoo T, Hiner B, Liu Z, Grutzendler J (2010) Embolus extravasation is an alternative mechanism for cerebral microvascular recanalization. Nature 465:478–482.

Lauwers F, Cassot F, Lauwers-Cances V, Puwanarajah P, Duvernoy H (2008) Morphometry of the human cerebral cortex microcirculation: General characteristics and space-related profiles. NeuroImage 39:936–948.

Lécuyer M-A, Kebir H, Prat A (2016) Glial influences on BBB functions and molecular players in immune cell trafficking. Biochim Biophys Acta BBA - Mol Basis Dis 1862:472–482.

Lee J, Wu W, Boas DA (2016) Early capillary flux homogenization in response to neural activation. J Cereb Blood Flow Metab 36:375–380.

Lee J, Wu W, Lesage F, Boas DA (2013) Multiple-capillary measurement of RBC speed, flux, and density with optical coherence tomography. J Cereb Blood Flow Metab 33:1707–1710.

Leenders KL, Perani D, Lammertsma AA, Heather JD, Buckingham P, Jones T, Healy MJR, Gibbs JM, Wise RJS, Hatazawa J, Herold S, Beaney RP, Brooks DJ, Spinks T, Rhodes C, Frackowiak RSJ (1990) CEREBRAL BLOOD FLOW, BLOOD VOLUME AND OXYGEN UTILIZATIONNORMAL VALUES AND EFFECT OF AGE. Brain 113:27–47.

Leeuwis AE, Smith LA, Melbourne A, Hughes AD, Richards M, Prins ND, Sokolska M, Atkinson D, Tillin T, Jäger HR, Chaturvedi N, van der Flier WM, Barkhof F (2018) Cerebral Blood Flow and Cognitive Functioning in a Community-Based, Multi-Ethnic Cohort: The SABRE Study. Front Aging Neurosci 10 Available at: https://www.ncbi.nlm.nih.gov/pmc/articles/PMC6154257/ [Accessed October 19, 2019].

Li B, Esipova TV, Sencan I, Kılıç K, Fu B, Desjardins M, Moeini M, Kura S, Yaseen MA, Lesage F, Østergaard L, Devor A, Boas DA, Vinogradov SA, Sakadžić S (2019a) More homogeneous capillary flow and oxygenation in deeper cortical layers correlate with increased oxygen extraction Charpak S, Behrens TE, Charpak S, Linninger A, eds. eLife 8:e42299.

Li B, Lee J, Boas DA, Lesage F (2016) Contribution of low- and high-flux capillaries to slow hemodynamic fluctuations in the cerebral cortex of mice. J Cereb Blood Flow Metab 36:1351–1356.

Li B, Ohtomo R, Thunemann M, Adams SR, Yang J, Fu B, Yaseen MA, Ran C, Polimeni JR, Boas DA, Devor A, Lo EH, Arai K, Sakadžić S (2019b) Two-photon microscopic imaging of capillary red blood cell flux in mouse brain reveals vulnerability of cerebral white matter to hypoperfusion. J Cereb Blood Flow Metab:10.1177/0271678X19831016.

Longden TA, Dabertrand F, Koide M, Gonzales AL, Tykocki NR, Brayden JE, Hill-Eubanks D, Nelson MT (2017) Capillary K^+-sensing initiates retrograde hyperpolarization to increase local cerebral blood flow. Nat Neurosci 20:717–726.

Lücker A, Secomb TW, Barrett MJP, Weber B, Jenny P (2018a) The Relation Between Capillary Transit Times and Hemoglobin Saturation Heterogeneity. Part 2: Capillary Networks. Front Physiol 9 Available at: https://www.frontiersin.org/articles/10.3389/fphys.2018.01296/full [Accessed October 21, 2019].

Lücker A, Secomb TW, Weber B, Jenny P (2018b) The Relation Between Capillary Transit Times and Hemoglobin Saturation Heterogeneity. Part 1: Theoretical Models. Front Physiol 9 Available at: https://www.frontiersin.org/articles/10.3389/fphys.2018.00420/full [Accessed October 21, 2019].

Lugo-Hernandez E, Squire A, Hagemann N, Brenzel A, Sardari M, Schlechter J, Sanchez-Mendoza EH, Gunzer M, Faissner A, Hermann DM (2017) 3D visualization and quantification of microvessels in the whole ischemic mouse brain using solvent-based clearing and light sheet microscopy. J Cereb Blood Flow Metab 37:3355–3367.

Lyons DG, Parpaleix A, Roche M, Charpak S (2016) Mapping oxygen concentration in the awake mouse brain. eLife 5:e12024.

Ma J, Ma Y, Shuaib A, Winship IR (2019) Impaired Collateral Flow in Pial Arterioles of Aged Rats During Ischemic Stroke. Transl Stroke Res:10.1007/s12975-019-00710–00711.

Mann DM, Eaves NR, Marcyniuk B, Yates PO (1986) Quantitative changes in cerebral cortical microvasculature in ageing and dementia. Neurobiol Aging 7:321–330.

Mapelli L, Gagliano G, Soda T, Laforenza U, Moccia F, D'Angelo EU (2017) Granular Layer Neurons Control Cerebellar Neurovascular Coupling Through an NMDA Receptor/NO-Dependent System. J Neurosci Off J Soc Neurosci 37:1340–1351.

Marín-Padilla M (2012) The human brain intracerebral microvascular system: development and structure. Front Neuroanat 6 Available at: https://www.frontiersin.org/articles/10.3389/fnana.2012.00038/full [Accessed January 15, 2020].

Martin AJ, Friston KJ, Colebatch JG, Frackowiak RS (1991) Decreases in regional cerebral blood flow with normal aging. J Cereb Blood Flow Metab Off J Int Soc Cereb Blood Flow Metab 11:684–689.

Masamoto K, Takuwa H, Seki C, Taniguchi J, Itoh Y, Tomita Y, Toriumi H, Unekawa M, Kawaguchi H, Ito H, Suzuki N, Kanno I (2014) Microvascular Sprouting, Extension, and Creation of New Capillary Connections with Adaptation of the Neighboring Astrocytes in Adult Mouse Cortex under Chronic Hypoxia. J Cereb Blood Flow Metab 34:325–331.

Mattson MP, Arumugam TV (2018) Hallmarks of Brain Aging: Adaptive and Pathological Modification by Metabolic States. Cell Metab 27:1176–1199.

Mehina EMF, Murphy-Royal C, Gordon GR (2017) Steady-State Free Ca2+ in Astrocytes Is Decreased by Experience and Impacts Arteriole Tone. J Neurosci 37:8150–8165.

Meier-Ruge W, Hunziker O, Schulz U, Tobler HJ, Schweizer A (1980) Stereological changes in the capillary network and nerve cells of the aging human brain. Mech Ageing Dev 14:233–243.

Meier-Ruge W, Schulz-Dazzi U (1987) Effects of brovincamine on the stereological parameters of corticocerebral capillaries. Life Sci 40:943–949.

Menon BK, O'Brien B, Bivard A, Spratt NJ, Demchuk AM, Miteff F, Lu X, Levi C, Parsons MW (2013) Assessment of leptomeningeal collaterals using dynamic CT angiography in patients with acute ischemic stroke. J Cereb Blood Flow Metab 33:365–371.

Merat S, Fruebis J, Sutphin M, Silvestre M, Reaven PD (2000) Effect of aging on aortic expression of the vascular cell adhesion molecule-1 and atherosclerosis in murine models of atherosclerosis. J Gerontol A Biol Sci Med Sci 55:B85-94.

Milner R ed. (2014) Cerebral Angiogenesis: Methods and Protocols. Humana Press. Available at: https://www.springer.com/gp/book/9781493903191 [Accessed November 5, 2019].

Mishra A, Reynolds JP, Chen Y, Gourine AV, Rusakov DA, Attwell D (2016) Astrocytes mediate neurovascular signaling to capillary pericytes but not to arterioles. Nat Neurosci 19:1619–1627.

Moeini M, Lu X, Avti PK, Damseh R, Bélanger S, Picard F, Boas D, Kakkar A, Lesage F (2018) Compromised microvascular oxygen delivery increases brain tissue vulnerability with age. Sci Rep 8:8219.

Moeller JR, Ishikawa T, Dhawan V, Spetsieris P, Mandel F, Alexander GE, Grady C, Pietrini P, Eidelberg D (1996) The metabolic topography of normal aging. J Cereb Blood Flow Metab Off J Int Soc Cereb Blood Flow Metab 16:385–398.

Morland C et al. (2017) Exercise induces cerebral VEGF and angiogenesis via the lactate receptor HCAR1. Nat Commun 8:1–9.

Mostany R, Chowdhury TG, Johnston DG, Portonovo SA, Carmichael ST, Portera-Cailliau C (2010) Local Hemodynamics Dictate Long-Term Dendritic Plasticity in Peri-Infarct Cortex. J Neurosci 30:14116–14126.

Murman DL (2015) The Impact of Age on Cognition. Semin Hear 36:111–121.

Murugesan N, Demarest TG, Madri JA, Pachter JS (2012) Brain regional angiogenic potential at the neurovascular unit during normal aging. Neurobiol Aging 33:1004.e1-1004.e16.

Namdee K, Carrasco-Teja M, Fish MB, Charoenphol P, Eniola-Adefeso O (2015) Effect of Variation in hemorheology between human and animal blood on the binding efficacy of vascular-targeted carriers. Sci Rep 5:1–14.

Ndubuizu OI, Tsipis CP, Li A, LaManna JC (2010) Hypoxia Inducible Factor-1 (HIF-1) Independent Microvascular Angiogenesis in the Aged Rat Brain. Brain Res 1366:101–109.

Ng YS, Stein J, Ning M, Black-Schaffer RM (2007) Comparison of clinical characteristics and functional outcomes of ischemic stroke in different vascular territories. Stroke 38:2309–2314.

Nielsen RB, Egefjord L, Angleys H, Mouridsen K, Gejl M, Møller A, Brock B, Brændgaard H, Gottrup H, Rungby J, Eskildsen SF, Østergaard L (2017) Capillary dysfunction is associated with symptom severity and neurodegeneration in Alzheimer's disease. Alzheimers Dement 13:1143–1153.

Nishimura N, Rosidi NL, Iadecola C, Schaffer CB (2010) Limitations of Collateral Flow after Occlusion of a Single Cortical Penetrating Arteriole. J Cereb Blood Flow Metab 30:1914–1927.

Noda A, Ohba H, Kakiuchi T, Futatsubashi M, Tsukada H, Nishimura S (2002) Age-related changes in cerebral blood flow and glucose metabolism in conscious rhesus monkeys. Brain Res 936:76–81.

Noda K, Nakao S, Ishida S, Ishibashi T (2012) Leukocyte Adhesion Molecules in Diabetic Retinopathy. J Ophthalmol 2012 Available at: https://www.ncbi.nlm.nih.gov/pmc/articles/PMC3216271/ [Accessed November 5, 2019].

Nortley R, Korte N, Izquierdo P, Hirunpattarasilp C, Mishra A, Jaunmuktane Z, Kyrargyri V, Pfeiffer T, Khennouf L, Madry C, Gong H, Richard-Loendt A, Huang W, Saito T, Saido TC, Brandner S, Sethi H, Attwell D (2019) Amyloid β oligomers constrict human capillaries in Alzheimer's disease via signaling to pericytes. Science 365:eaav9518.

Noumbissi ME, Galasso B, Stins MF (2018) Brain vascular heterogeneity: implications for disease pathogenesis and design of in vitro blood–brain barrier models. Fluids Barriers CNS 15:12.

Nyberg L, Salami A, Andersson M, Eriksson J, Kalpouzos G, Kauppi K, Lind J, Pudas S, Persson J, Nilsson L-G (2010) Longitudinal evidence for diminished frontal cortex function in aging. Proc Natl Acad Sci 107:22682–22686.

Nyúl-Tóth Á, Suciu M, Molnár J, Fazakas C, Haskó J, Herman H, Farkas AE, Kaszaki J, Hermenean A, Wilhelm I, Krizbai IA (2016) Differences in the molecular structure of the blood-brain barrier in the cerebral cortex and white matter: an in silico, in vitro, and ex vivo study. Am J Physiol-Heart Circ Physiol 310:H1702–H1714.

O'Brown NM, Pfau SJ, Gu C (2018) Bridging barriers: a comparative look at the blood-brain barrier across organisms. Genes Dev 32:466–478.

Oghabian Z, Jafari AH (2018) Quantitative Measurement of Oxygen Extraction Fraction (OEF) Using Respiratory Modulated Perfusion MRI. Iran J Radiol 15 Available at: http://iranjradiol.com/en/articles/64253.html [Accessed November 8, 2019].

Ohata M, Sundaram U, Fredericks WR, London ED, Rapoport SI (1981) Regional cerebral blood flow during development and ageing of the rat brain. Brain J Neurol 104:319–332.

Okpala I, Daniel Y, Haynes R, Odoemene D, Goldman J (2002) Relationship between the clinical manifestations of sickle cell disease and the expression of adhesion molecules on white blood cells. Eur J Haematol 69:135–144.

Østergaard L, Engedal TS, Moreton F, Hansen MB, Wardlaw JM, Dalkara T, Markus HS, Muir KW (2016) Cerebral small vessel disease: Capillary pathways to stroke and cognitive decline. J Cereb Blood Flow Metab 36:302–325.

Østergaard L, Jespersen SN, Engedahl T, Jiménez EG, Ashkanian M, Hansen MB, Eskildsen S, Mouridsen K (2015) Capillary Dysfunction: Its Detection and Causative Role in Dementias and Stroke. Curr Neurol Neurosci Rep 15:37.

Park L, Anrather J, Girouard H, Zhou P, Iadecola C (2007) Nox2-derived reactive oxygen species mediate neurovascular dysregulation in the aging mouse brain. J Cereb Blood Flow Metab Off J Int Soc Cereb Blood Flow Metab 27:1908–1918.

Peppiatt CM, Howarth C, Mobbs P, Attwell D (2006) Bidirectional control of CNS capillary diameter by pericytes. Nature 443:700–704.

Peters A, Schweiger U, Pellerin L, Hubold C, Oltmanns KM, Conrad M, Schultes B, Born J, Fehm HL (2004) The selfish brain: competition for energy resources. Neurosci Biobehav Rev 28:143–180.

Pugh KG, Lipsitz LA (2002) The microvascular frontal-subcortical syndrome of aging. Neurobiol Aging 23:421–431.

Raz N, Lindenberger U, Rodrigue KM, Kennedy KM, Head D, Williamson A, Dahle C, Gerstorf D, Acker JD (2005) Regional Brain Changes in Aging Healthy Adults: General Trends, Individual Differences and Modifiers. Cereb Cortex 15:1676–1689.

Reeson P, Choi K, Brown CE (2018) VEGF signaling regulates the fate of obstructed capillaries in mouse cortex Kleinfeld D, ed. eLife 7:e33670.

Richter V, Rassoul F, Purschwitz K, Hentschel B, Reuter W, Kuntze T (2003) Circulating vascular cell adhesion molecules VCAM-1, ICAM-1, and E-selectin in dependence on aging. Gerontology 49:293–300.

Riddle DR, Sonntag WE, Lichtenwalner RJ (2003) Microvascular plasticity in aging. Ageing Res Rev 2:149–168.

Rieke GK (1987) Thalamic arterial pattern: An endocast and scanning electron microscopic study in normotensive male rats. Am J Anat 178:45–54.

Roche M, Chaigneau E, Rungta RL, Boido D, Weber B, Charpak S (2019) In vivo imaging with a water immersion objective affects brain temperature, blood flow and oxygenation Kleinfeld D, ed. eLife 8:e47324.

Roy CS, Sherrington CS (1890) On the Regulation of the Blood-supply of the Brain. J Physiol 11:85-158.17.

Ruitenberg A, Heijer T den, Bakker SLM, Swieten JC van, Koudstaal PJ, Hofman A, Breteler MMB (2005) Cerebral hypoperfusion and clinical onset of dementia: The Rotterdam study. Ann Neurol 57:789–794.

Rungta RL, Chaigneau E, Osmanski B-F, Charpak S (2018) Vascular Compartmentalization of Functional Hyperemia from the Synapse to the Pia. Neuron 99:362-375.e4.

Sakadžić S, Roussakis E, Yaseen MA, Mandeville ET, Srinivasan VJ, Arai K, Ruvinskaya S, Devor A, Lo EH, Vinogradov SA, Boas DA (2010) Two-photon high-resolution measurement of partial pressure of oxygen in cerebral vasculature and tissue. Nat Methods 7:755–759.

Santisakultarm TP, Paduano CQ, Stokol T, Southard TL, Nishimura N, Skoda RC, Olbricht WL, Schafer AI, Silver RT, Schaffer CB (2014) Stalled cerebral capillary blood flow in mouse models of essential thrombocythemia and polycythemia vera revealed by in vivo two-photon imaging. J Thromb Haemost JTH 12:2120–2130.

Schaffer CB, Friedman B, Nishimura N, Schroeder LF, Tsai PS, Ebner FF, Lyden PD, Kleinfeld D (2006) Two-Photon Imaging of Cortical Surface Microvessels Reveals a Robust Redistribution in Blood Flow after Vascular Occlusion. PLOS Biol 4:e22.

Schager B (2019) Microvessel Density Analysis. GitHub Available at: https://github.com/bschager/Microvessel-Density-Analysis [Accessed August 2, 2019].

Schager B, Brown CE (2020) Susceptibility to capillary plugging can predict brain region specific vessel loss with aging. J Cereb Blood Flow Metab:0271678X19895245.

Schmid F, Barrett MJP, Jenny P, Weber B (2017a) Vascular density and distribution in neocortex. NeuroImage Available at: http://www.sciencedirect.com/science/article/pii/S1053811917305165 [Accessed June 6, 2019].

Schmid F, Tsai PS, Kleinfeld D, Jenny P, Weber B (2017b) Depth-dependent flow and pressure characteristics in cortical microvascular networks. PLoS Comput Biol 13:e1005392.

Schmidt S, Moser M, Sperandio M (2013) The molecular basis of leukocyte recruitment and its deficiencies. Mol Immunol 55:49–58.

Scioli MG, Bielli A, Arcuri G, Ferlosio A, Orlandi A (2014) Ageing and microvasculature. Vasc Cell 6:19.

Shao W-H, Li C, Chen L, Qiu X, Zhang W, Huang C-X, Xia L, Kong J-M, Tang Y (2010) Stereological Investigation of Age-Related Changes of the Capillaries in White Matter. Anat Rec 293:1400–1407.

Shih AY, Blinder P, Tsai PS, Friedman B, Stanley G, Lyden PD, Kleinfeld D (2013) The smallest stroke: occlusion of one penetrating vessel leads to infarction and a cognitive deficit. Nat Neurosci 16:55–63.

Shih AY, Rühlmann C, Blinder P, Devor A, Drew PJ, Friedman B, Knutsen PM, Lyden PD, Mateo C, Mellander L, Nishimura N, Schaffer CB, Tsai PS, Kleinfeld D (2015) Robust and fragile aspects of cortical blood flow in relation to the underlying angioarchitecture. Microcirc N Y N 1994 22:204–218.

Shin W, Horowitz S, Ragin A, Chen Y, Walker M, Carroll TJ (2007) Quantitative cerebral perfusion using dynamic susceptibility contrast MRI: evaluation of reproducibility and age- and gender-dependence with fully automatic image postprocessing algorithm. Magn Reson Med 58:1232–1241.

Shweiki D, Itin A, Soffer D, Keshet E (1992) Vascular endothelial growth factor induced by hypoxia may mediate hypoxia-initiated angiogenesis. Nature 359:843–845.

Smith AF, Doyeux V, Berg M, Peyrounette M, Haft-Javaherian M, Larue A-E, Slater JH, Lauwers F, Blinder P, Tsai P, Kleinfeld D, Schaffer CB, Nishimura N, Davit Y, Lorthois S (2019) Brain Capillary Networks Across Species: A few Simple Organizational Requirements Are Sufficient to Reproduce Both Structure and Function. Front Physiol 10 Available at: https://www.frontiersin.org/articles/10.3389/fphys.2019.00233/full [Accessed January 15, 2020].

Snyder HM et al. (2015) Vascular contributions to cognitive impairment and dementia including Alzheimer’s disease. Alzheimers Dement 11:710–717.

Society for Neuroscience (2019) Considerations for Design of Studies of Normal Aging, Accelerated Aging, and Neurodegeneration. J Neurosci 39:7032–7033.

Spence JD (2019) Blood Pressure Gradients in the Brain: Their Importance to Understanding Pathogenesis of Cerebral Small Vessel Disease. Brain Sci 9 Available at: https://www.ncbi.nlm.nih.gov/pmc/articles/PMC6406272/ [Accessed November 5, 2019].

Stephan BC, Matthews FE, Khaw K-T, Dufouil C, Brayne C (2009) Beyond mild cognitive impairment: vascular cognitive impairment, no dementia (VCIND). Alzheimers Res Ther 1:4.

Sturrock RR (1977) Quantitative and morphological changes in neurons and neuroglia in the indusium griseum of aging mice. J Gerontol 32:647–658.

Swain RA, Harris AB, Wiener EC, Dutka MV, Morris HD, Theien BE, Konda S, Engberg K, Lauterbur PC, Greenough WT (2003) Prolonged exercise induces angiogenesis and increases cerebral blood volume in primary motor cortex of the rat. Neuroscience 117:1037–1046.

Szpak GM, Lechowicz W, Lewandowska E, Bertrand E, Wierzba-Bobrowicz T, Dymecki J (1999) Border zone neovascularization in cerebral ischemic infarct. Folia Neuropathol 37:264–268.

Talahalli R, Zarini S, Tang J, Li G, Murphy R, Kern TS, Gubitosi-Klug RA (2013) Leukocytes regulate retinal capillary degeneration in the diabetic mouse via generation of leukotrienes. J Leukoc Biol 93:135–143.

Tang Y, Wang L, Wang J, Lin X, Wang Y, Jin K, Yang G-Y (2016) Ischemia-induced Angiogenesis is Attenuated in Aged Rats. Aging Dis 7:326–335.

Tarantini S, Tran CHT, Gordon GR, Ungvari Z, Csiszar A (2017) Impaired neurovascular coupling in aging and Alzheimer's disease: contribution of astrocyte dysfunction and endothelial impairment to cognitive decline. Exp Gerontol 94:52–58.

Tennant KA, Brown CE (2013) Diabetes Augments In Vivo Microvascular Blood Flow Dynamics after Stroke. J Neurosci 33:19194–19204.

Tong X-K, Trigiani LJ, Hamel E (2019) High cholesterol triggers white matter alterations and cognitive deficits in a mouse model of cerebrovascular disease: benefits of simvastatin. Cell Death Dis 10:89.

Tran CHT, Peringod G, Gordon GR (2018) Astrocytes Integrate Behavioral State and Vascular Signals during Functional Hyperemia. Neuron 100:1133-1148.e3.

Tsai PS, Kaufhold JP, Blinder P, Friedman B, Drew PJ, Karten HJ, Lyden PD, Kleinfeld D (2009) Correlations of Neuronal and Microvascular Densities in Murine Cortex Revealed by Direct Counting and Colocalization of Nuclei and Vessels. J Neurosci 29:14553–14570.

Uhlirova H et al. (2016) Cell type specificity of neurovascular coupling in cerebral cortex Nelson SB, ed. eLife 5:e14315.

Ungvari Z, Tucsek Z, Sosnowska D, Toth P, Gautam T, Podlutsky A, Csiszar A, Losonczy G, Valcarcel-Ares MN, Sonntag WE, Csiszar A (2013) Aging-Induced Dysregulation of Dicer1-Dependent MicroRNA Expression Impairs Angiogenic

Capacity of Rat Cerebromicrovascular Endothelial Cells. J Gerontol Ser A 68:877–891.

van der Wijk A-E, Lachkar N, de Vos J, Grootemaat AE, van der Wel NN, Hordijk PL, Bakker ENTP, vanBavel E (2019) Extravasation of Microspheres in a Rat Model of Silent Brain Infarcts. Stroke 50:1590–1594.

Vermeer SE, Longstreth WT, Koudstaal PJ (2007) Silent brain infarcts: a systematic review. Lancet Neurol 6:611–619.

Viboolvorakul S, Patumraj S (2014) Exercise Training Could Improve Age-Related Changes in Cerebral Blood Flow and Capillary Vascularity through the Upregulation of VEGF and eNOS. BioMed Res Int Available at: https://www.hindawi.com/journals/bmri/2014/230791/ [Accessed July 8, 2019].

Villar-Cheda B, Sousa-Ribeiro D, Rodriguez-Pallares J, Rodriguez-Perez AI, Guerra MJ, Labandeira-Garcia JL (2009) Aging and Sedentarism Decrease Vascularization and VEGF Levels in the Rat Substantia Nigra. Implications for Parkinson’s Disease. J Cereb Blood Flow Metab 29:230–234.

Villena A, Vidal L, Díaz F, Vargas IPD (2003) Stereological changes in the capillary network of the aging dorsal lateral geniculate nucleus. Anat Rec A Discov Mol Cell Evol Biol 274A:857–861.

Wälchli T, Ulmann-Schuler A, Hintermüller C, Meyer E, Stampanoni M, Carmeliet P, Emmert MY, Bozinov O, Regli L, Schwab ME, Vogel J, Hoerstrup SP (2017)

Nogo-A regulates vascular network architecture in the postnatal brain. J Cereb Blood Flow Metab 37:614–631.

Walls JR, Coultas L, Rossant J, Henkelman RM (2008) Three-Dimensional Analysis of Vascular Development in the Mouse Embryo. PLOS ONE 3:e2853.

Warrington JP, Ashpole N, Csiszar A, Lee YW, Ungvari Z, Sonntag WE (2013) Whole Brain Radiation-Induced Vascular Cognitive Impairment: Mechanisms and Implications. J Vasc Res 50:445–457.

Warrington JP, Csiszar A, Johnson DA, Herman TS, Ahmad S, Lee YW, Sonntag WE (2011) Cerebral microvascular rarefaction induced by whole brain radiation is reversible by systemic hypoxia in mice. Am J Physiol - Heart Circ Physiol 300:H736–H744.

Warrington JP, Csiszar A, Mitschelen M, Lee YW, Sonntag WE (2012) Whole Brain Radiation-Induced Impairments in Learning and Memory Are Time-Sensitive and Reversible by Systemic Hypoxia. PLoS ONE 7 Available at: https://www.ncbi.nlm.nih.gov/pmc/articles/PMC3261195/ [Accessed November 9, 2019].

Wilkinson JH, Hopewell JW, Reinhold HS (1981) A quantitative study of age-related changes in the vascular architecture of the rat cerebral cortex. Neuropathol Appl Neurobiol 7:451–462.

Xiong B, Peng J, Li A, Lou Y, Chen S, Long B, Peng J, Yang Z, Xu T, Yang X, Li X, Jiang T, Luo Q, Gong H (2017) Precise Cerebral Vascular Atlas in Stereotaxic Coordinates of Whole Mouse Brain. Front Neuroanat 11:128.

Xu X, Wang B, Ren C, Hu J, Greenberg DA, Chen T, Xie L, Jin K (2017) Age-related Impairment of Vascular Structure and Functions. Aging Dis 8:590–610.

Yanev P, Dijkhuizen RM (2012) In Vivo Imaging of Neurovascular Remodeling After Stroke. Stroke 43:3436–3441.

Zaletel M, Strucl M, Pretnar-Oblak J, Zvan B (2005) Age-related changes in the relationship between visual evoked potentials and visually evoked cerebral blood flow velocity response. Funct Neurol 20:115–120.

Zarrinkoob L, Ambarki K, Wåhlin A, Birgander R, Eklund A, Malm J (2015) Blood flow distribution in cerebral arteries. J Cereb Blood Flow Metab 35:648–654.

Zhang R, Kadar T, Sirimanne E, MacGibbon A, Guan J (2012) Age-related memory decline is associated with vascular and microglial degeneration in aged rats. Behav Brain Res 235:210–217.

Zhang S, Boyd J, Delaney K, Murphy TH (2005) Rapid Reversible Changes in Dendritic Spine Structure In Vivo Gated by the Degree of Ischemia. J Neurosci 25:5333–5338.

Zlokovic BV (2005) Neurovascular mechanisms of Alzheimer's neurodegeneration. Trends Neurosci 28:202–208.